Numerical Modeling of The Initial Stages of Dam-Break Problems

Thesis Submitted to the University of Ottawa in Partial Fulfillment of the Requirements for the

Degree of Master of Applied Science in Civil Engineering

By

Saeid Esmaeeli Mohsenabadi

Supervisors:

Professor Ioan Nistor

Professor Majid Mohammadian

Department of Civil Engineering

Faculty of Engineering

University of Ottawa

Ottawa, Ontario,

Canada

Abstract

Cases of dam failure occur around the world almost each year. Dam failures can result in the formation and propagation of fast-moving unsteady flows that can cause loss of life as well as significant environmental and economic consequences in downstream flooded areas. The initial stages of a dam break are important due to wave-breaking front and the associated turbulence. Furthermore, characteristics of the river bed downstream of the dam (topography and bathymetry) as well as the presence of obstacles in the dam break wave path such as man-made or natural obstacles like bridges, trees, and local sills affect flow dynamics, which can lead to the formation of hydraulic jumps and the reflection of the flood wave. Accordingly, the precise prediction of flood parameters such as arrival times, free surface profiles, and flow velocity profiles is essential in order to mitigate flood hazards.

This study aimed to assess the performance of various turbulence models in predicting and estimating dam-break flows and related positive and negative flood wave characteristics over different downstream bed conditions. Three-dimensional (3-D) Computational Fluid Dynamics (CFD) models were created to solve the unsteady Reynolds equations in order to determine the initial stages of the free surface profiles over dry and wet beds and to investigate the generation and propagation of dam-break flows and reflected flood waves in the presence of a bed obstacle. The performance of different Reynolds-averaged Navier-Stokes (RANS) turbulence models has been investigated, and the standard $k-\varepsilon$, RNG $k-\varepsilon$, realizable $k-\varepsilon$, $k-\omega$ SST, and v^2-f turbulence models have been studied using OpenFOAM software. Dam-breaks were modelled using the Volume of Fluid (VOF) method employing the Finite Volume Method (FVM).

Both qualitative and quantitative comparisons of numerical simulations with laboratory experiments were completed in order to assess the suitability of different turbulence models. The results of the first study showed that the RNG $k-\varepsilon$ model exhibited better performance in capturing the flood wave free surface profiles over both dry- and wet-bed downstream conditions, while from the second study, it was concluded that the $k-\omega$ SST model was able to accurately predict the formation and propagation of reflected waves against a bottom obstacle in terms of free surface profiles and negative bore propagation speeds.

Acknowledgements

First, I would like to express my sincere gratitude to my supervisors, Dr. Ioan Nistor and Dr. Majid Mohammadian, for their continued advice, assistance, support and resources throughout all stages of my Master's studies. Both supervisors kindly helped me step-by-step during my academic career at the university of Ottawa with their great skills, vast knowledge, and technical expertise. Their guidance and support provided me with the chance to improve my skills in the field of hydraulic engineering.

I would also like to thank Mr. Hossein Kheirkhah Gildeh, from Golder Associates Ltd., who provided me with countless advice and guidance during my Masters. His experience in the field of hydraulic engineering and numerical modelling was extremely helpful and essential to complete this work.

Last but not least, I would like to thank my beloved parents with their endless support, constant encouragement, and care. Without them, I would not have been able to complete and finish this degree.

Table of Contents

List of Figures

List of Tables

List of Symbols

English Symbols

D	Initial reservoir depth [m], and Diffusion coefficient [m^2/s]
Dk_{eff}	The effective diffusivity for k [m^2/s]
$D\varepsilon_{eff}$	The effective diffusivity for ε [m^2/s]
$D\omega_{eff}$	The effective diffusivity for ω [m^2/s]
d	Water depth [m]
d_0	Initial Water depth [m]
f	Relaxing factor
G_k	The production of turbulent kinetic energy
g	Gravity acceleration [m/s^2]
h	Water surface elevation [m]
h_0	Reservoir water depth [m]
h_1	Tailwater depth [m]
k	Turbulence kinetic energy [m^2/s^2]
L	Length scale [m]
n	Number of samples
P	Pressure [N/m^2]
R	The renormalization term
S_0	Bed slope
S_0^x	Bottom slope
S_{ij}	Strain-rate tensor
T	Dimensionless time, and Turbulence time
t	Time [s]
u	Velocity in the x-direction [m/s]
v	Velocity in the y-direction [m/s]

v^2 Velocity variance

w Velocity in the z-direction [m/s]

$X_{obs,i}$ Observed values at time/place i

$X_{model,i}$ Modelled values at time/place i

x Distance from the dam [m]

Greek Symbols

α Depth ratio

ε Turbulent dissipation rate [m^2/s^3]

μ Dynamic viscosity [$N.s/m^3$]

μ_t Turbulent dynamic viscosity [$N.s/m^3$]

ν Kinematic viscosity [m^2/s]

ν_t Turbulent kinematic viscosity [m^2/s]

σ_ε Turbulent Prandtl number for ε

σ_k Turbulent Prandtl number for k

η The additional expansion parameter

ρ Mass density [kg/m^3]

ω Specific turbulent dissipation [m^2/s^3]

List of Acronyms

CCD	Charge-Coupled Devices
CFD	Computational Fluid Dynamics
CFL	Courant–Friedrichs–Lewy
COBRAS	Conell Breaking-Waves and Structures
DNS	Direct Numerical Simulation
FEM	Finite Element Method
FVM	Finite Volume Method
ICOLD	International Commission on Large Dams
LES	Large Eddy Simulation
LRR	Launder, Reece and Rodi
NRMSE	Normalized Root Mean Square Error
OpenFOAM	Open Field Operation And Manipulation
RANS	Reynolds-averaged Navier-Stokes
RMSE	Root Mean Square Error
RNG	Renormalized Group Theory
SST	Shear Stress Transport
SW	Shallow Water
SWE	Shallow Water Equations
VOF	Volume of Fluid

Chapter 1. Introduction

1.1. Background

During recent years, investigation into dam-break flows has been of significant research interest in both theoretical and practical developments. Dams are important and often strategic structures which can fail due to poor initial design and construction, lack of maintenance, structural deficiencies, or due to extreme climate events not accounted for at the design stage. The failure of a dam holding back a large amount of water in its reservoir can result in devastating consequences such as loss of life, property loss, significant morphological changes, and downstream infrastructure destruction due to the formation and propagation of fast-moving flood waves. The failures of the Gleno Dam in Lombardy, Italy in 1923, the Saint Francis Dam in California, USA in 1928, the Malpasset Dam in Côte d'Azur, France in 1959, the Teton Dam in Idaho, USA in 1976, the Burmadinho Dam in Brumadinho, Minas Gerais, Brazil in 2019, and the Edenville Dam in Edenville, Michigan, USA in 2020, are examples of major dam failures during the past hundred years (Figures 1.1 and 1.2).

The initial stages of a dam break are important due to wave-breaking and the presence of turbulence. In particular, by considering the fact that pressure is not hydrostatic, a dam-break front wave is strongly affected by vertical acceleration. Rapidly varying unsteady flows resulting from dam-breaks are affected by changes in downstream channel topography such as the presence of bed slopes or due to man-made and natural obstacles like bridges, trees, and local sills. The presence of obstacles in a river's path affects flow dynamics, which can lead to the formation of hydraulic jumps and the reflection of flood waves. Furthermore, irregularities in a channel cross-section such as channel contractions and expansions have effects on the behaviour and characteristics of the flow.

Dam-break flood waves have been studied by many researchers in order to investigate unsteady flows, and there are a number of idealized analytical solutions for dam-break problems in the literature. Ritter (1892) provided an analytical solution for the hydrodynamic problem of an instantaneous dam-break flow in a horizontal frictionless channel, and Stoker (1957) and Chanson

(2006) extended Ritter's solution to the case of a wet-bed condition and to the case of a dam-break flow over a frictionless sloping bed, respectively. Also, while several experimental studies have focused on the early stages of the dam-break process (e.g., Dressler, 1954; Bell et al., 1992; Bellos et al., 1992; Lauber and Hager, 1998), previous studies have mostly focused on dam-break flows with initially dry or wet bed conditions due to significant differences in their flow characteristics. Many recent numerical studies have employed one- and two-dimensional models that were not able to properly capture some observed hydraulic aspects like water depth, velocity, and arrival time, particularly in the near field (e.g., Robb and Vasquez, 2015; Hu et al., 2018; Yang et al., 2018)

Investigations into dam-break wave behaviour such as the formation and propagation of dam-break waves during flooding events by predicting both the spatial and temporal evolutions of floods are very important in order to reduce or mitigate the risks the impacts of flood waves. However, selecting a suitable numerical model is an essential step in performing accurate simulations to analyse dam-break flow characteristics.

Figure 1.1. Edenville Dam failure. Photo editing by Sarah Tilotta, 20 May 2020

Figure 1.2. Burmadinho dam disaster, 25 January 2019. Photo by Ibama from Brazil - Brumadinho, Minas Gerais, CC BY-SA 2.0

1.2. Study Objectives

In order to investigate the behaviour of dam-break flood waves to mitigate the impacts of downstream flooding, numerical modeling is one of the best options to capture details such as their spatial and temporal evolutions. Since dam-break flows are one of the most complex types of rapidly varying unsteady flows, and since they propagate over complex and irregular domain topographies, assessing their maximum flow depths and the characteristics of their flow regimes is important. Therefore, selecting and using an appropriate model to properly simulate and reproduce dam-break flow characteristics is an essential step in numerical modeling. This study is mainly focused on evaluating and investigating the capability and performance of the computational fluid dynamics OpenFOAM numerical model in simulating dam-break flows immediately downstream of a dam gate.

Specifically, the main objectives of this research are:

- To numerically investigate the initial stages of dam-break flow propagation over dry and wet bed conditions;
- To simulate the formation and propagation of dam-break waves numerically in the presence of a downstream obstacle;
- To choose and assess appropriate 3D numerical models with a wide range of turbulence models to simulate and reproduce dam-break flood waves while preserving numerical stability.
- To provide a comprehensive comparison of the numerical results with selected available experimental data, focusing on the free surface profiles.

In order to accomplish the objectives of this thesis, 3D numerical studies on dam-break flows during their initial stages have been conducted. The tests were carried out using the OpenFOAM numerical model, which is further detailed in Chapters 3 and 4.

1.3. Contributions and Novelty

During recent decades, theoretical studies on idealized dam-break waves have provided a way to predict and estimate dam-break flow hydrodynamics (Ritter, 1892; Dressler, 1952; Chanson, 2009); however, these analytical solutions are not applicable for complex prototype cases. Also, many of the experimental studies on dam-break waves have focused on free surface profiles and water depths, while fewer studies have investigated the flow velocity field and pressure distributions. In terms of numerical modelling, considering the recent developments in computational resources, selecting a suitable and accurate numerical and mathematical model is complicated, but important in order to reproduce flood-wave characteristics. According to the author's knowledge, most of the numerical studies have been done via one- and two-dimensional numerical simulations to represent dam-break wave behavior, and little three-dimensional (3D) numerical modelling has been conducted which motivates further 3D studies.

In this study, three-dimensional numerical modelling is performed to simulate the initial stages of dam-break flows under dry- and wet-bed conditions. Also, the generation and propagation of dam-break flood waves in the presence of a downstream obstacle are investigated numerically by employing a three-dimensional numerical model. Moreover, various turbulence closure models are examined in this study in order to evaluate the performance and the accuracy of the models in predicting induced dam-break flows in comparison with experimental data.

1.4. Outline

The thesis is organized based on the technical papers written by the author and is divided into 5 chapters as follows:

Chapter 1 presents a brief introduction on the topic of the current research study and provides an outline of its objectives, scope, and novelty, while Chapter 2 provides a comprehensive literature review of recent analytical, experimental, and numerical studies on dam-break flow characteristics under various conditions.

Chapter 3 is the first technical paper of the author of this thesis, which provides CFD simulations of the initial stages of dam-break flows under both dry- and wet-bed conditions. OpenFOAM is used to perform the simulations, and the performance of two turbulence models is evaluated. Also, a qualitative and quantitative comparison of the computed results with available measured data is provided.

Chapter 4 is the second technical paper, which expands the study of chapter 3 with more test cases and more turbulence models. In this chapter, there are 2 test cases which numerically investigate the initial stages of dam-break flow under dry- and wet-bed conditions and the formation and propagation of induced dam-break flows in the presence of a downstream obstacle. The numerical modelling is conducted using OpenFOAM with a wide range of turbulence models to simulate dam-break flood waves. The performance of the numerical models is investigated by comparing the numerical results with available experimental data.

Chapter 5 contains the final conclusions of the research along with some suggestions and recommendations for future work.

Chapter 2. Literature Review

2.1. Introduction

A dam-break flow, which is in the form of a rapidly varied unsteady flow resulting from a sudden release of a large amount of water from behind a dam gate can have devastating effects on urban areas and farmlands downstream and can causes huge damage and loss of lives. Investigating dam-break flood waves is complex, especially when they involve abruptly varying and irregular topography and bathymetry of the floodplain due to the presence of natural and man-made contractions and expansions such as trees, dikes, debris, and bridges, which can act as obstacles to the flow. The presence of obstacles such as buildings and bridges in urban areas and bottom sills and debris in natural riverbeds can cause negative wave formation, raising the flow depth and changing flow patterns and direction. In order to mitigate the hazards of dam-break flood waves, accurate investigations into dam-break flow characteristics such as flow depths and velocities are needed.

2.2. Dam-break induced flows

A study on one-dimensional and two-dimensional flood waves was conducted by Stoner et al. (1992) and a complete set of data for various tests in straight and curved channels was recorded and made available. The testing apparatus consisted of a recirculating water supply system including a reservoir, flume, storage tank, and two pumps (Figure 2.1). The plate separating the reservoir from the channel was removed instantaneously by a dam-break mechanism, and thus positive and negative waves respectively in the channel and reservoir were generated. A smooth channel bottom and a rough channel bottom were used to conduct the tests. Different water levels were used as the initial conditions in the reservoir. As well, the downstream channel was either dry or had a pre-specified water level with no initial flow in the channel.

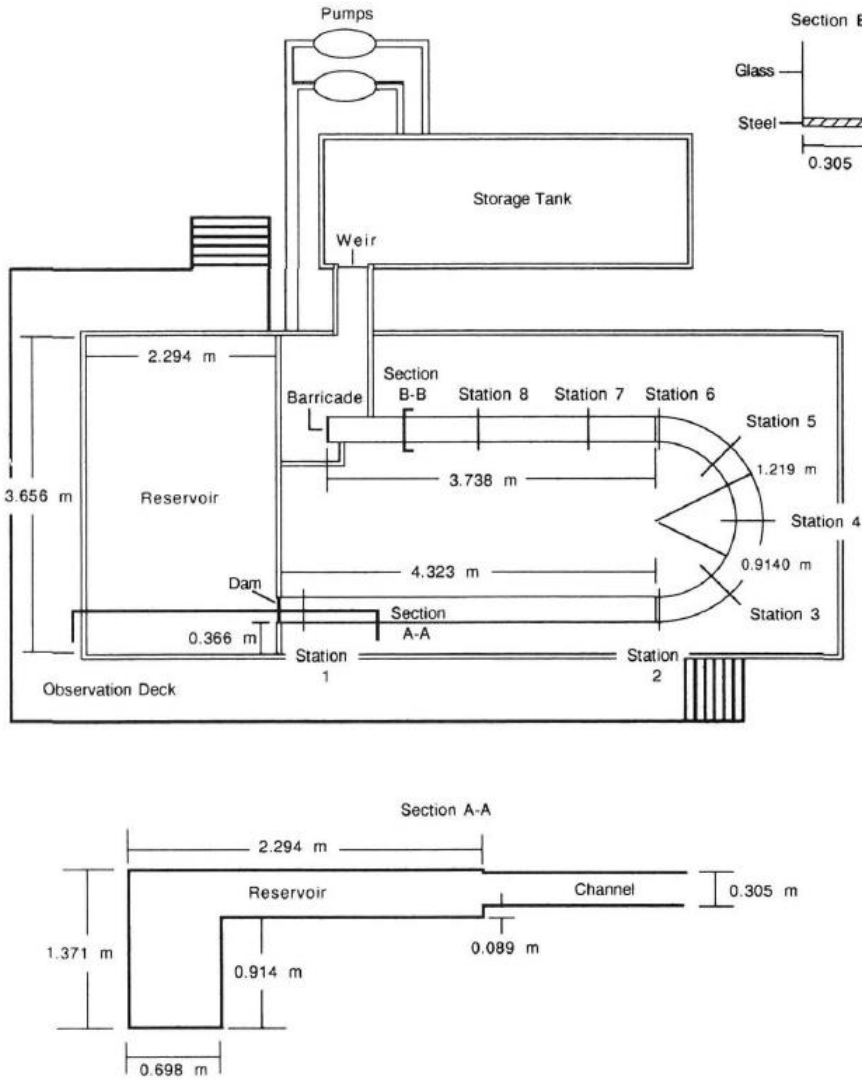

Figure 2.1. Test facility (Stoner et al. 1992)

In their study, variations of the water level in the downstream channel and upstream reservoir in addition to plan views of the wave front at different times were considered. Based on the results, Stoner et al. (1992) found that the wave front had a super-elevation on the outside of the channel in the curved part, and moreover, in the wave front, the outer front edge led the inner edge in time.

Bellos et al. (1992) experimentally investigated the motion of flood waves due to an instantaneous dam-break in order to provide data on unsteady, two-dimensional flows in open channels in dry and wet bed conditions. In order to produce a two-dimensional effect in subcritical and supercritical flows, a converging-diverging flume configuration was chosen. A flat bottom, vertical side walls, and mild side wall contractions and expansions were used to avoid three-dimensional flow effects. An instantaneous rising gate which was operated manually was used to simulate dam failure. Bed conditions were applied in the form of both dry and wet on the downstream side of the dam using various bed slopes. To represent unsteady flow characteristics, it was decided to measure the water depths and static pressures with respect to time at various cross-sections along the centerline flow of the flume so as to avoid side boundary layer effects.

Figures 2.2. and 2.3. demonstrate the comparison between numerical the scheme developed by MacCormack (1969) (which is a two-step explicit scheme with second-order accuracy) and experimental measurements of the stage hydrographs under a dry bed condition at various locations along the flume with two different bottom slopes (S_0^x). In order to illustrate the gravitational force effect, it was decided to use a series of experiments with various bed slopes in dry bed conditions. For the upstream and downstream of the flume, which had subcritical and supercritical flow regimes, respectively, comparisons between the computed and measured results were in good agreement and were well predicted. As expected, the flood routing was faster with high bottom slopes in dry bed conditions. The idea behind the testing of the geometric flume was to understand the physical flow characteristics and produce two-dimensional subcritical and supercritical unsteady flow regimes that could be adequately described by a numerical approach.

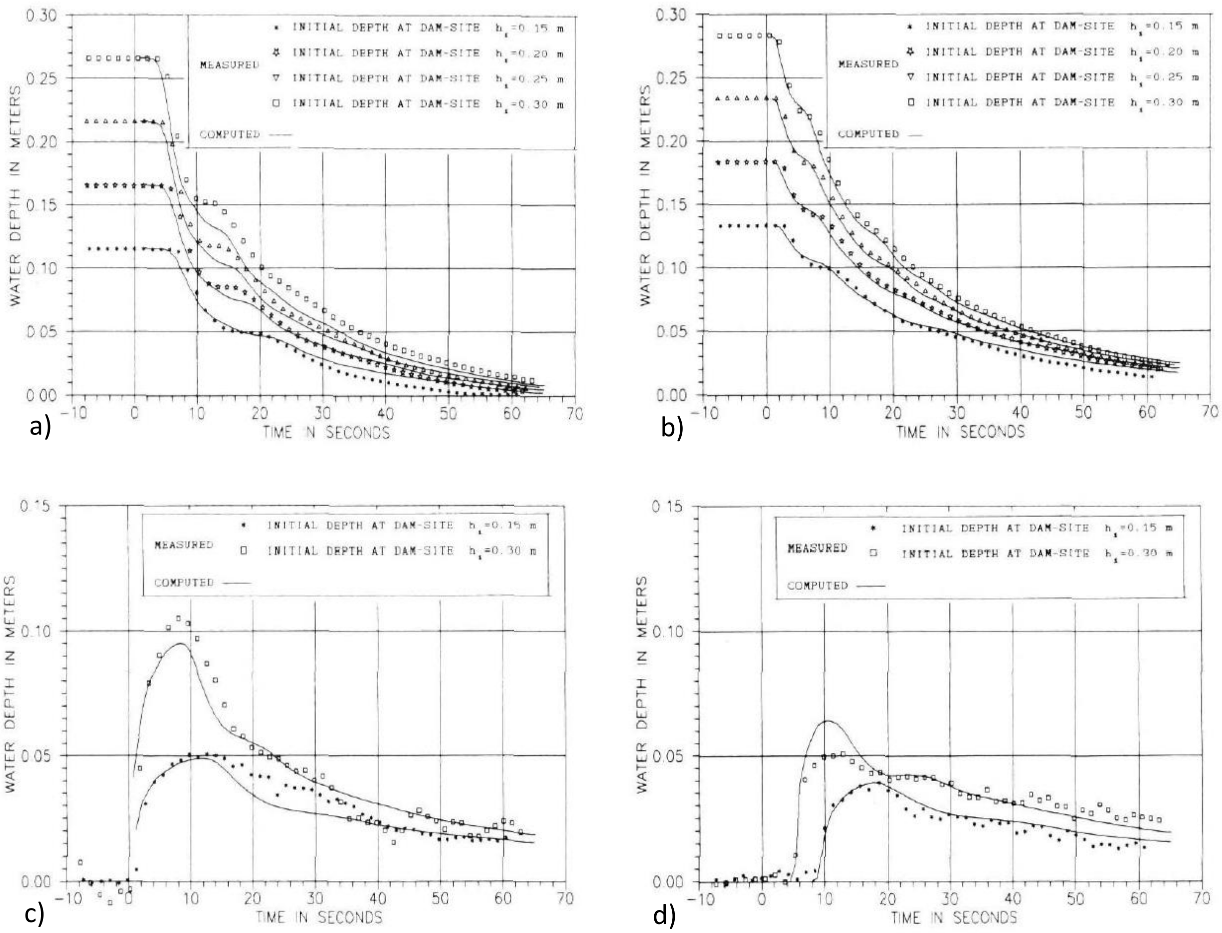

Figure 2.2. Comparison between predicted and measured water levels at (a) $x = -8.5\ m$, $S_0^x = 0.004$; (b) $x = -4.0\ m$, $S_0^x = 0.004$; (c) $x = +2.5\ m$, $S_0^x = 0.004$; and (d) $x = +10\ m$, $S_0^x = 0.004$ (presented by Bellos et al., 1992)

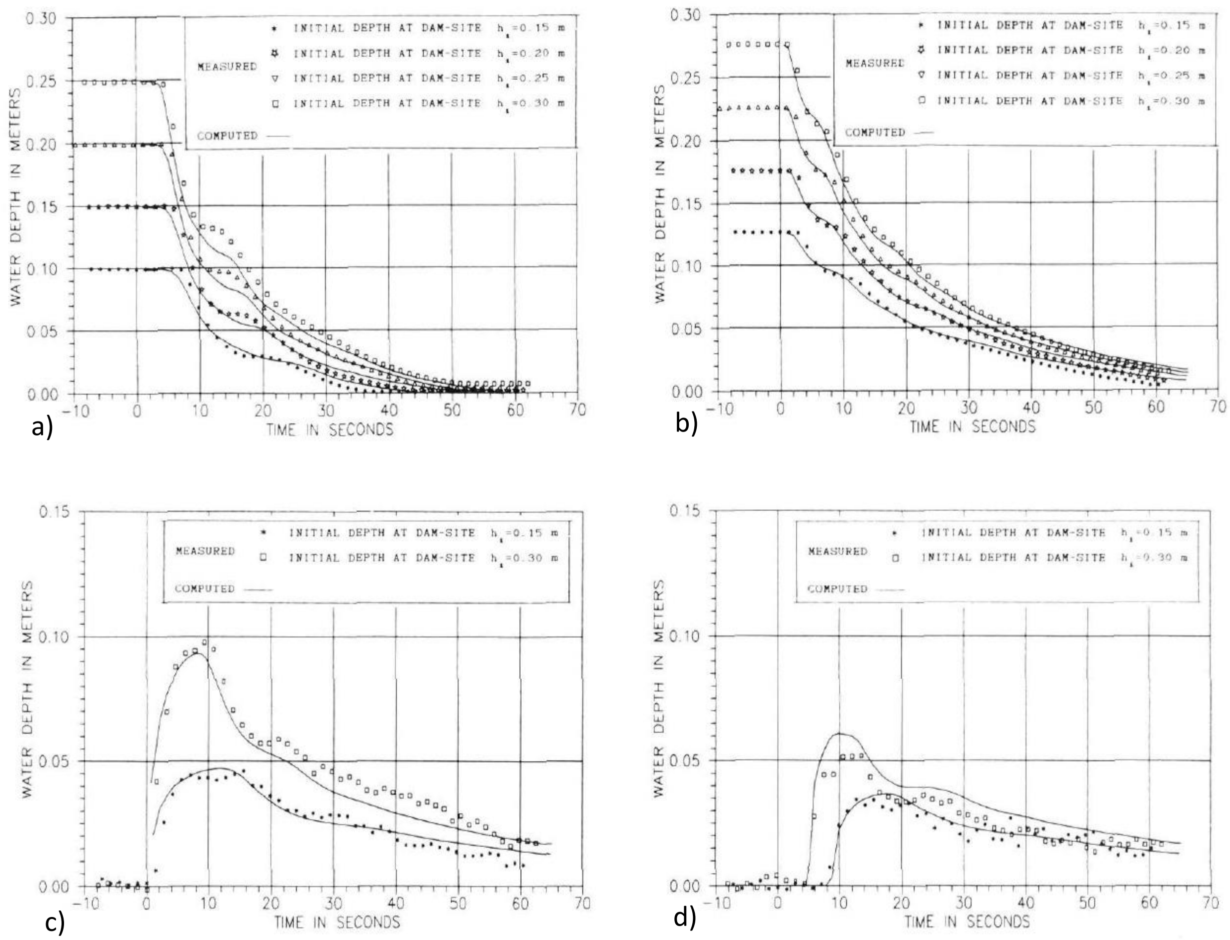

Figure 2.3. Comparison between predicted and measured water levels at (a) $x = -8.5\ m$, $S_0^x = 0.006$; (b) $x = -4.0\ m$, $S_0^x = 0.006$; (c) $x = +2.5\ m$, $S_0^x = 0.006$; and (d) $x = +10\ m$, $S_0^x = 0.006$ (presented by Bellos et al., 1992)

LaRocque et al. (2013) investigated two-dimensional dam-break flows to experimentally and numerically measure the flow depths and velocity profiles along a rectangular channel. The objectives of the research were to measure the spatio-temporal evolution of the water surface and velocity upstream and downstream of the flooded areas, simulate the problem numerically, and compare the results of the numerical models with the measured data. The experiments were carried out in a smooth wooden flume 7.31 m long, 0.18 m wide, and 0.42 m deep with a bottom slope of 0.93% that was coated with several water-resistant paint layers. A wooden plate located 3.37 m from the upstream end of the flume was lifted suddenly to simulate dam failure. A total number of

24 tests were conducted with single probes installed at eight locations upstream and downstream of the gate and with three reservoir water elevations of 0.25, 0.3, and 0.35 m.

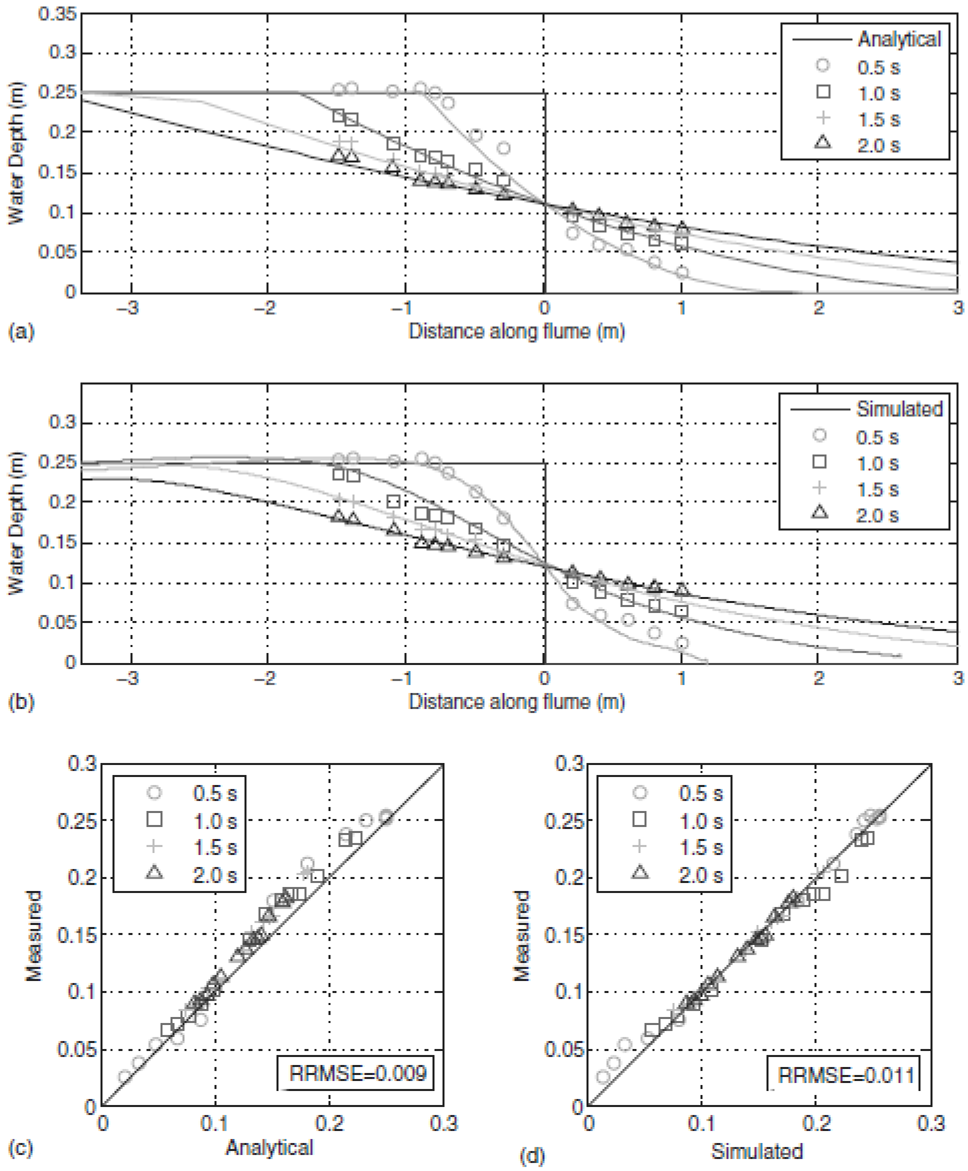

Figure 2.4. Comparison of water depth between the (a) analytical solution (Chanson 2006); and (b) the numerical simulation and experimental data (LaRocque et al., 2013)

A commercial CFD package, FLUENT, which was based on the volume of fluid (VOF) method to track the dam-break flow along the entire channel, was used to perform the numerical simulations.

As an initial condition, the volumes of fluids at rest were defined at the upstream of the gate as the reservoir, while the downstream of the gate was initially dry. For the boundary conditions, the upstream and bottom boundaries were set as walls, and the downstream and top boundaries were defined as pressure outlets. A system of uniform meshes in the x and y directions was used with sizes of 0.01 and 0.005 m, respectively. The Large Eddy Simulation (LES) turbulence approach was used to solve the Reynolds-averaged conservation equations.

The analytical, experimental, and numerical results for the water depth at various times for the upstream reservoir head of 0.25 m were compared and are provided in Figure 2.4. The analytical solutions for the water surface profiles with time along the length of the channel were described by the following equation (Chanson, 2006):

$$\frac{d}{D} = \frac{1}{9}\left(2 + \frac{1}{2}\sqrt{\frac{g}{D}}S_0 t - \frac{x}{t\sqrt{gD}}\right)^2 \tag{2.1}$$

where $d(x,t) =$ water depth; $D =$ initial reservoir depth; $x =$ distance from the dam; $t =$ time; and $S_0 =$ bed slope. Equation (1) is valid for the following range:

$$-1 \leq \frac{x}{t\sqrt{gD}} \leq 2 + \frac{1}{2}\sqrt{\frac{g}{D}}S_0 t \tag{2.2}$$

The comparison showed that both the numerical and analytical solutions were able to adequately predict the flow depth at 0.5, 1.0, 1.5, and 2.0 s after the gate removal. However, at t=1.0 s, t=1.5 s, and t=2.0 s, the numerical simulation performed better with the experimental data compared to the analytical solution. The root mean square error data are provided in figures 2.4 (c) and (d) for the analytical and numerical results, respectively. LaRocque et al. (2013) concluded that the numerical simulation with the LES turbulence model was able to predict the behaviour of the dam-break flow with good agreement. They also found that the downstream velocity profile was affected significantly due to the turbulence modelling, while upstream of the dam, the turbulence modelling did not affect the velocity profile.

2.3. The initial stages of dam-break waves

In 1998, Stansby et al. carried out an experimental study to investigate the initial stages of dam-break flows in a horizontal rectangular channel. The experiments were conducted in a flume with a horizontal bed 15.24 m long, 0.4 m wide, and 0.4 m high (Figure 2.5). The dam gate was in the form of a metal plate which was attached to a 7 kg weight by a wire rope. Quasi-instantaneous dam-breaks were simulated by releasing the weight from 0.8 m above the floor. The experiments were conducted for two various upstream reservoir water depths of 0.1 m and 0.36 m and three downstream tailwater depths giving depth ratios of 0, 0.1, and 0.45.

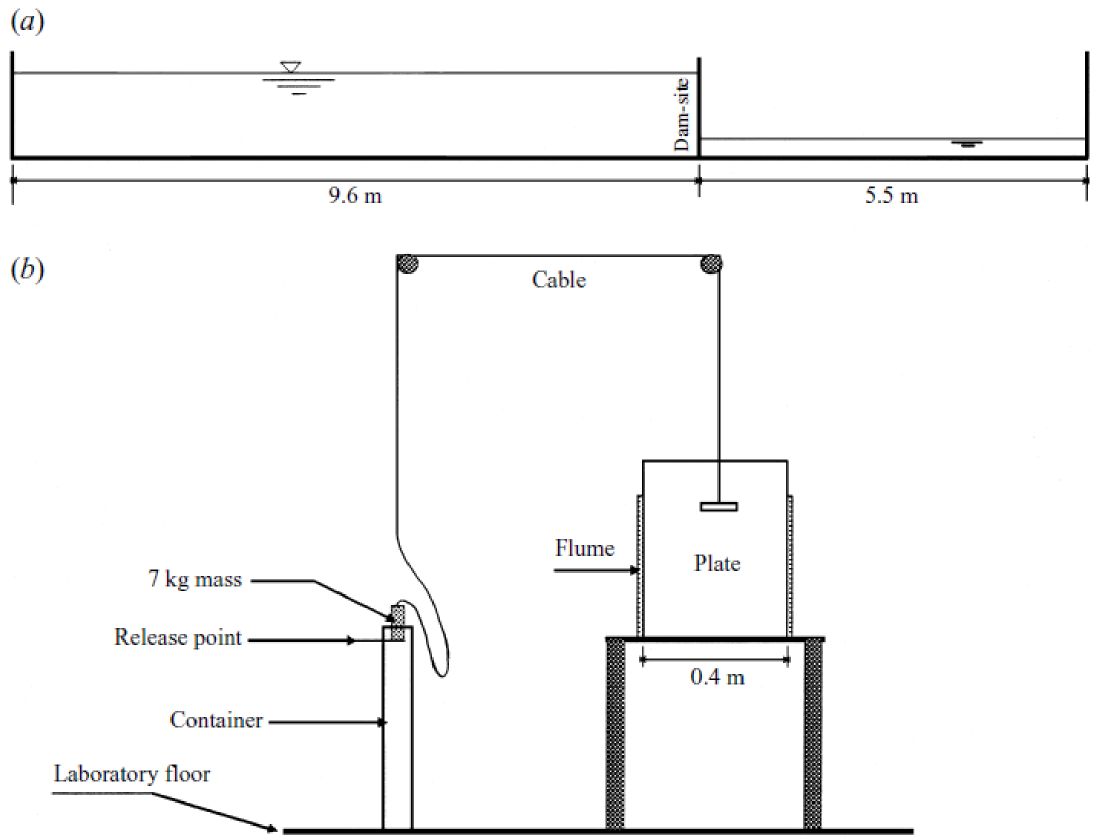

Figure 2.5. Experimental setup: (a) side view; (b) pulley/weight system (Stansby et al., 1998)

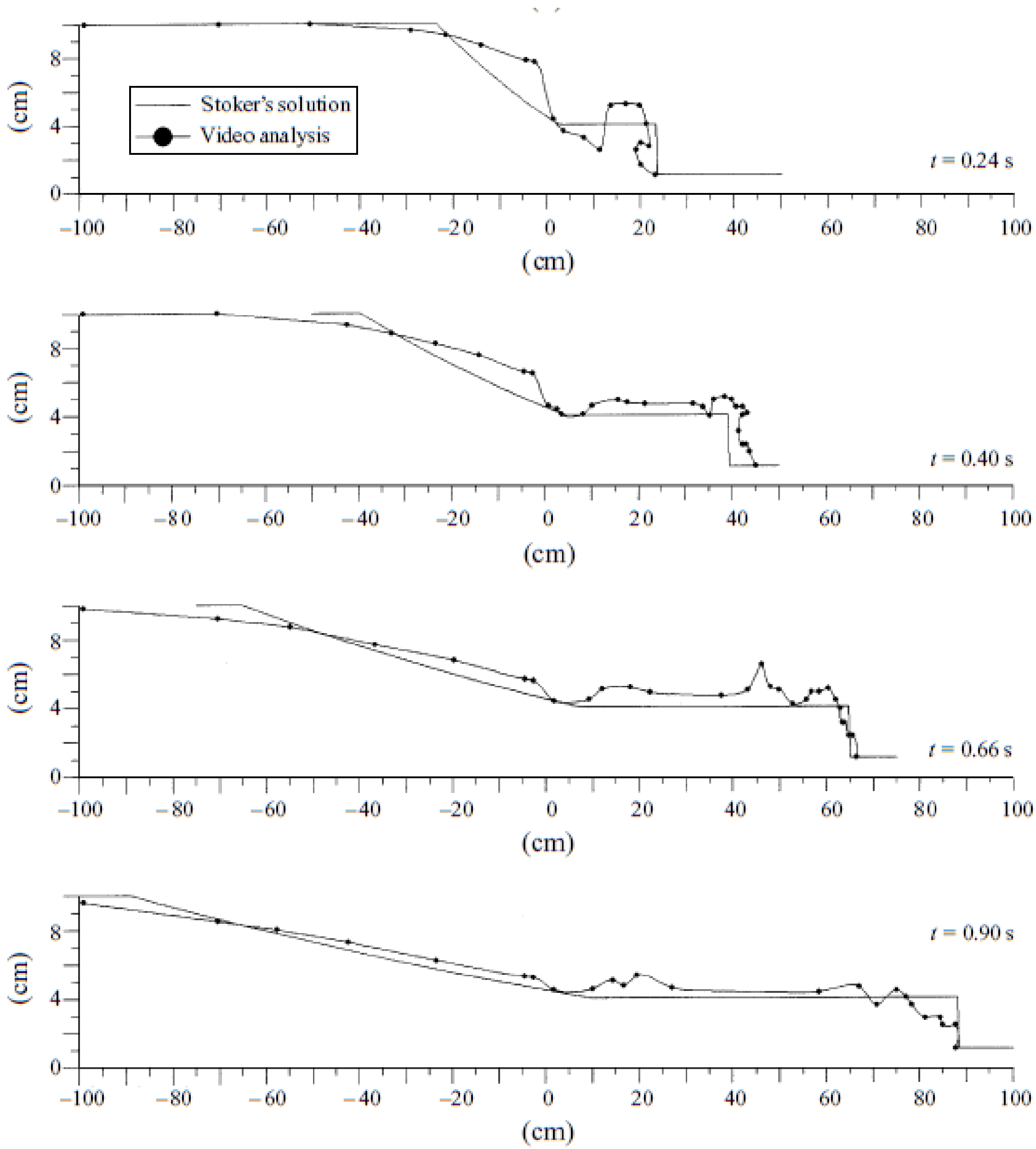

Figure 2.6. Comparison of free surface profiles between experimental results and analytical solution under wet bed condition with a depth ratio of 0.1 (Stansby et al., 1998)

The experimental results demonstrated that a horizontal jet and a vertical, mushroom-like jet were formed after the gate removal under downstream dry and wet bed conditions, respectively. Stansby et al. (1998) found that the vertical mushroom-like jet occurred in the wet bed condition due to the interaction between the upstream reservoir water and the downstream tailwater. In addition, their experimental results were compared to Stoker's (1957) analytical solution with shallow water equations (Figure 2.6). The comparison illustrated that the analytical solution was not able to accurately simulate dam-break flows in both the dry and wet bed conditions, specifically during the initial stages. The differences between the experimental results and analytical solution resulted from the assumption that the pressure was hydrostatic and the velocity uniform over depth. As time passes, however, the analytical solution adequately simulates the dam-break waves compared to measured data.

In 2010, Cagatay and Kocaman studied and compared the initial flow propagation of the dam-break problem both experimentally and numerically. The experiments were conducted using a rectangular horizontal channel made of glass (Figure 2.7). In order to simulate dam-breaks, a mechanism including a plastic plate (for the dam gate), a steel rope, pulleys, and a weight of 15 kg was used. The dam-breaks were modelled by releasing the weight from 1.50 m above the floor, which caused a sudden (between 0.06 and 0.08 s) removal of the dam gate. As the initial condition, a constant reservoir water depth ($h_0 = 0.25$ m) was chosen. A total of three experimental tests with various downstream bed conditions were carried out, with one dry bed and two different wet bed conditions ($h_1 = 0.025$ and 0.10 m). Digital image processing was used to capture the free surface profile via a system of three cameras, a computer, and a frame-grabber card.

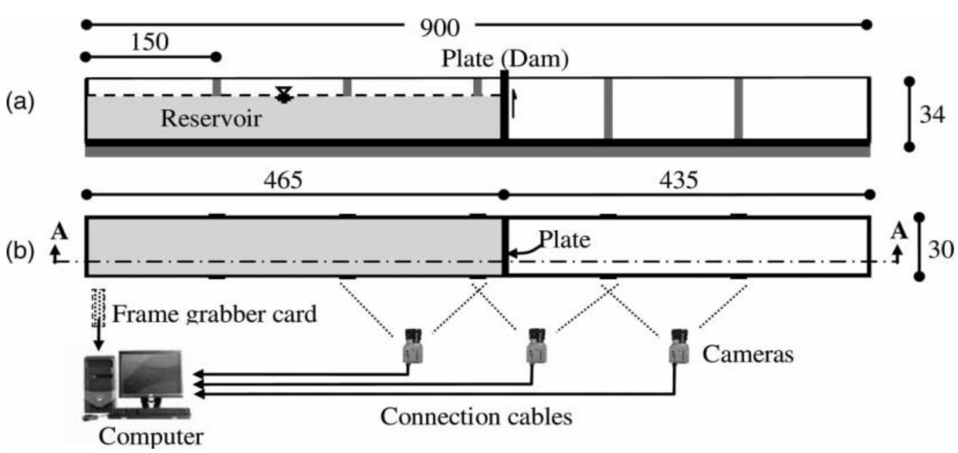

Figure 2.7. Experimental setup: (a) section A-A; (b) Plan, Length in (cm) (Cagatay and Kocaman, 2010)

For the numerical simulation, a commercial CFD program (Flow-3D) was used to compare the experimental results with the numerical ones. Reynolds-averaged Navier-Stokes (RANS) equations with the standard $k - \varepsilon$ turbulence closure model and shallow water equations (SWE) were used as the solvers of the numerical model. Figure 2.8 illustrates the qualitative comparison between the experimental and numerical results. In spite of some disagreement between the experimental and numerical results during the early stage of dam-break caused by the friction of the bottom bed in the dry bed condition, Cagatay and Kocaman (2010) concluded that both numerical models predicted the initial stages of the dam-breaks reasonably and accurately.

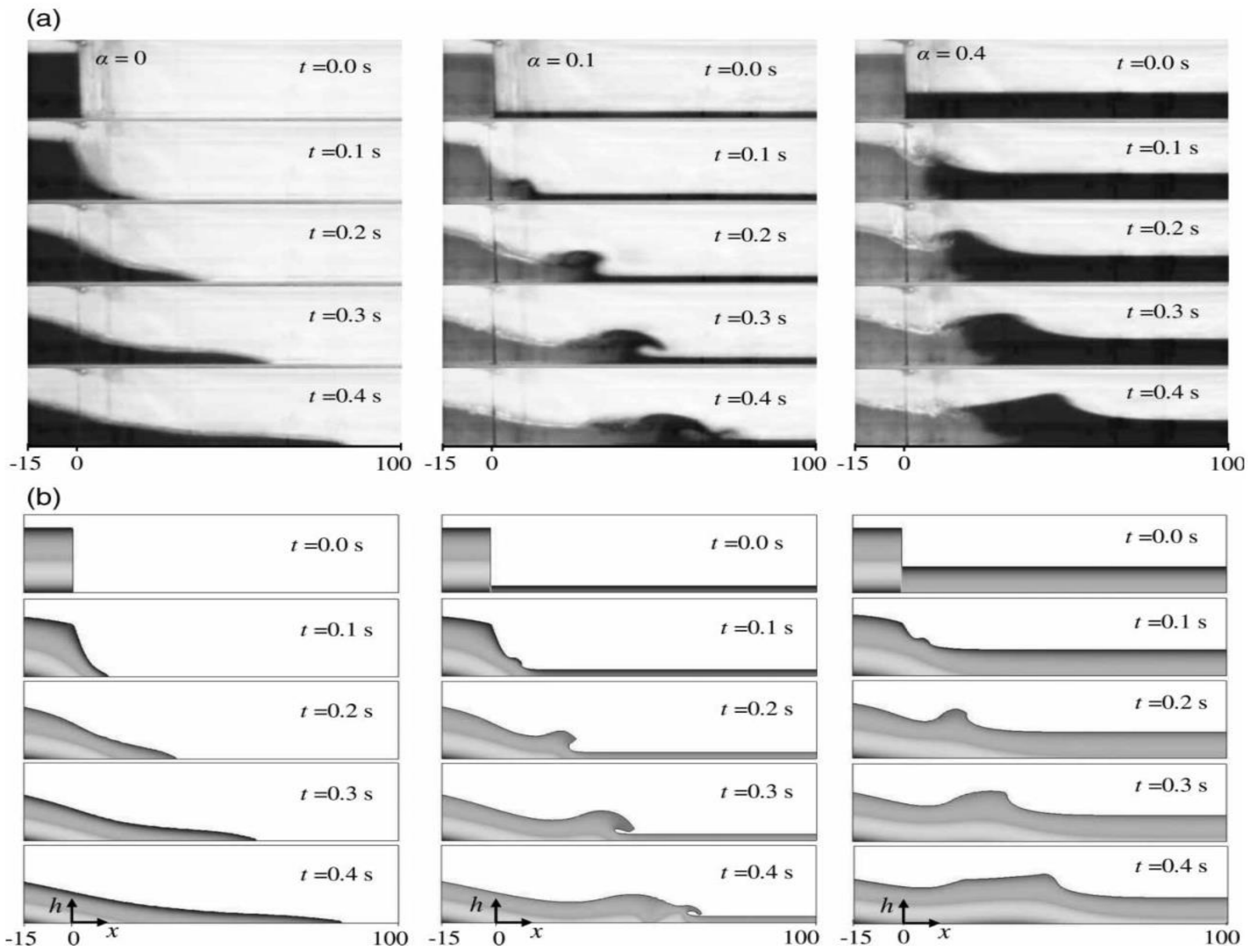

Figure 2.8. Evolution of free surface profiles: (a) Measured; and (b) RANS computed, α = depth ratio (h_1= downstream tailwater depth / h_0= reservoir water depth) (Cagatay and Kocaman, 2010)

2.4. Dam-break flow in presence of an obstacle

An experimental and numerical investigation of dam-break waves in the presence of an obstacle in a horizontal rectangular flume was performed by Cagatay and Kocaman (2011). In order to study the effect of abrupt channel bottom variations on dam-break flow propagation and the formation and evolution of a negative bore in the upstream direction behind an obstacle, an experiment was carried out in an initially dry-bed rectangular channel over a trapezoidal bottom sill (Figure 2.9). To model the dam-breaks, the dam's gate was removed instantaneously by releasing a weight from 1.5 m above the floor. Using digital image processing including three CCD cameras, a computer, and a frame grabber, the free surface profiles were recorded without repetition of the experiment and flow disturbances.

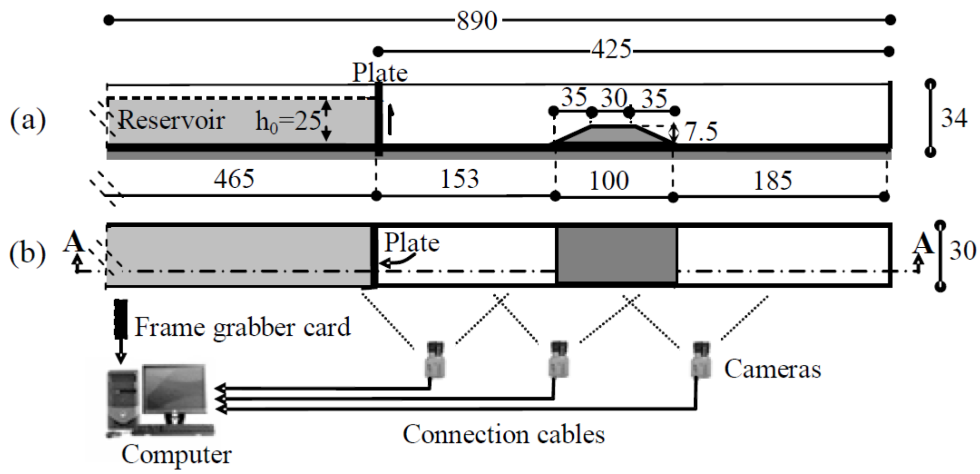

Figure 2.9. Test arrangement: (a) section A-A; and (b) plan view, length in cm (Cagatay and Kocaman, 2011).

In order to simulate dam-break waves numerically, the VOF-based available CFD program Flow-3D was used to solve Reynolds-Averaged Navier-Stokes (RANS) equations with the standard $k-\varepsilon$ turbulence model and the Shallow Water Equations (SWEs). Fixed rectangular cells of various sizes were used for the computational mesh. The mesh sizes were chosen as 2, 5, and 20 mm in both the lateral and longitudinal directions in order to analyze the mesh sensitivity.

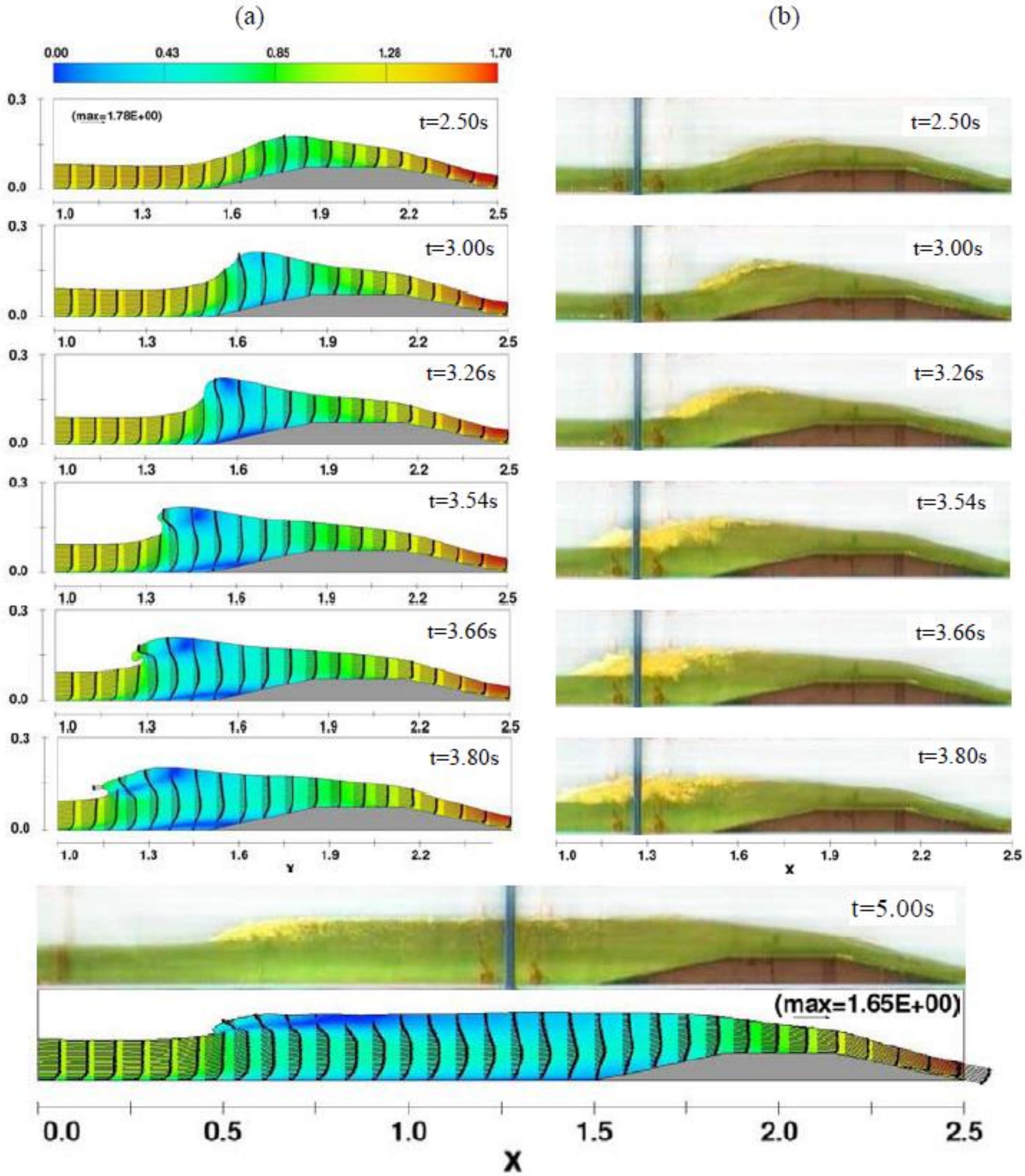

Figure 2.10. Negative wave evolution: (a) CFD RANS simulation; and (b) measured data (Cagatay and Kocaman, 2011)

The experimental and CFD simulation results of the flow patterns and propagation of the negative bore after the gate's removal are shown in Figure 2.10. When the flow reaches the obstacle, a part of the flow moves forward up to the hump, while the other part is reflected and propagates in the upstream direction. One of the obvious differences between the measured and computed results is in the various types of the reflected wave front. The experiments illustrate a spilling-type wave-breaking, while the numerical results demonstrate a plunging-type wave-breaking. The RANS simulations are in a good agreement with experimental data at most stages in predicting the velocity of the reflected wave fronts and the free surface profiles.

Cagatay and Kocaman (2014) conducted research to investigate dam-break flood-wave propagation in a horizontal rectangular channel with a triangular-shaped bottom obstacle. The hump was placed 1.5 meters downstream from the dam gate in the initially dry bed condition in order to scrutinize the effect of bottom slope and an abrupt change in channel geometry on dam-break flows. To model the dam-breaks, a vertical plate (dam gate) which was attached to the dam gate using a steel rope was removed suddenly by releasing a 15 kg weight from 1.5 m above the floor. A digital imaging system was used to define the water's free surface profile and water level variations with time. The advantage of using this system was in being able to visualize the flow characteristics along the entire flume without changing camera positions or repeating the tests.

In order to model dam-breaks numerically, simulations were carried out using the CFD commercial software package FLOW-3D. Two numerical solutions, including RANS with the standard $k - \varepsilon$ turbulence closure and SWE, were chosen to numerically simulate the dam-breaks. Figure 2.11 shows the computational domain of the RANS solution. To represent the dam reservoir, a 0.25 m-high and 4.65 m-long volume of fluid was used as the initial condition for the simulation. The upstream and bottom boundaries were chosen as walls, since there was no inflow to the flume. The downstream boundary was selected as the outflow. The upper boundary was set as a pressure outlet in order to consider the atmospheric pressure on the free surface. Also, the grid size for the uniform mesh was set at 5 mm in both directions ($\Delta x = \Delta z = 5\ mm$).

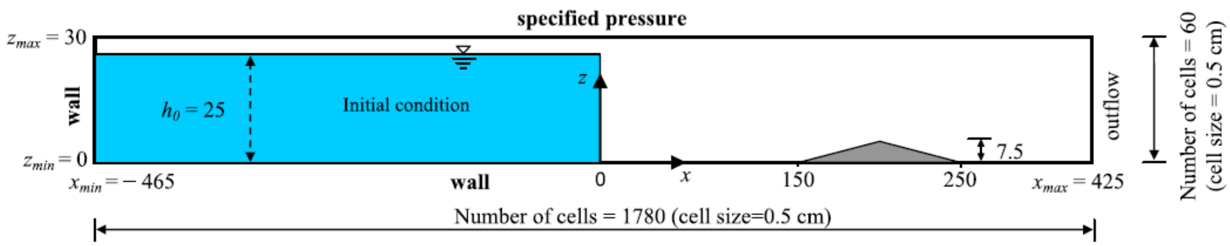

Figure 2.11. Geometry and boundary conditions of solution domain (RANS), dimensions in [cm] (Cagatay and Kocaman, 2014)

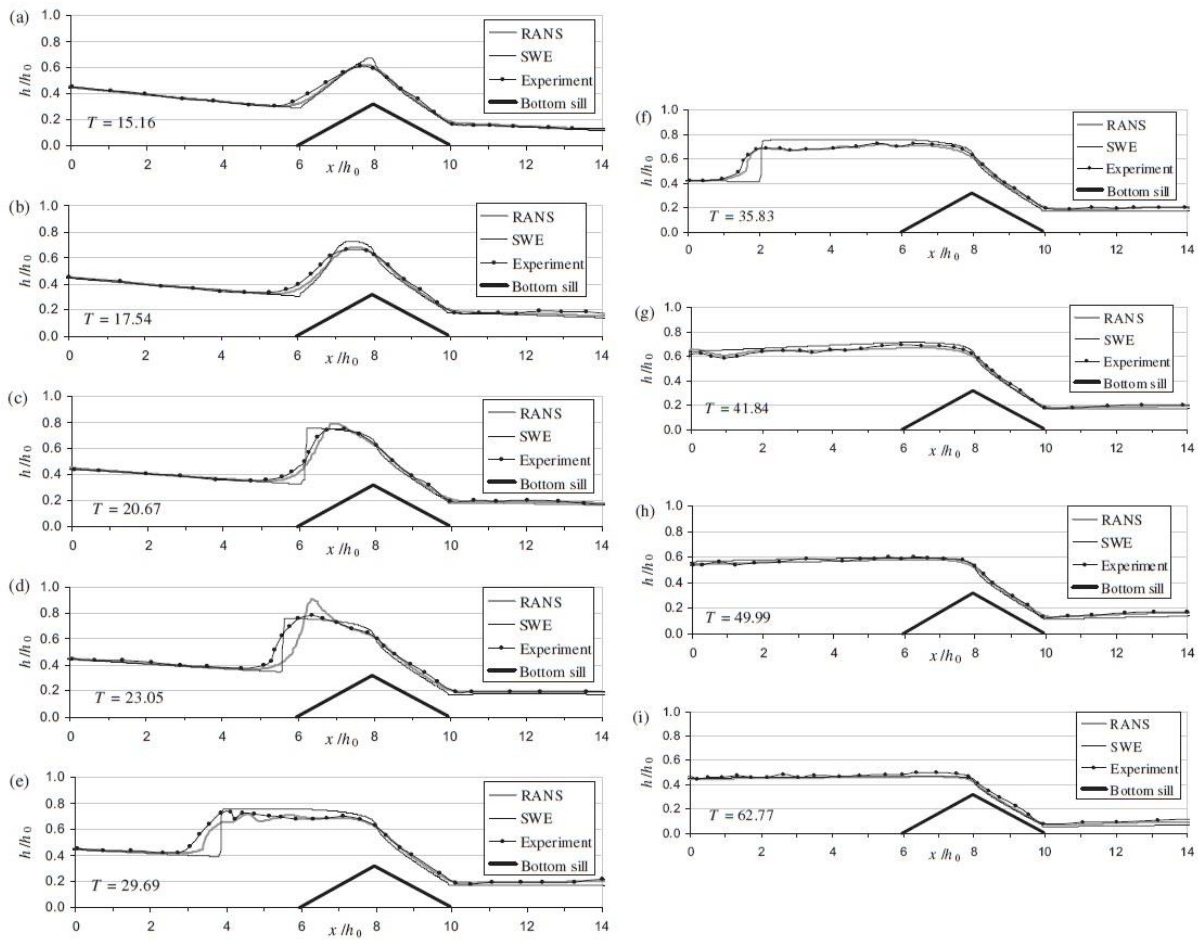

Figure 2.12. Experimental and numerical results of the free surface profile at different dimensionless time steps T=(a) 15.16, (b) 17.54, (c) 20.67, (d) 23.05, (e) 29.69, (f) 35.83, (g) 41.84, (h) 49.99, and (i) 62.77 (Cagatay and Kocaman, 2014)

The dam-break flows propagated over the dry bed after sudden removal of the dam gate. Figure 2.12 illustrates the comparison between the measured data and both sets of numerical results (RANS and SWE) for the free surface profile at various times. The presence of the obstacle resulted in a rise in water depth upstream of the hump and the creation of a negative bore, while flood waves were reflected against the hump. For most stages, RANS was able to predict the free surface profile and reproduce the velocity of the reflected waves with a reasonable agreement, while SWE showed discrepancies when reproducing the velocities and free surface profiles.

In 2015, Kocaman and Cagatay investigated the formation and propagation of dam-break reflected waves in the presence of a vertical wall at the downstream end of a rectangular horizontal flume over an initially wet bed condition with two different tailwater levels. A vertical plate was placed near the middle of the flume, dividing it in two parts: the first part represented the dam reservoir, and the second one represented the channel downstream with an initial wet bed condition (Figure 2.13). The dam-break flow was modelled by the sudden removal of the dam gate which was connected to a weight by a steel rope. By releasing the weight from 1.5 m above the floor, the dam gate was rapidly removed. The flow measurement was conducted in three steps by digital image processing including a computer, three CCD cameras, and a frame grabber: first the flow was recorded by high-speed cameras which were located at equal intervals, and the recorded flow was transferred to a computer using the frame grabber card. Then, the recorded images were calibrated and finally combined, providing a panoramic view of the entire channel without test repetitions (Figure 2.13).

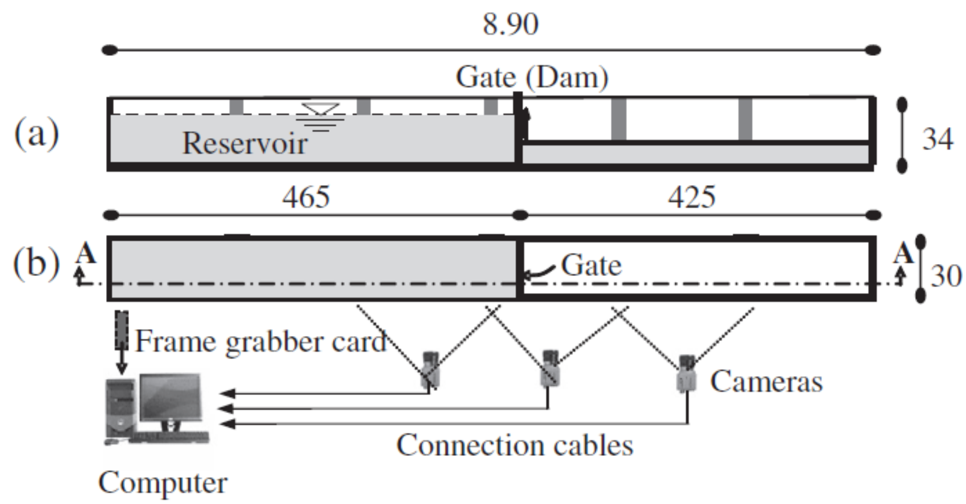

Figure 2.13. Experimental facility: (a) Section A-A; and (b) Plan view, lengths in cm (Kocaman and Cagatay, (2015)

FLOW-3D, which is a CFD package based on the Finite Volume Method, was used to simulate the dam-break reflected waves in the presence of a vertical wall. The solutions for the numerical model were chosen as RANS with the standard $k - \varepsilon$ turbulence closure to solve the governing mass and momentum equations for Newtonian incompressible fluid flows and SWE. The flume was filled with three various volumes of fluid for the upstream and downstream tailwaters, at 0.025 m and 0.10 m. As long as there were no inflows or outflows, the upstream and downstream boundaries were chosen as walls, and were installed with vertical steel gates. The top and bottom boundaries were set as symmetry and wall, respectively. All the channel surfaces were assumed to be smooth. A mesh of fixed rectangular cells with 5 mm sizes in both directions were applied in the computational domain.

Figure 2.14 illustrates the dam-break flow and reflected wave evolutions with time in the presence of a downstream vertical wall in shallow ($\alpha = depth\ ratio = \frac{tailwater\ depth}{reservoir\ depth} = 0.1$) and deep ($\alpha = 0.4$) tailwaters. In order to get a clear recognition of the reservoir and tailwater interactions along the entire channel, light (green) and dark (red) colours were chosen for the reservoir and tailwaters, respectively. Figures 2.14. (a) and (b) represent the formation and propagation of the dam-break flows and reflected waves, respectively. During the initial stages of the dam-break, after an instantaneous gate removal, the reservoir water dragged the tailwater due to gravity, and hence the wave front was broken and a jet was formed ($\alpha = 0.1$). However, the tailwater resisted the drag force of the reservoir water and forced the flow to move in a vertical direction for $\alpha = 0.4$.

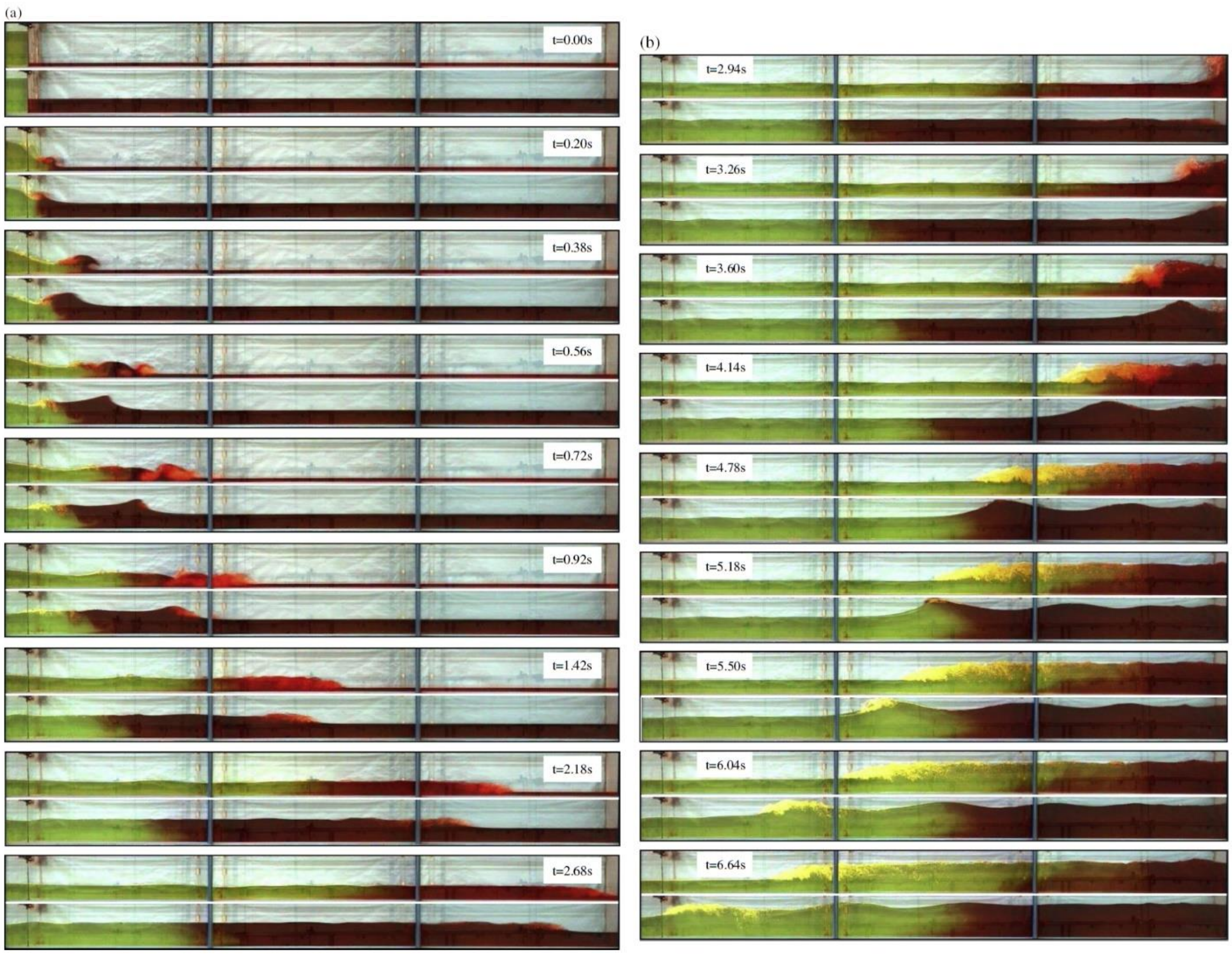

Figure 2.14. Experimental results of formation and propagation of: (a) the flood waves; and (b) the reflected waves with time in shallow and deep tailwaters (Kocaman and Cagatay, 2015)

According to Figure 2.14 (a), the wave front travel speed in the shallower wet bed condition ($\alpha = 0.1$) was much higher than that in the deep wet bed condition ($\alpha = 0.4$). When the flood wave for $\alpha = 0.1$ started to reflect against the vertical wall and move in the upstream direction ($t = 2.94\ s$), the flood waves for $\alpha = 0.4$ just arrived at the vertical wall. Despite the flooding waves, the travel speed of the reflected waves was much higher for $\alpha = 0.4$ than for $\alpha = 0.1$. To compare the numerical results with the experimental data, RANS was able to reproduce the reflected wave front and undulations on the free surface with a general good agreement for both depth ratios. However, SWE demonstrated some disagreements in predicting the reflected wave front for the lower depth ratio and for the undulations on the free surface for the high depth ratio.

2.5. Partial-breach dam-break flow

LaRocque et al. (2013) conducted research to numerically simulate the experiment by Fraccarollo and Toro (1995) in 3D in order to study laboratory-scale dam-break waves by using LES and $k - \varepsilon$ models for turbulence closure. Turbulence has a significant impact on near-field (i.e., initial stages) dam-break flows, which are mainly influenced by vertical acceleration due to gravity, and hence the hydrostatic pressure distribution is not valid. Despite their ability to predict dam-break flows, SWE models are not able to properly capture some hydraulic aspects. A set of comparisons between measured data and numerical results for water depth, bottom pressure, and depth-averaged velocity was done by LaRocque et al. (2013) in order to investigate the performance of various turbulence approaches.

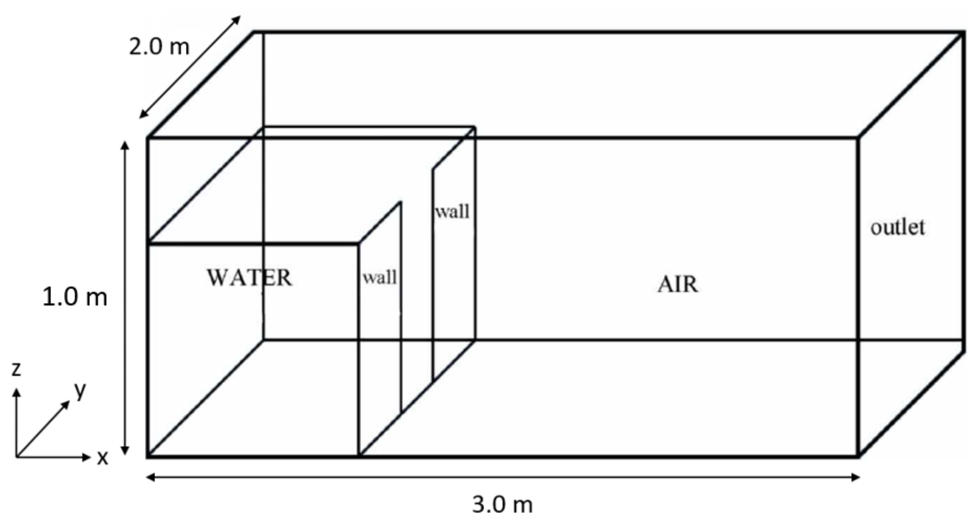

Figure 2.15. Schematic of the numerical model (LaRocque et al., 2013)

The numerical simulations were conducted using a rectangular horizontal tank 3.0 m long, 2.0 m wide, and 1.0 m high with an initially dry downstream bed (Figure 2.15). The upstream reservoir was filled with a volume of water 1.0 m long, 2.0 m wide, and 0.6 m high with a 0.4 m gate opening to reproduce partial dam-break flows. The grid size for the computational domain was uniform, with 3 cm × 4 cm in the x and y directions, respectively. In the vertical or z direction, a total number of 50 grids was defined with a near-bed size of 1 mm. The upstream, side walls, reservoir walls, and bottom boundary conditions were set as walls. The top and downstream boundaries were defined as pressure outlets. In order to investigate the performance of the numerical models, static pressures at the bottom of the flume as well as velocity components and water depths were compared with existing experimental data.

The dam-break flows passed through the dam gate opening and propagated in both the downstream and lateral directions after the instantaneous dam gate removal. During the initial stage of the partial dam-break, one part of the flood waves expanded downstream of the gate, while the other part reached and reflected against the sidewalls and then travelled towards the downstream end. The experimental and numerical results for the water depth at various locations downstream can be seen in Figure 2.16. Qualitative and quantitative comparison of the results demonstrated that both numerical modeling approaches were able to simulate partial dam-break flow characteristics with a reasonable agreement; however, the LES model performed better in reproducing experimental results such as fluctuations in temporal variations of water depth and velocity compared to the $k-\varepsilon$ model.

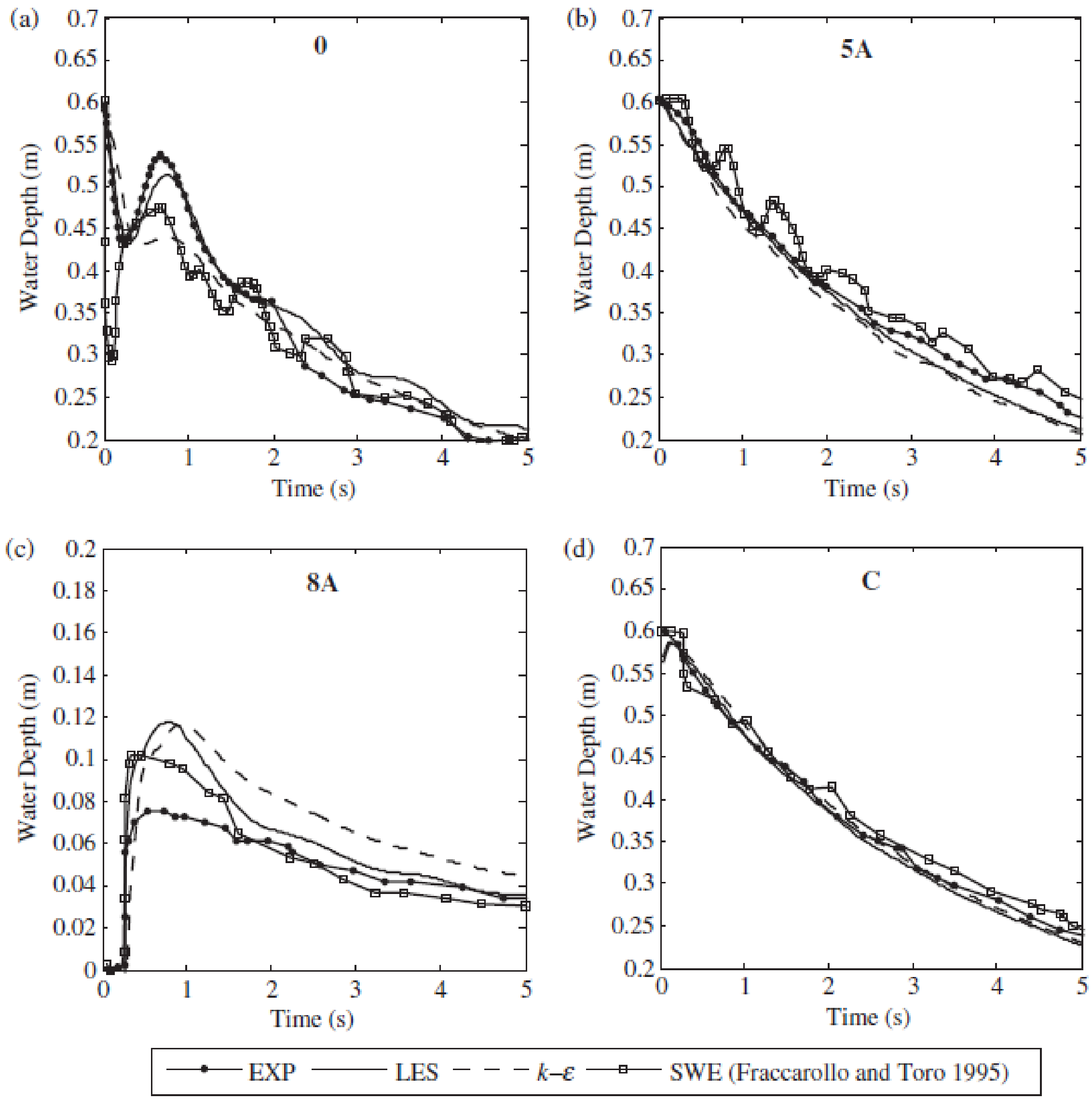

Figure 2.16. Comparison between measured (Fraccarollo and Toro, 1995) and simulated (LaRocque et al., 2013) water depths at 4 positions

In 2010, Biscarini et al. presented a study investigating dam-break free-surface flows numerically by comparing the SWE approach to fully three-dimensional (RANS) simulations based on the Volume of Fluid method. The comparisons between the numerical, experimental, and analytical results were carried out in three test cases in order to validate and investigate the performance of the numerical models. The cases were: 1. a dam break over a dry bed without friction (Fennema and Chaundry, 1990); 2. a dam break over a triangular bottom sill (Soarez, 2002); and 3. a dam break flow over a 90° bend (Soarez Frazao and Zech, 2002). The objective was to highlight the differences and compare one- or two-dimensional shallow water approaches with a fully three-dimensional Reynolds-averaged Navier-Stokes approach.

In their results, Biscarini et al. (2010) found that both numerical approaches were able to reproduce dam-break flow characteristics such as flow depth and arrival time in various situations with a reasonable agreement. However, by comparing the results of the first test case, the water free surface in the RANS model was respectively lower and higher compared to that in the SW model immediately downstream and upstream of the dam gate. Also, the water travelled much faster in the two-dimensional SW model compared to three-dimensional RANS model. Furthermore, the results of the second and third test cases demonstrated that the SW model was not able to properly reproduce flow depth profiles and wave front velocity, while the three-dimensional RANS model performed quite well in representing the unsteady flow characteristics.

2.6. Dam-break waves over channels with varying topography

In 2012, Kocaman and Cagatay conducted some experiments to investigate and better understand dam-break flows and the formation and propagation of negative waves resulting from the presence of a lateral triangular-shaped channel contraction over a horizontal rectangular flume with an initial dry bed condition. A schematic and plan view of the test arrangement are shown in Figure 2.17. A plate was located near the middle of the flume to separate the channel upstream, which was filled with water to represent the dam reservoir, while the channel downstream was initially dry. To reproduce lateral contraction, two symmetrical triangular-shaped sidewalls were placed in the channel downstream. A mechanism was set up to simulate a dam-break flow by lifting the dam gate instantaneously. In order to capture the experimental data, digital image processing with three CCD cameras was used. This technique allowed the authors to determine the continuous free surface profiles along the entire channel without test repetitions.

To simulate dam-break flows numerically and to solve continuity and Reynolds-averaged Navier-Stokes equations, FLOW-3D, which is a commercial CFD program, was used. Among the various turbulence closure approaches, the standard $k - \varepsilon$ turbulence closure was chosen to determine the turbulence viscosity. For the solution domain, the longitudinal centre line was considered as the symmetry axis because the lateral contraction was symmetrical and only half of the channel, which was 8.9 m long, 0.15 wide, and 0.3 m high, was modelled. As long as there was no inflow to the channel, the upstream and bottom boundaries were set as walls. The downstream boundary was chosen as the outflow, since the channel downstream was initially dry. The computational domain consisted of about 3.2 million square cells of 5 mm in size in all directions.

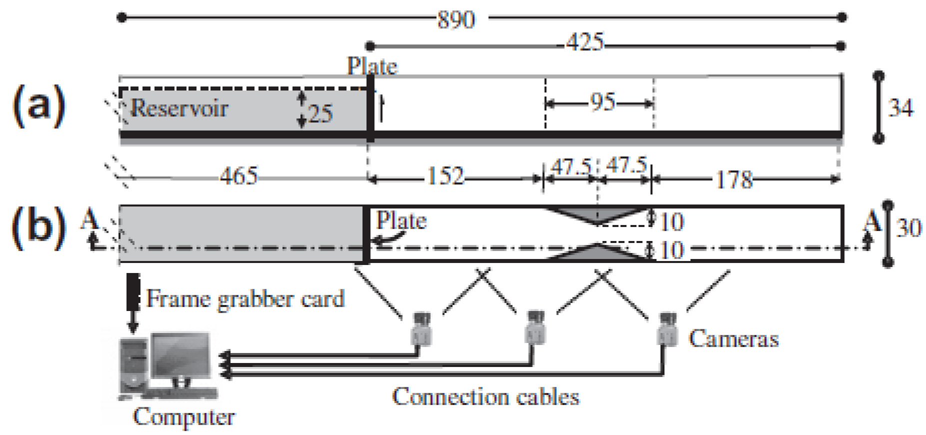

Figure 2.17. Experimental facility: (a) section A–A; and (b) plan, lengths in (cm) (Kocaman and Cagatay, 2012)

After sudden removal of the dam gate, flooding waves formed and moved towards the lateral contraction. When the dam-break flow reached the contraction, one part of the flow passed through the narrowest part of the channel while the other part jammed on the upstream side of the contraction, and the water level rapidly increased. Meanwhile, dam-break waves reflected against the contraction, and hence a negative bore formed and started to travel in the upstream direction. The rising water level and occurrence of the hydraulic jump, and hence the formation and propagation of the negative bore, can be explained by the conversion of the kinetic energy to potential energy and the transition of the flow regime between subcritical to supercritical, and vice versa when the flood waves passed through the lateral contraction.

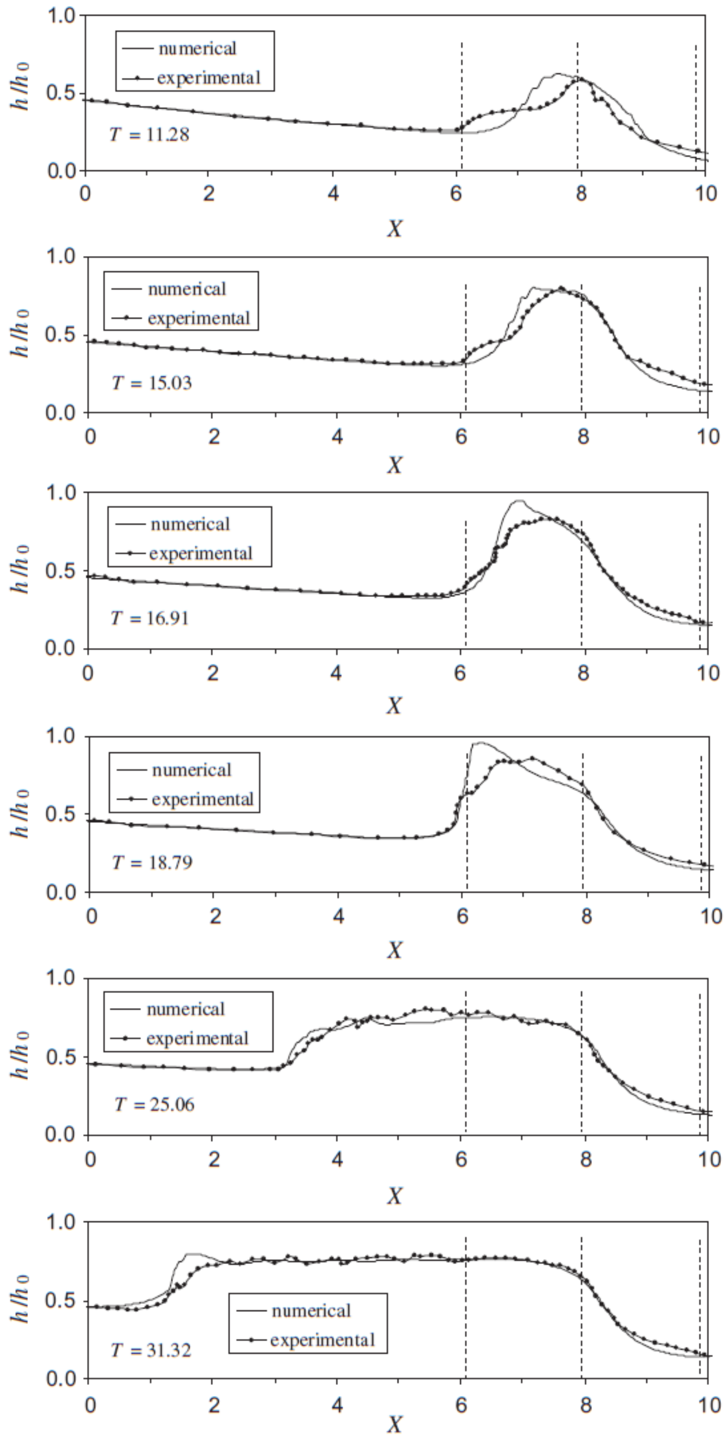

Figure 2.18. Comparison between measured data and numerical results for free surface profiles at various times (Kocaman and Cagatay, 2012)

Figure 2.18 illustrates a comparison of the free surface profile results for the measured data and the three-dimensional numerical simulation based on the RANS approach. There was a satisfactory agreement in reproducing dam-break waves in a channel with a local contraction; however, there were some discrepancies in predicting the magnitudes and locations of the maximum water levels, specifically upstream of the narrowest section of the channel.

Kocaman and Cagatay (2015) also conducted research to investigate the formation and propagation of dam-break flows and reflected waves in an initially dry bed channel with a varying cross-section. Symmetrical, trapezoidal-shaped obstructions were placed on both downstream sidewalls of the rectangular horizontal channel to create an abrupt contraction in the channel's cross-section (Figure 2.19). The dam-break was modelled by a sudden gate removal using a mechanism including dam gate, rope, and a weight. Instantaneous gate removal was achieved by releasing the weight, which was attached to the gate by the rope, from 1.5 m above the floor. Digital image processing, which is an advance measuring technique, was used to obtain continuous free surface profiles and the time evolution of the water level through the entire flume without any test repetition.

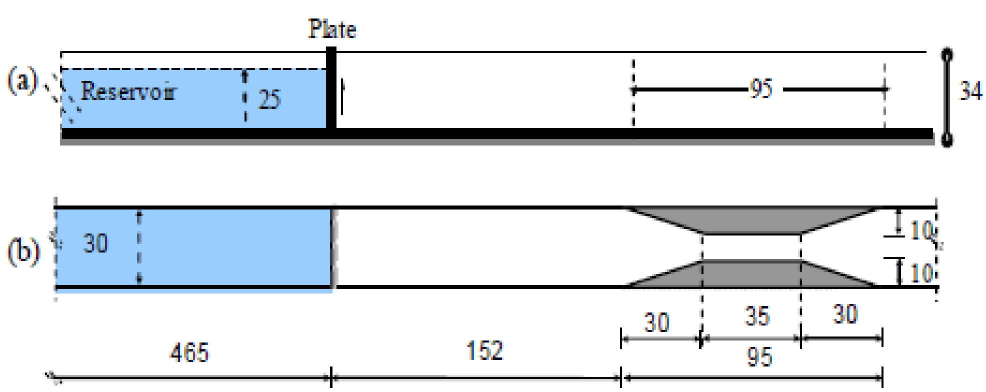

Figure 2.19. Experimental setup: (a) Section view; and (b) plan view, lengths in cm (Kocaman and Cagatay, 2015)

In order to simulate the dam-break flow numerically, FLOW-3D, which is VOF-based CFD commercial software based on the Finite Volume Method, was used. The RANS solution for the numerical model was chosen in order to solve the continuity and momentum equations with the standard $k - \varepsilon$ turbulence closure. For the initial condition, a volume of fluid with no inflow was defined as the dam reservoir. The upstream, bottom, and side wall boundaries were set as walls, since there was no inflow to the flume. The downstream boundary was chosen as the outflow to keep the channel end open. The top boundary was set as symmetry to consider the atmospheric pressure on the free surface. All the channel surfaces and obstacles were assumed as smooth.

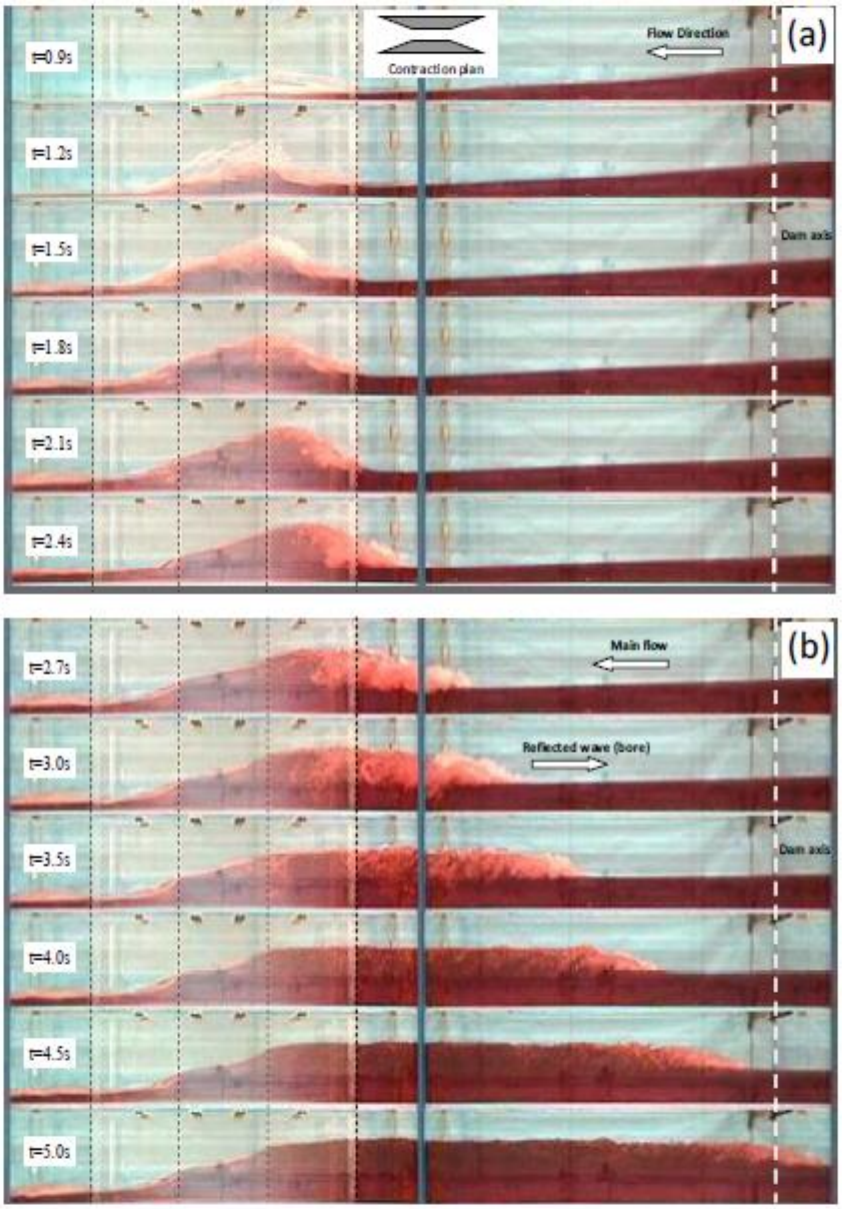

Figure 2.20. (a) Formation of negative bore; and (b) Propagation of reflected wave (Kocaman and Cagatay, 2015)

Dam-break waves moved through the channel after the instantaneous gate removal. A part of the flow was reflected and moved in the upstream direction once it reached the channel contraction, while the other parts passed the channel contraction and traveled in the downstream direction. Figure 2.20 shows the formation and propagation of the reflected waves through the horizontal rectangular flume. The white and black dashed lines represent the dam gate and local contraction locations, respectively. A significant hydraulic jump formed at the entrance of the local contraction, resulting in a rapid rise in water levels and the formation and propagation of a negative bore just upstream of the contraction. The flood waves reflected and propagated in the upstream direction because the specific energy of the flood wave was lower that the minimum energy necessary to pass through the contraction region.

2.7. Reservoir geometry impacts on dam-break flows

A series of comprehensive experimental studies was conducted by Feizi Khankandi et al. (2012) to investigate and assess the effects of reservoir geometry and initial upstream depth on the propagation of dam-break flows. Dam-break flow characteristics such as water free-surface profiles, velocity components, and maximum discharge were investigated experimentally under both downstream dry and wet bed conditions. Four different reservoir shapes, including wide, long, trapezoid-shaped, and one with a 90° bend were considered for the experimental setups (Figure 2.21). The dam-breaks were simulated by the instantaneous removal of a plate by using a pneumatic jack. The gate opening time was about 0.14 s, which satisfied the instantaneous gate opening time criterion provided by Vischer and Hager (1998) (i.e., a gate opening time less than 0.23 s).

The experimental results for the water surface profiles were compared to Ritter's (1892) analytical solution, and Feizi Khankandi et al. (2012) concluded that the experimental results for the water level variations for the long and 90°-bend reservoirs were close to Ritter's analytical solution in the dry bed condition (Figure 2.22). However, there were notable discrepancies in the comparison between the experimental results and the analytical solution for the trapezoidal and wide reservoirs. This was because of the presence of 2D effects due to the flow constrictions at the channel entrance for the wide and trapezoidal reservoirs, while the flow was 1D for the long the 90°-bend reservoirs. It was also concluded that the highest velocity components, maximum discharge values, and severe cross-wave propagation were observed in the experiments with the wide reservoir geometry compared to the other reservoir shapes.

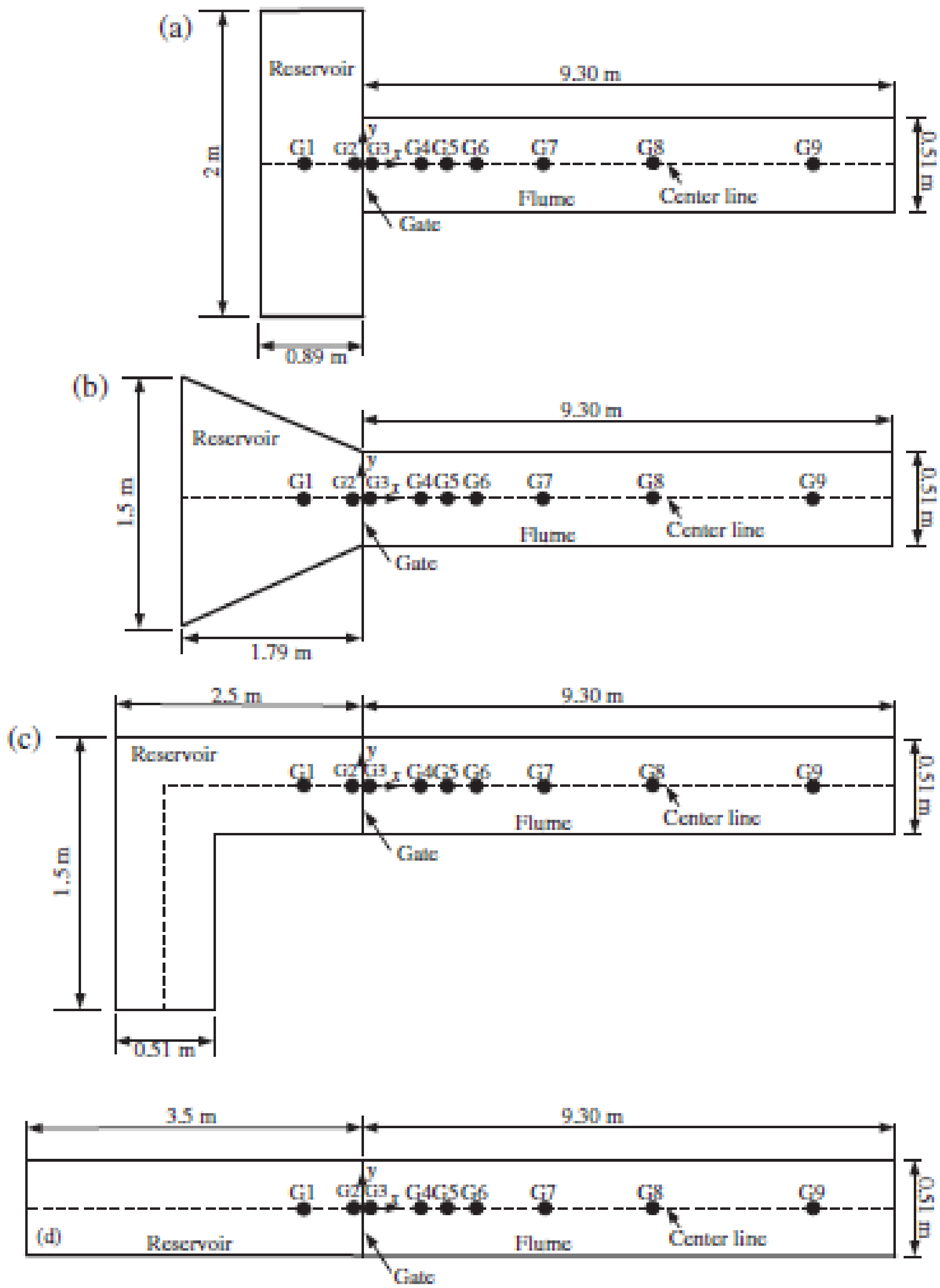

Figure 2.21. Various reservoir geometry: (a) wide, (b) trapezoidal, (c) 90° bend, and (d) long reservoirs (Feizi Khankandi et al., 2012)

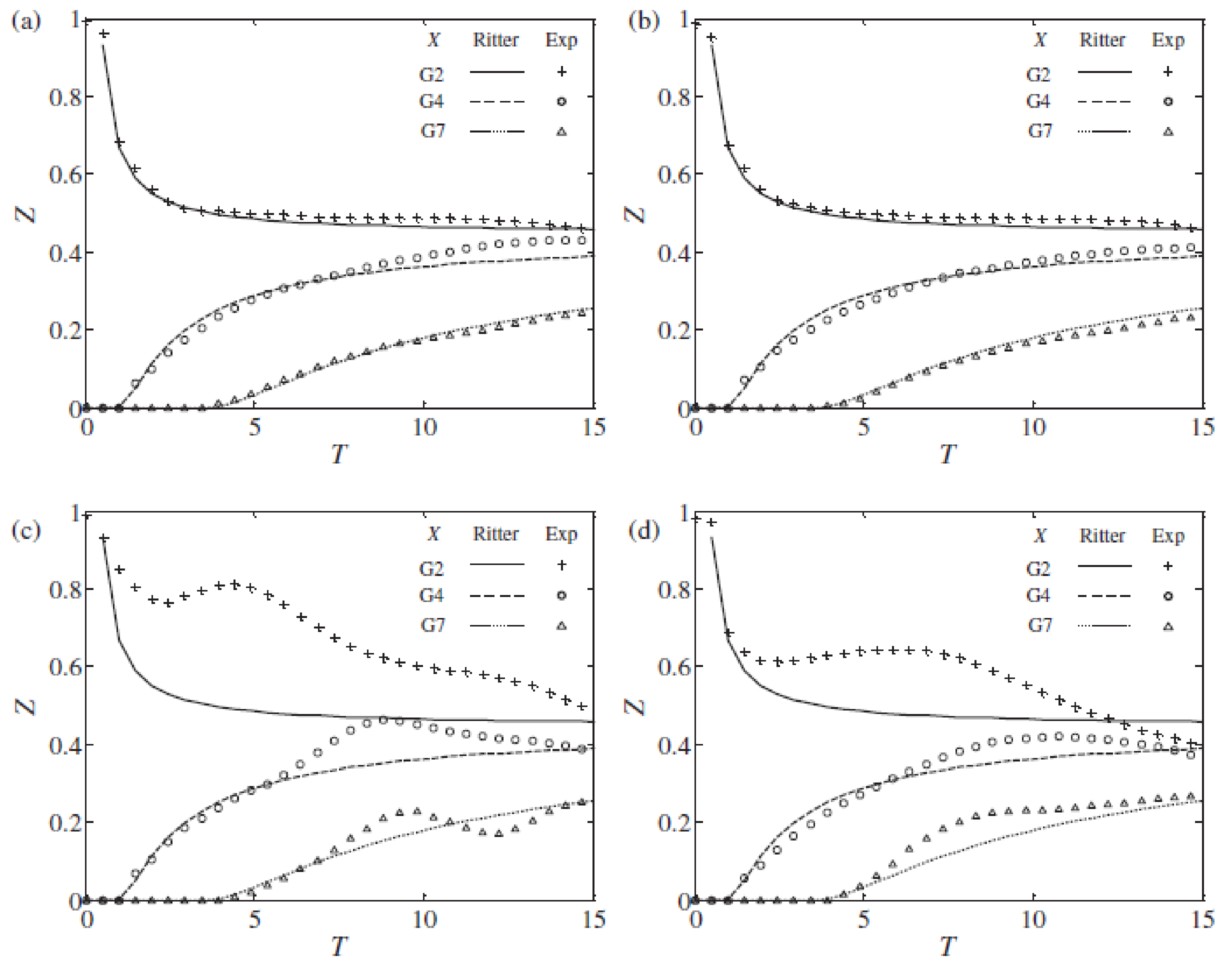

Figure 2.22. Comparison between experimental results and analytical solution of temporal water levels for different reservoir shapes: (a) 90° bend, (b) long, (c) wide, and (d) trapezoidal reservoirs (Feizi Khankandi et al., 2012)

In 2017, Liu et al. conducted a series of hydraulic experiments involving dam-break flows in order to investigate the variations of free surface profiles and flow velocities in an open channel under both downstream dry and wet bed conditions. The influence of water head settings, upstream reservoir lengths, and downstream water depths on the movement of dam-break flows were also investigated. A horizontal rectangular flume 6.5 m long and 0.4 m wide was used to perform the laboratory experiments (Figure 2.23). A steel plate representing the dam gate was placed 1.5 m from the upstream end, and to investigate the influence of reservoir length, another steel plate was installed 0.75 m upstream of the dam gate in some experiments. To measure the water levels and flow velocities, two specific locations were defined: one immediately downstream of the gate (0.15 m) to capture the initial stages of dam-break, and one far from the gate (1.5 m) where the flow becomes steady and stable.

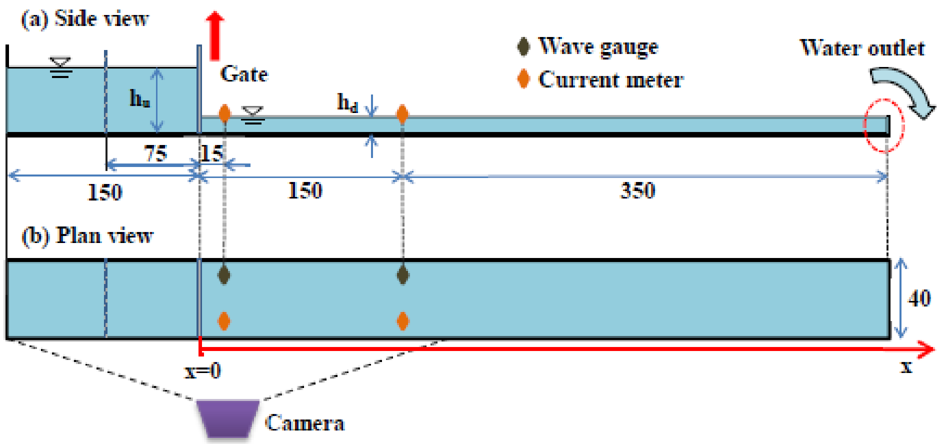

Figure 2.23. Hydraulic experimental setup: (a) side view, (b) plan view (Liu et al., 2017)

Froude and Reynolds numbers are some of the dimensionless parameters to validate models when considering gravity and viscous effects. Liu et al. (2017) mentioned that the Froude number was more important in such validations because dam-break flow characteristics is dominated by gravity rather than viscosity. Further, it was concluded that the water surface profile and flow velocity showed significant differences between the dry and wet downstream bed conditions, even when keeping the reservoir head constant. The temporal water level results at immediately after the gate illustrated that only one peak occurred under the dry bed condition, while there were two peaks for the wet bed condition due to the interaction of the reservoir water with the downstream tailwater (Figure 2.24). Moreover, the flow velocity was lower under the wet bed condition with deeper tailwater than that under the wet bed condition with shallower tailwater (Figure 2.24). It was also concluded that the water level and velocity variations were influenced by increasing the upstream reservoir length while keeping the reservoir volume of water the same.

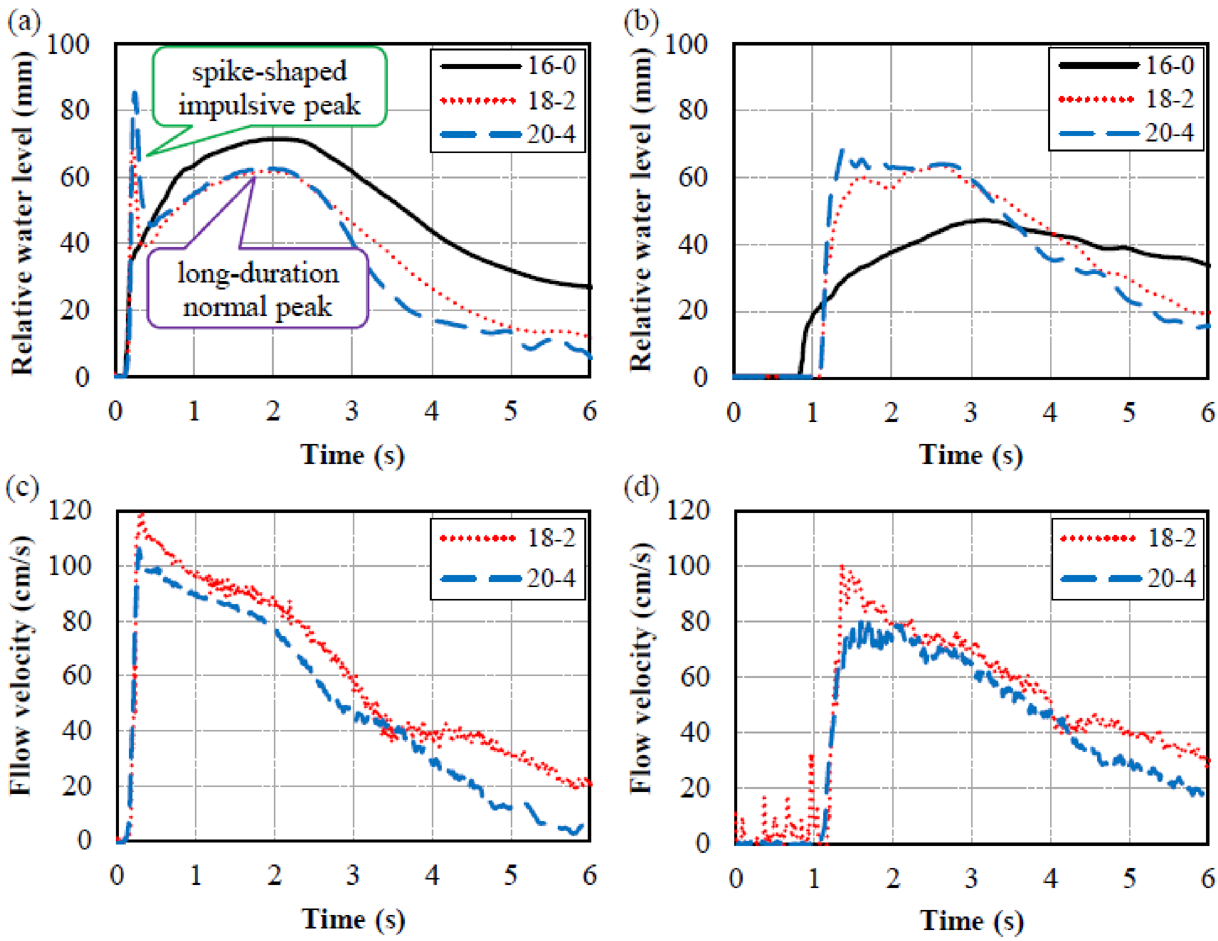

Figure 2.24. Water level evolution (a and b) and velocity evolution (c and d) with time at 0.15 m (left graphs) and 1.5 m downstream of the gate (Liu et al., 2017)

2.8. Numerical Studies on dam-break waves

The accurate estimation of dam-break flow characteristics such as arrival time, free surface profile, velocity, and pressure distribution is essential in order to reduce dam-break flood wave damage. Consequently, numerical modelling was employed to simulate complex dam-break flows and flood wave behaviour with detailed spatial and temporal gradients. In 2004, Shigematsu et al. conducted a numerical study to investigate dam-break flood waves during the initial stage. The COBRAS (Conell Breaking-Waves and Structures) numerical model, which was developed by Lin and Liu (1998) and is based on the Reynolds-Averaged Navier-Stokes (RANS) equations with the $k - \varepsilon$

turbulence model, was used for the numerical simulations. To track the free surface, the volume of fluid method was employed on the COBRAS model.

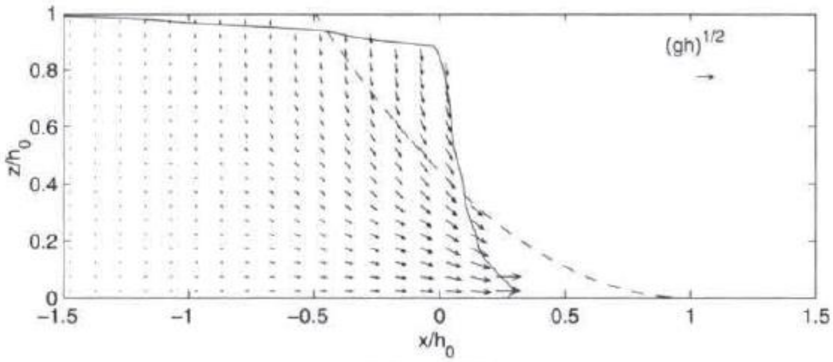

(a) $t_* = 0.5$

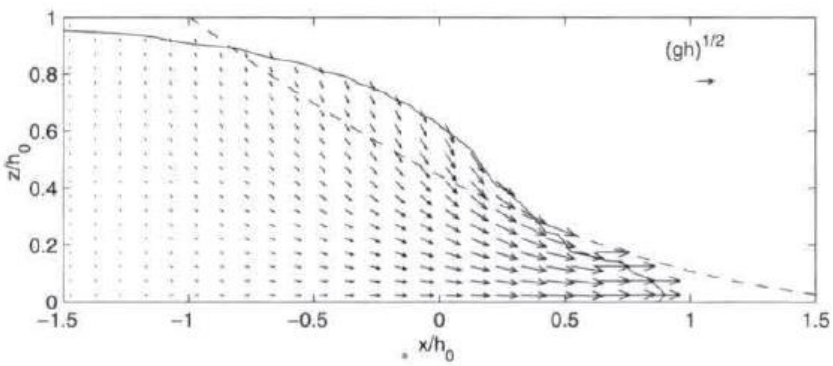

(b) $t_* = 1.0$

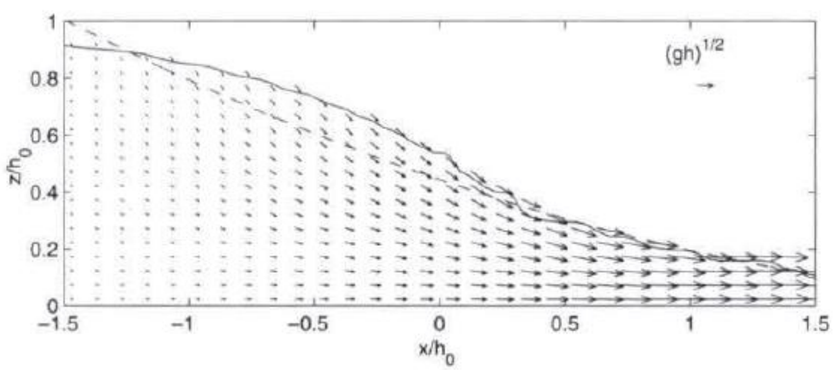

(c) $t_* = 1.5$

Figure 2.25. Numerical results for the velocity distribution at various times (Shigematsu et al., 2004)

The numerical results were compared with available experimental data and analytical solutions, and comparison of the numerical results and the analytical solution (Ritter, 1892) showed that theoretical assumptions of hydrostatic pressure and ignoring the vertical velocity components are not valid during the initial stages of a dam-break. Figure 2.25 illustrated the existence of significant vertical velocity components at the top of the dam-break wave when a dam gate was removed instantaneously. However, when compared to the experimental data, it was concluded that the COBRAS model adequately simulated complex dam-break flows under both downstream dry and wet bed conditions.

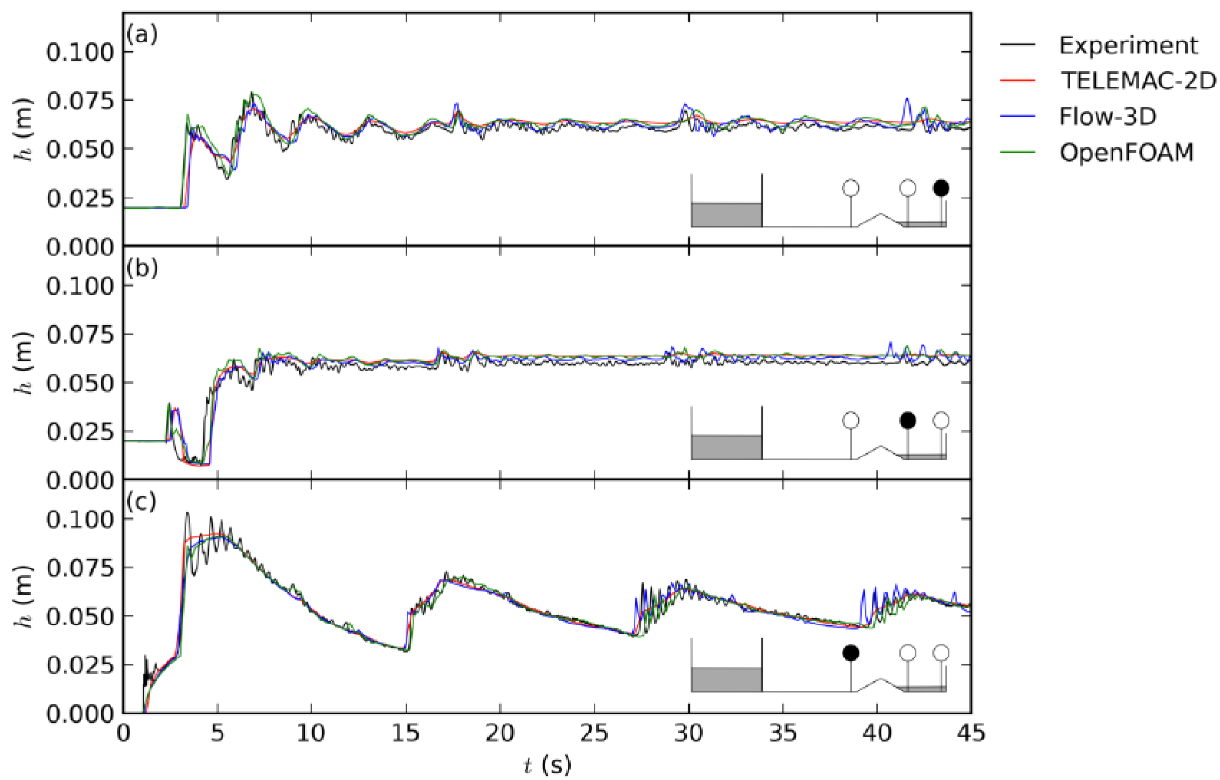

Figure 2.26. Comparison between computed and measured results of water level evolution at two locations upstream and one location downstream of the bottom sill (Robb and Vasquez, 2015)

Robb and Vasques (2015) studied the performance of three numerical models in reproducing dam-break flows in the presence of obstacles. Sudden dam-break flows in the presence of a triangular bottom sill obstacle over an initially dry bed condition and the impact of dam-break flows on an isolated downstream obstacle were numerically investigated. For the 2D numerical simulations, TELEMAC-2D, which is free and open-source code, was used to solve the two-dimensional shallow water equations. In the case of the 3D modeling, FLOW-3D, which is commercially available software, and OpenFOAM, which is open-source computational fluid dynamic code, were used to solve the 3D Reynolds-Averaged Navier-Stokes equations based on the VOF method. The RNG $k - \varepsilon$ turbulence model was applied for both of the 3D numerical simulations.

Robb and Vasquez (2015) found that all three numerical models were able to successfully simulate and reproduce dam-break flood waves in the presence of a downstream obstacle with a reasonable agreement (Figure 2.26). It was also concluded that 2D modelling was sufficient to capture the water depth; however, 3D numerical modeling performed better in investigating the initial stages of dam-break flows and the impact of flood waves on an obstacle because of the creation of vertical acceleration due to the water level increasing behind the obstacle.

Considering the rapid development of computational fluid dynamics, dam-break wave characteristics can be accurately simulated by CFD numerical models to determine the detailed fluctuation process with lower cost and higher efficiency compared to analytical solutions and experimental studies. Yang et al. (2018) conducted a series of systematic comparisons between analytical solutions, experimental data, and numerical simulations of the generation and propagation of dam-break waves under both dry bed and wet bed downstream conditions, and the calculation accuracy and efficiency of the numerical models were also investigated.

Two-dimensional numerical simulations were performed by Yang et al. (2018) using FLOW-3D, which is a commercial CFD package based on the volume of fluid method, to solve the Reynold-Averaged Navier-Stokes equations and Euler equations. The turbulent kinematic viscosity was calculated in the RANS numerical model by three different turbulence models: the standard $k - \varepsilon$, RNG $k - \varepsilon$, and $k - \omega$ turbulence models. The computational domain included about 150,000 grids with the size of 0.005 m in both the x and z directions. The upstream, downstream, and bottom boundaries were set as wall boundaries with a no-slip condition. The channel sidewall boundaries were set as symmetry, since the numerical model was two-dimensional. The top boundary was considered as a pressure boundary to account for the atmospheric pressure.

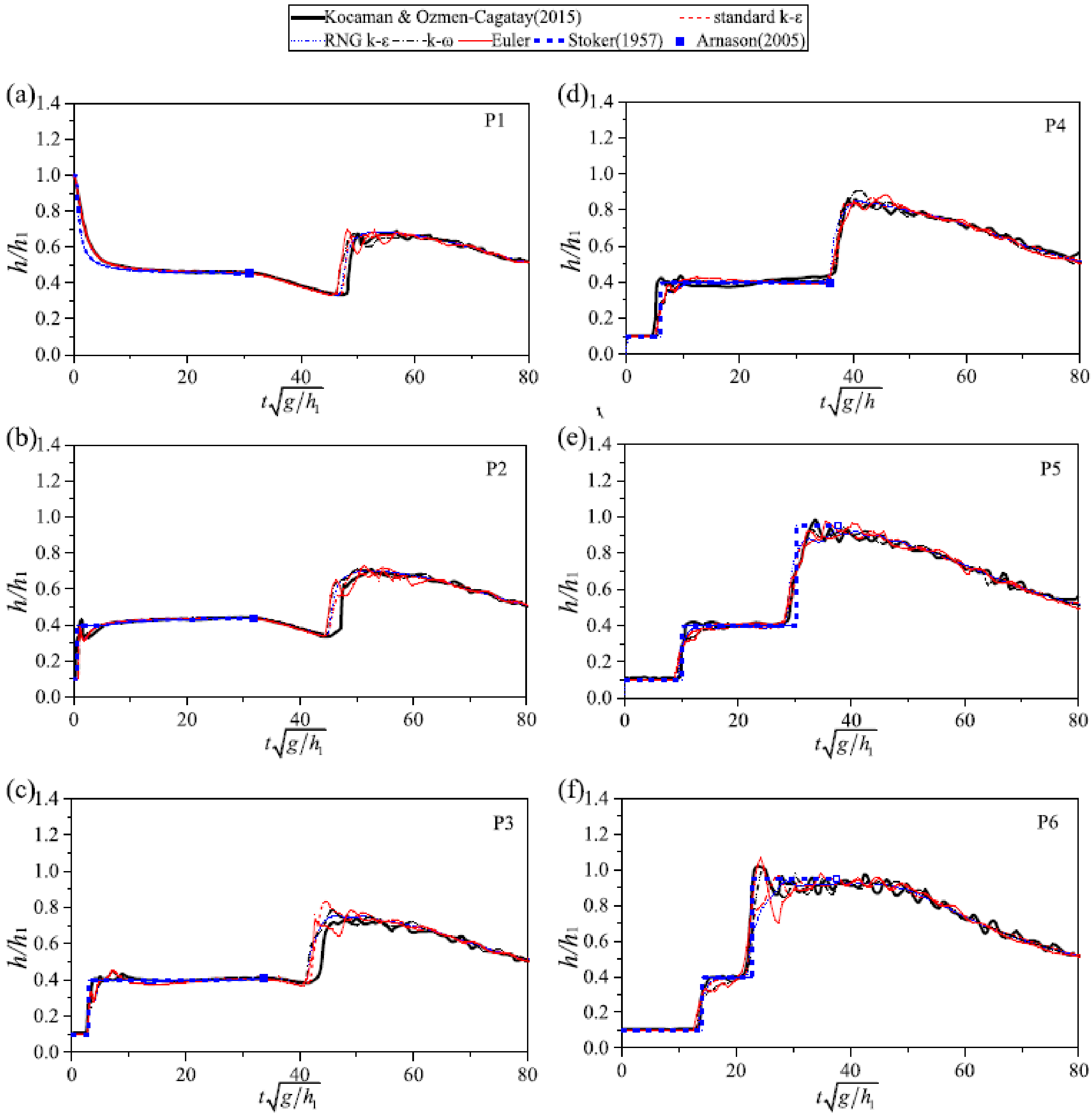

Figure 2.27. Wave height time history comparisons at various locations downstream and upstream of the dam gate over a wet bed condition (depth ratio 0.1) (Yang et al., 2018)

Yang et al. (2018) concluded that RANS simulations with the three classic turbulence models were able to reproduce the formation and propagation processes of dam-break waves accurately under dry and wet bed conditions (Figure 2.27). It was also found that the numerical results of the three turbulence models almost coincided over both the dry and wet bed conditions. However, there were some discrepancies in the numerical results for the maximum wave heights and arrival times compared to experimental data. Furthermore, the Euler equations performed reasonably well over the wet bed conditions while showing significant differences compared to the experimental data since they ignored water viscosity and turbulence.

Hu et al. (2018) performed numerical simulations to evaluate the capability and efficiency of 3D models by using a simplified 3D model, MIKE 3 FM, and a Flow-3D model to simulate dam-break flows. Various hydrodynamic parameters such as free surface profiles, water depth variations, and velocity evolution were investigated numerically for a dam-break under dry and wet bed conditions with various tailwater depths. To analyze and evaluate the accuracy and applicability of numerical models to simulate dam-break flows, the results of the simplified 3D SWE, detailed RANS model, and analytical solutions were compared with available experimental data.

The results of Ritter's (1892) analytical solution for dry bed conditions and Stoker's (1957) analytical solution for wet bed conditions were compared with the results of the three-dimensional numerical models. The Ritter's 1D analytical solution for an idealized dam failure under a dry frictionless bed condition can be expressed by:

$$h = \frac{1}{9g}\left[2(gh_0)^{1/2} - \frac{x}{t}\right]^2 \tag{2.3}$$

$$u = \frac{2}{3}\left[\frac{x}{t} + (gh_0)^{1/2}\right]^2 \tag{2.4}$$

where $h =$ water surface elevation, $h_0 =$ initial water depth, $u =$ velocity in the x-direction, and $t =$ time. Flow-3D, which is a commercially available CFD package based on the VOF method, was used to solve the RANS equations using a finite-difference approximation. For the turbulence model, the standard $k - \varepsilon$ turbulence closure was chosen to determine the turbulence viscosity. MIKE 3 FM, which is a modelling system based on an unstructured and flexible finite volume mesh approach, was used to solve the 3D incompressible RANS equations numerically. Using Smagorinsky's formulation and the standard $k - \varepsilon$ method as turbulence models, the eddy viscosity was determined in the horizontal and vertical directions, respectively. During the validation, mesh sensitivity analysis was done for both numerical models with various mesh sizes, and hence the mesh size for the Flow-3D model was chosen as 0.005 m in the x and y directions, while the mesh size was set to 0.05 m.

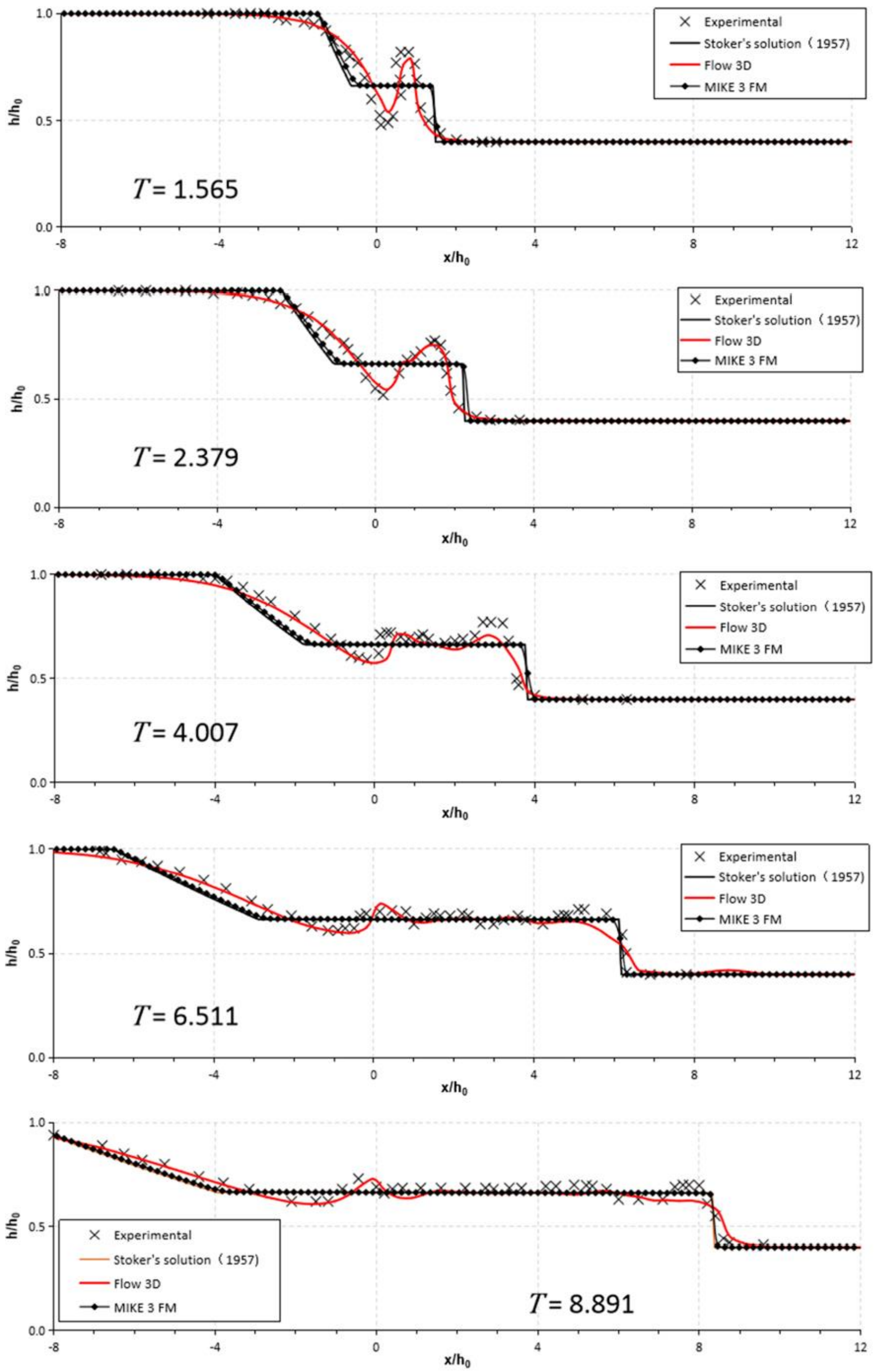

Figure 2.28. Comparison of the calculated and measured (Cagatay and Kocaman, 2010) free surface profiles at various times for the wet bed condition with deeper tailwater (Hu et al., 2018)

Hu et al. (2018) concluded that both the 3D Flow-3D and MIKE 3 FM models were able to provide complete and detailed results for the free surface profile, water depth, and flow velocity. For the initial stages of the dam-break, the free surface profiles of the wave front under both dry and wet bed conditions were reproduced by Flow-3D with a reasonable agreement, while the results of the MIKE 3 FM and 1D analytical solutions showed a vertical drop rather than a curved profile for the wet bed condition (Figure 2.28). However, during the late stages, MIKE 3 FM performed better than Flow-3D in simulating the free surface profile of the wave front. In terms of computational demand, Flow-3D was much more complicated and time-consuming to use compared to MIKE 3 FM.

2.9. Discussion

This literature review has summarized the current research relating to the initial stages of dam-break flood waves over a channel under both dry and wet bed conditions, as well as the formation and propagation of positive and negative bores in the presence of a downstream obstacle, reservoir and channel geometry effects, and partial breach dam-break flows. Numerical modelling is becoming an essential alternative tool as a complement to laboratory experiments for the simulation of dam-break problems, and with the rapid development of computational fluid dynamics (CFD) technology, CFD numerical models are becoming ever-more capable of providing detailed results for dam-break flood waves with a lower cost and higher efficiency compared to analytical solutions and experiments.

To the best of the author’s knowledge, only a few three-dimensional numerical studies that simulate the initial stages of dam-break flows under dry and wet bed conditions and that predict the formation and propagation of dam-break waves against a bottom obstacle are available in the literature, with most of the recent research being conducted with one-dimensional or two-dimensional numerical models to simulate dam-break flows. Furthermore, the performance and accuracy of various turbulence models to solve RANS equations and estimate dam-break flood wave behaviour have not been evaluated by many researchers during recent years. In addition, the capability and efficiency of OpenFOAM to perform three-dimensional numerical modelling simulating dam-break flow characteristics under various conditions have not been investigated previously.

Due to the importance of better understanding and predicting water surface profiles and flow propagation during flood events to reduce the hazards from flood impacts, this research has been focused on performing three-dimensional numerical modelling based on RANS equations with different turbulence models to investigate the performance of those turbulence models in simulating the initial stages of dam-breaks. However, it is clear that further research needs to be undertaken to improve the accuracy and efficiency of numerical models in properly reproducing dam-break flow characteristics.

Chapter 3. CFD Modelling of Near-Field Dam Break Flow [1]

3.1. Introduction

Dam break is one of the risks associated with the dams. There are several cases of dam failures every year globally. The propagation of a flood wave created by a sudden break is often catastrophic in downstream floodplain due to a large volume of water released in a short time (i.e. time to failure). It is therefore very important to estimate the maximum flood level, maxim flood depth and flood arrival time to reduce loss of life and flood damages. There are several experimental studies focused on the early stages of a dam break process (e.g. Dressler, 1954; Bell et al., 1992; Bellos et al., 1992; Lauber and Hager, 1998). There are also idealized analytical solutions for the dam break problems. For instance, Stoker (1957) extended Ritter's solution of 1829 to relate dry bed and wet bed by solving Saint-Venant equations using the method of characteristics. However, during the early stages of dam break the analytical solutions do not agree well with experimental data (Stansby et al., 1998; Cagatay and Kocaman, 2008). Dam break problems are unsteady-state flows that could be described by Reynolds-averaged Navier-Stokes (RANS) models. Shingematsu et al. (2004) solved the RANS equations using the finite difference formulation, in which the volume of fluid (VOF) was used to capture the free surface. Abdolmaleki et al. (2004) used an Eulerian finite volume method (FVM) in a Navier-Stokes solver to model the dam break problem. Quecedo et al. (2005) compared two different methods in dam break modelling: finite volume method (FVM) vs finite element method (FEM) to quantify the flood wave propagation along its flow path.

The initial stages of a dam break are critical due to wave breaking and presence of turbulence (Figure 1). In particular, the front wave resulted from a dam break is strongly affected by vertical accelerations which are not considered in the 1D and 2D shallow water equation (SWE) models.

[1] **Esmaeeli Mohsenabadi S**., Mohammadian M., Nistor I., Kheirkhah Gildeh H., "CFD Modelling of Near-Field Dam Break Flow", International Commission on Large Dams (ICOLD), Ottawa, Canada, June 2019.

However, this vertical acceleration is captured in RANS models and this makes it a reliable CFD tool to predict the complicated fluid characteristics in early stages of a dam break.

This study was mainly focused to verify the capability of an OpenFOAM model to simulate the dam break flow immediately downstream of a breach location. The free surface profiles were tracked and extracted over horizontal, dry and wet beds with two different tailwater levels. The results of the current study were compared to the experimental and numerical results of Cagatay and Kocaman (2010).

Figure 3.1. Teton Dam Failure; northwest view toward the breach. Photo by Mrs. Eunice Olson, 5 June 1976.

3.2. Numerical Model

Flood flows have been studied by using numerical models during the past years and CFD has become one of the most beneficial tools in water resources engineering in both academia and industry. To simulate dam break flows in this study, the OpenFOAM model was used. OpenFOAM (OPEN Field Operation And Manipulation) is an open-source computational fluid dynamics model written in C++ which has been used in hydraulic engineering problems more frequently in past years (Shaheed et al., 2018; Kheirkhah et al. a, 2015; Kheirkhah et al. b, 2014; Kheirkhah et al. c, 2014). OpenFOAM model has the feature of being open-source for changes and developments, and new ideas can be contributed by users to help in extending the software features. Simulation of flow fields using various numerical schemes and turbulence models are possible within the model. The model also has the capability of parallel processing. Two types of application are available with this model: solvers that designed to solve a specific fluid mechanics problem, and utilities which are used to perform data manipulation. OpenFOAM uses the FVM and includes various numerical schemes that are implemented for both time and space integrations. For further information about how to use and program OpenFOAM, see (OpenCFD, 2015). The solver used in this study is interFoam, which is mostly used for incompressible free surface turbulent flows.

3.2.1 Governing Equations

In this study, the Navier-Stokes and continuity equations have been used in the x, y and z directions to describe the flow, as written below.

Momentum in the x-direction:

$$\frac{\partial}{\partial t}(\rho u) + \frac{\partial}{\partial x}(\rho uu) + \frac{\partial}{\partial y}(\rho vu) + \frac{\partial}{\partial z}(\rho wu) = -\frac{\partial P}{\partial x} + \mu\left(\frac{\partial^2 u}{\partial x^2} + \frac{\partial^2 u}{\partial y^2} + \frac{\partial^2 u}{\partial z^2}\right) \quad (3.1)$$

Momentum in the y-direction:

$$\frac{\partial}{\partial t}(\rho v) + \frac{\partial}{\partial x}(\rho uv) + \frac{\partial}{\partial y}(\rho vv) + \frac{\partial}{\partial z}(\rho wv) = -\frac{\partial P}{\partial y} + (v + v_t)\left(\frac{\partial^2 v}{\partial x^2} + \frac{\partial^2 v}{\partial y^2} + \frac{\partial^2 v}{\partial z^2}\right) \quad (3.2)$$

Momentum in the z-direction:

$$\frac{\partial}{\partial t}(\rho w) + \frac{\partial}{\partial x}(\rho uw) + \frac{\partial}{\partial y}(\rho vw) + \frac{\partial}{\partial z}(\rho ww) = -\frac{\partial P}{\partial z} + (v + v_t)\left(\frac{\partial^2 w}{\partial x^2} + \frac{\partial^2 w}{\partial y^2} + \frac{\partial^2 w}{\partial z^2}\right) \quad (3.3)$$

Continuity:

$$\frac{\partial}{\partial x}(\rho u) + \frac{\partial}{\partial y}(\rho v) + \frac{\partial}{\partial z}(\rho w) = 0 \quad (3.4)$$

where the y-axis of the Cartesian coordinate system is aligned in the vertical direction; $u, v,$ and w are the velocity components in the x, y, and z directions, respectively; ρ is the mass density; μ is the viscosity; v_t is the turbulent kinematic viscosity; t is the time; and P is the pressure.

3.2.2 Turbulence Models

The simulation of turbulent flows is considered a complicated task because of the features that characterize this type of flow, such as three-dimensionality, unsteadiness, and the inclusion of many scales (Tajnesaie et al., 2018). Therefore, it is a delicate task to choose the most appropriate turbulence model, and the selection process will depend on factors like the physics encompassed in the flow, the level of accuracy desired, and the computational resources available (Kheirkhah, 2013).

In this study, the simulation of dam break flows has been performed by using two widely used turbulence models: the standard k-ε model and the RNG k-ε model. These two RANS models have been selected due to their computational efficiency and their wide usage compared to other RANS models such as LRR or Large Eddy Simulation (LES) models. The two models are described in the following.

3.2.2.1. Standard k-ε Model

The turbulence model that is most commonly used in CFD is the standard k–ε model. This model is based on the eddy viscosity concept. Two partial differential equations (transport equations) are solved in this type of turbulence model: the turbulent kinetic energy k and the turbulent eddy dissipation ε (i.e., the rate at which the turbulent kinetic energy dissipates) (Olsen, 2000). The incapability of capturing the subtler relationships between the turbulent energy production and the turbulent stresses caused by anisotropy of the normal stresses is one of the problems of some two-equation turbulence models such as the k–ε model. In addition, the performance of the k–ε model is considered poor in some cases, like: (1) some unconfined flows; (2) flows with large extra strains (e.g., curved boundary layers, swirling flows); (3) rotating flows; and (4) flows driven by anisotropy of normal Reynolds stresses (Versteeg and Malalasekera, 1995).

In this model, the following equations are used to obtain the turbulent kinetic energy and its rate of dissipation (Kheirkhah, 2013):

$$\frac{\partial k}{\partial t} + \frac{\partial k u_i}{\partial x_i} = \frac{\partial}{\partial x_i}\left(Dk_{eff}\frac{\partial k}{\partial x_i}\right) + G_k - \varepsilon \tag{3.5}$$

$$\frac{\partial \varepsilon}{\partial t} + \frac{\partial \varepsilon u_i}{\partial x_i} = \frac{\partial}{\partial x_i}\left(D\varepsilon_{eff}\frac{\partial \varepsilon}{\partial x_i}\right) + C_{1\varepsilon}\frac{\varepsilon}{k}G_k - C_{2\varepsilon}\frac{\varepsilon^2}{k} \tag{3.6}$$

where G_k is the generation of turbulent kinetic energy due to mean velocity gradients, and Dk_{eff} and $D\varepsilon_{eff}$ are the effective diffusivity for k and ε, respectively, which are calculated as shown below:

$$Dk_{eff} = \nu + \nu_t \tag{3.7}$$

$$D\varepsilon_{eff} = \nu + \frac{\nu_t}{\sigma_\varepsilon} \tag{3.8}$$

The equation for the turbulent kinematic viscosity at each point is:

$$\nu_t = C_\mu \frac{k^2}{\varepsilon} \tag{3.9}$$

where σ_ε is the turbulent Prandtl number for ε and is assumed as equal to 1.3. Furthermore, the constants $C_{1\varepsilon}$, $C_{2\varepsilon}$ and C_μ have the following values: $C_{1\varepsilon} = 1.44,\ C_{2\varepsilon} = 1.92,\ C_\mu = 0.09$.

G_k is the production of turbulent kinetic energy, which is common in most turbulence models, and is given by:

$$G_k = 2\nu_t {S_{ij}}^2 \tag{3.10}$$

where the strain-rate tensor S_{ij} is written as:

$$S_{ij} = 0.5\left(\frac{\partial u_j}{\partial x_i} + \frac{\partial u_i}{\partial x_j}\right) \tag{3.11}$$

3.2.2.2. RNG k-ε Model

Similar to the standard k-ε model, the RNG k-ε model is derived from the instantaneous Navier-Stokes equations, except that it uses a technique called renormalization group theory described by the Yakhot and Orszag (1986). The derivation that they used produces a model with different constants to those used in the standard k-ε model which adds new terms to the transport equations for the turbulent kinetic energy and its dissipation. The effect of swirl is also accounted for in the RNG k-ε model enhancing the accuracy of swirling flows. An analytical formula for turbulent Prandtl numbers is provided in this model while the standard model relies on user-specific constant values. Finally, assuming appropriate treatment of the near wall region, the RNG k-ε model uses an analytically derived differential formula for the effective turbulent viscosity which accounts for low Reynolds number flows. As a result of these differences, the transport equations are written as:

$$\frac{\partial k}{\partial t} + \frac{\partial k u_i}{\partial x_i} = \frac{\partial}{\partial x_i}\left(Dk_{eff}\frac{\partial k}{\partial x_i}\right) + G_k - \varepsilon \tag{3.12}$$

$$\frac{\partial \varepsilon}{\partial t} + \frac{\partial \varepsilon u_i}{\partial x_i} = \frac{\partial}{\partial x_i}\left(D\varepsilon_{eff}\frac{\partial \varepsilon}{\partial x_i}\right) + (C_{1\varepsilon} - R)\frac{\varepsilon}{k}G_k - C_{2\varepsilon}\frac{\varepsilon^2}{k} \tag{3.13}$$

Some items are obtained differently from the standard model. Dk_{eff} is calculated as:

$$Dk_{eff} = \nu + \frac{\nu_t}{\sigma_k} \tag{3.14}$$

The renormalization term, R, is formulated as:

$$R = \frac{\eta(1-\frac{\eta}{\eta_0})}{1+\beta\eta^3} \tag{3.15}$$

$$\eta = S_{ij}\frac{k}{\varepsilon} \tag{3.16}$$

All model constants are defined as: $C\mu$= 0.0845, $C_{1\varepsilon}$= 1.42, $C_{2\varepsilon}$= 1.68, σ_k= 0.71942, σ_ε= 0.71942, η_0= 4.38, β= 0.012.

3.2.3. Model Setup and Boundary Conditions

A rectangular tank 9.0 m long, 0.3 m high and 0.5 m wide was modelled to perform the numerical experiments. As initial condition, a 4.65 m long and 0.25 high VOF was defined as reservoir. An additional VOF of 4.35 m long and 0.025 m, 0.10 m high as tailwater for the wet bed tests was defined. All channel surfaces were assumed smooth. The time steps dt were determined according to the Courant–Friedrichs–Lewy condition (CFL). In the numerical computations, the upstream boundary was set as wall due to no inflow into the reservoir and constant reservoir length. The downstream boundary was set as outflow for the dry bed test. For wet-bed tests, it was set as wall because the downstream end was closed by a vertical steel plate in the study by Cagatay and Kocaman (2010). The lower boundary was set as wall. The upper boundary was set as symmetry to account for the atmospheric pressure on the free surface. Since the water surface is defined by VOF, zero shear stress and constant atmospheric pressure were applied as boundary conditions over the air–water interface (Hirt and Nichols, 1981). The channel sidewalls were chosen as symmetry, implying no flux and shear of any property across it. The Standard wall function was employed to specify boundary conditions at the walls.

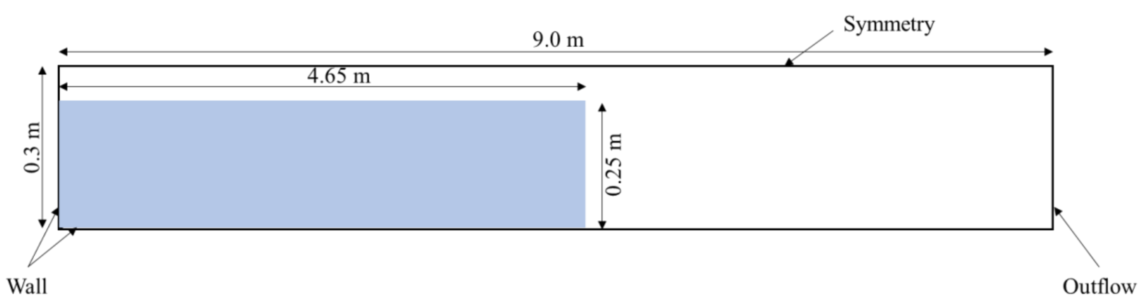

Figure 3.2. 2D View of Numerical Model Setup and Boundary Conditions for Dry Bed Scenario

3.3. Numerical Results and Discussion

Figure 3.3 shows a qualitative comparison of the current study model results with those of the experimental and numerical study by Cagatay and Kocaman (2010). Three conditions were assessed: a) dry condition downstream of the dam; wet condition downstream of the dam with water depth of 0.025 m and c) wet condition downstream of the dam with water depth of 0.1 m. There is a good general agreement between the current study and previous data, however, there are some disagreements which are more evident is the upper frame (t=0.1 s) and especially for the dry bed. The turbulence effect during the early dam-break stages was extensively studied by Shigematsu et al. (2004) for dry bed cases. They explained that the surface profiles are mostly parabolic and wave front becomes convex as time progresses, with pressure lower being than hydrostatic. As time passes, pressure increases, and it becomes higher than hydrostatic due to bottom friction and causes a free surface vortex. Lauber and Hager (1998) concluded in their study that a dam break wave over a dry bed can be divided into an initial wave and a dynamic wave passing the initial stage at a defined section which is in line with the dry bed wave propagation in Figure 3.3.

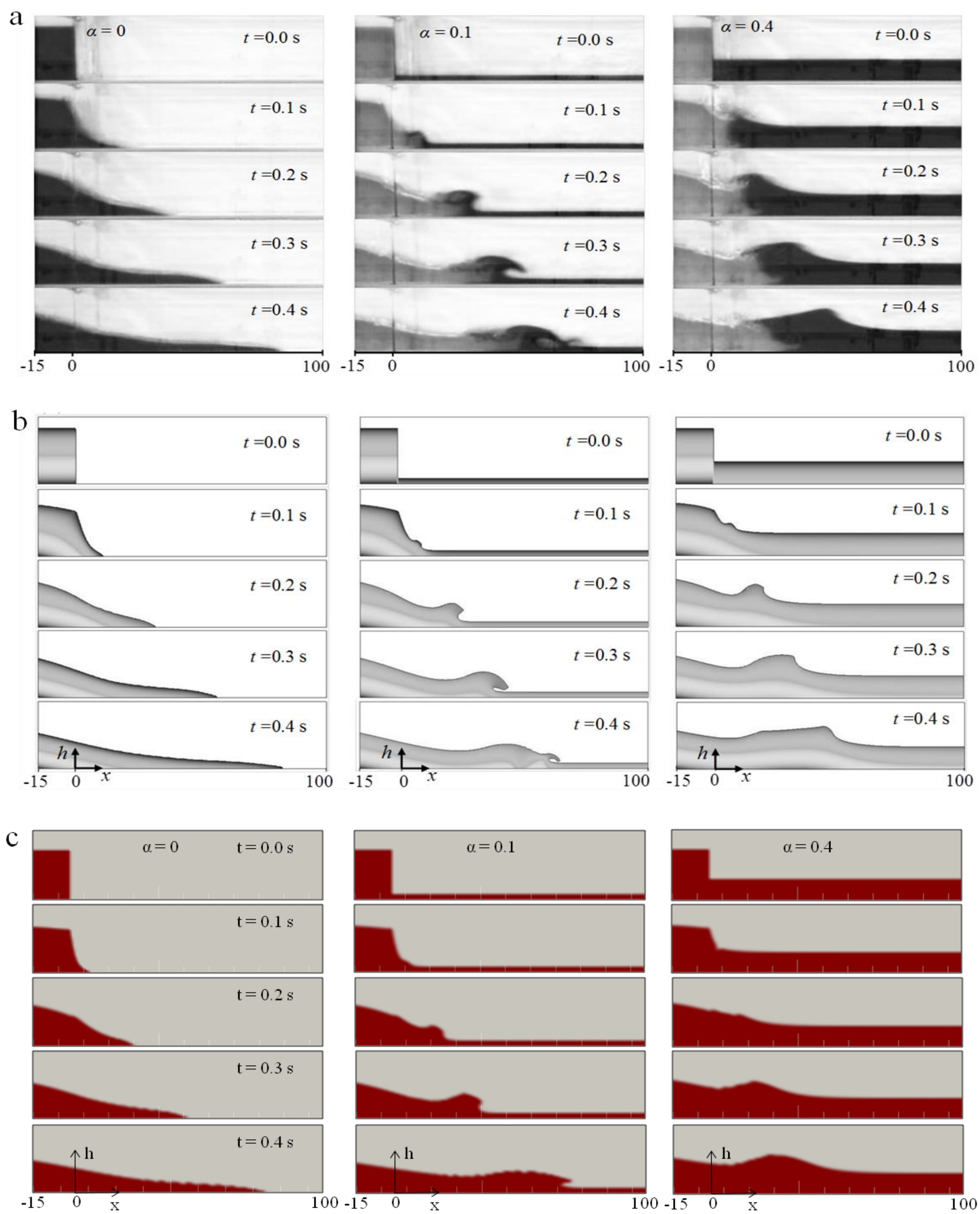

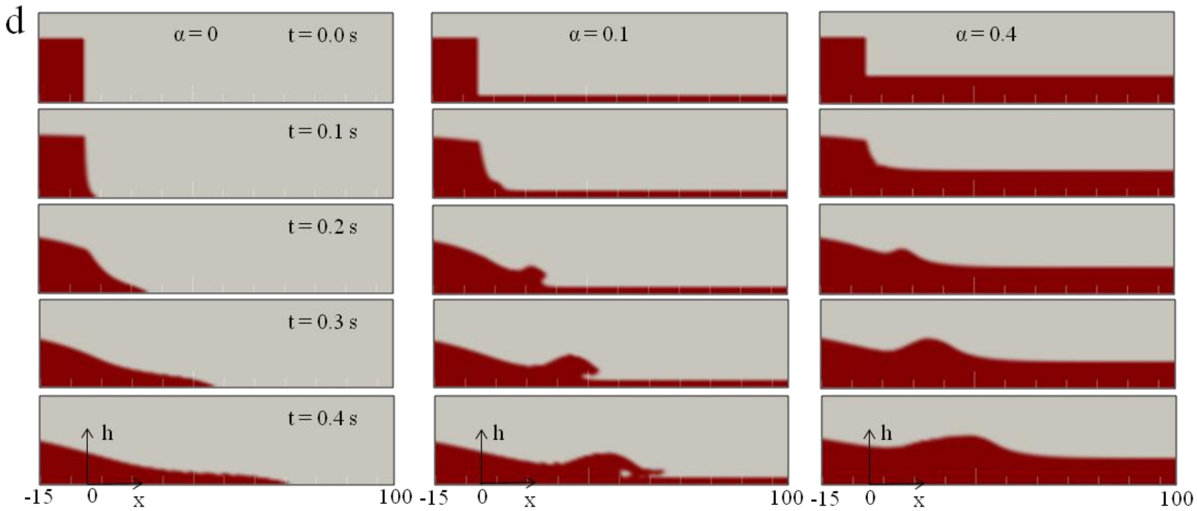

Figure 3.3. Evolution of free surface profiles. (a) measured (Cagatay and Kocaman, 2010), (b) k-ε model (Cagatay and Kocaman, 2010), (c) k-ε model OpenFOAM (this study), (d) RNG k-ε model OpenFOAM (this study).

In the wet bed scenario, when the dam breaks, the breached water would drag the tailwater and the tailwater resists the drag forces applied and thus the wave front breaks and a jet-like flow would form downstream during the initial stage (Stansby et al., 1998). Wave breaking would delay even more when the tailwater depth increases.

Figures 3.4-3.6 compare the experimental results with the numerical results for both standard and RNG k-ε models for the initial free surface profiles for the dry and wet channels. Flow depth and distance along the channel were non-dimensionalized by the initial water depth h_0. Time t was also multiplied by $(g/h_0)^{1/2}$ to get the dimensionless time $T=t(g/h_0)^{1/2}$. $\alpha=h_1/h_0$ is defined as the depth ratio (i.e. tailwater depth over the reservoir depth).

Figure 3.4 shows the comparisons between the present study and previous experimental and numerical data for the dry bed scenario with α=0.0. Both turbulence models in this study showed a good agreement with the experimental data, especially as time progresses and flood wave travels more downstream along the channel. At T=1.13, the RNG k-ε model overpredicts the water depth and standard k-ε model underestimates it. However, for the next frames (i.e. after T=1.13), the RNG k-ε model agrees well with the experimental free surface profile; while standard k-ε model overestimates the flood depth between x/h_0 = -4 and 0. As time progresses, both turbulence models predict the flood profile similarly except the edge of inundation, where flood depth is small, that the RNG k-ε model showed better results compared to the experimental data. It should be noted that RANS models are not able to capture small eddies in turbulent flows where they may cause the higher observed depth as seen at time T=5.01 between x/h_0 = 4 and 8.

Figure 3.5 shows the comparisons between the present study and previous experimental and numerical data for wet bed scenario with α=0.1. Based on the results, it is evident that the RNG k-ε model is better capable of capturing the flood peaks than the standard k-ε model. Modelled flood timing is also in good agreement with that from experiment. The RNG k-ε model examined in this study performs better comparing to k-ε and SWE models from Cagatay and Kocaman (2010). Falling limb of the wave front is accurately captured using the RNG k-ε model, where it meets the tailwater downstream of the dam. None of the models (current study and previous study) could accurately capture multiple wave formations as time progresses and wave breaks more frequently.

Figure 3.6 plots the surface profile resulted from the present study compared to those from previous experimental and numerical data for the wet bed scenario with α=0.4. Similar to the previous scenario (i.e. wet bed scenario with α=0.1), the RNG k-ε model shows a better performance for all times plotted. The RNG k-ε model was also capable to capture the wave peak patterns the best among other models. For wet-bed conditions, the pressure evolution with time is similar in the current study and the experiment, resulting in a curved downstream free surface profiles at maximum flow depth. For the wet-bed scenarios studied here, the present model results compare reasonably well with measurements as the tailwater depth increases. Note that, in most of the scenarios and times, the RNG model was more capable of capturing the wave front and free surface profile.

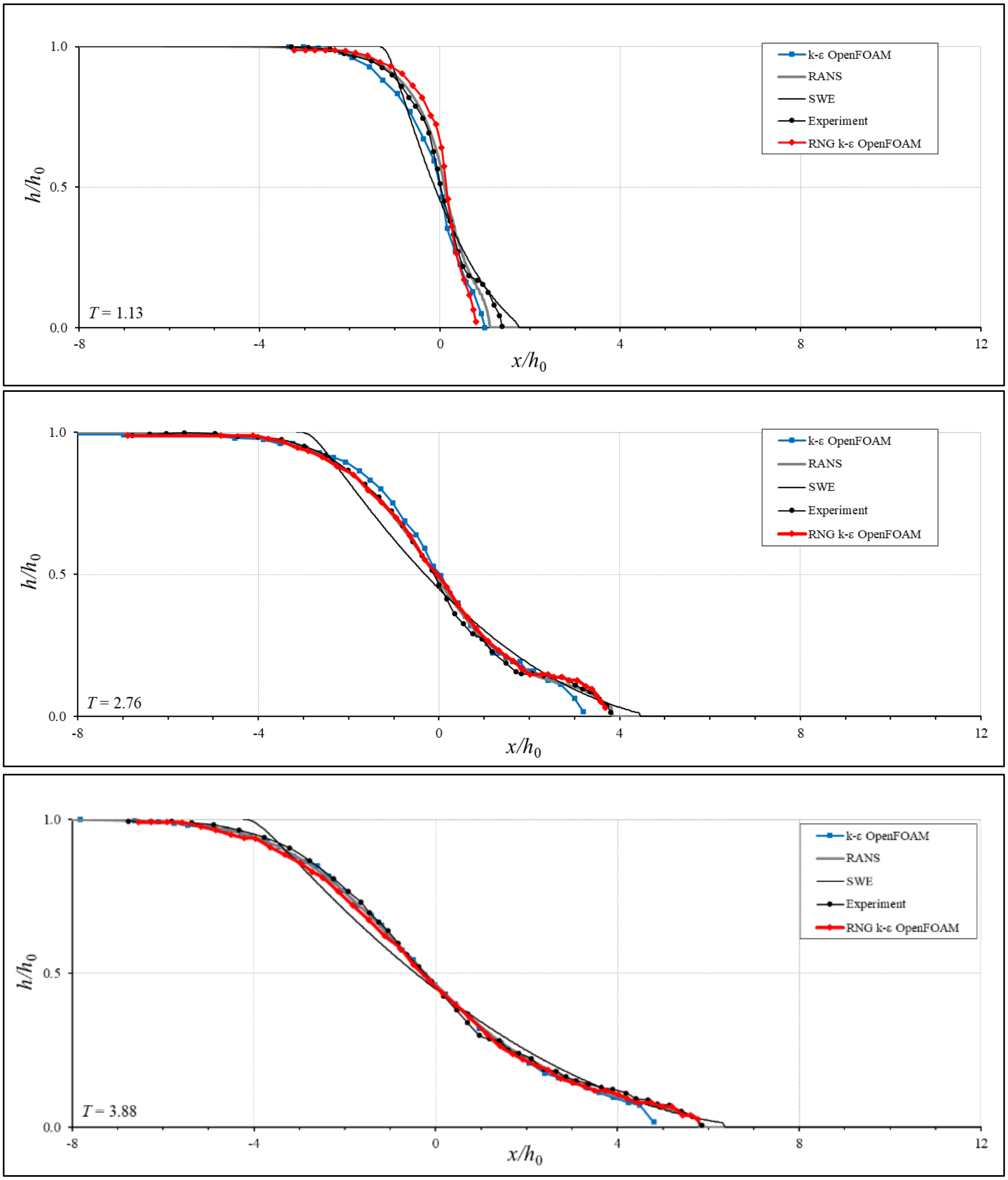
k-ε OpenFOAM
RANS
SWE
Experiment
RNG k-ε OpenFOAM
h/h_0
x/h_0
T = 1.13
T = 2.76
T = 3.88

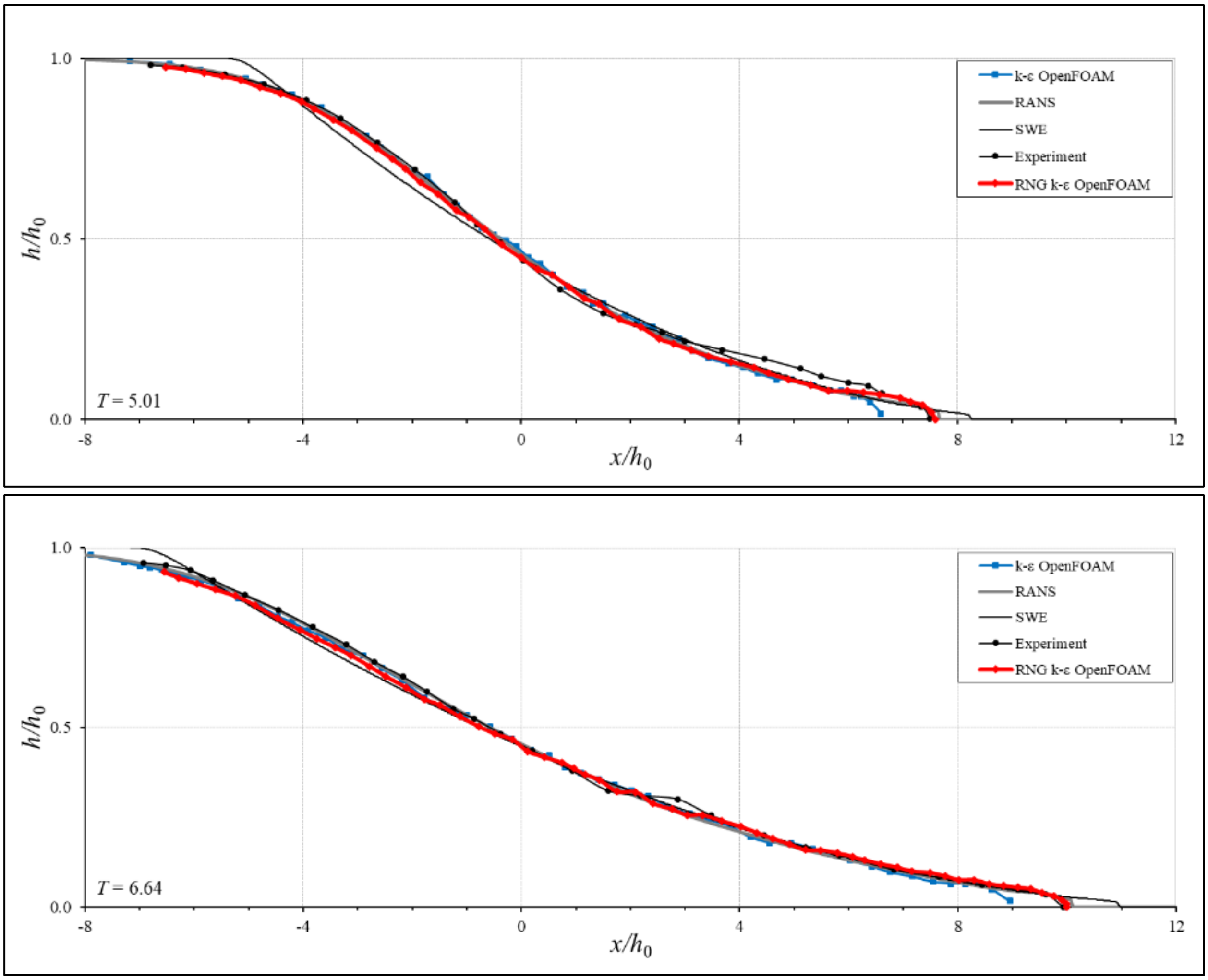

Figure 3.4. Model results of free surface profiles $h/h_0(x/h_0)$ during initial stages of dam break at various times $T=t(g/h_0)^{1/2}$ for dry bed with α=0.0. OpenFOAM models are for the current study.

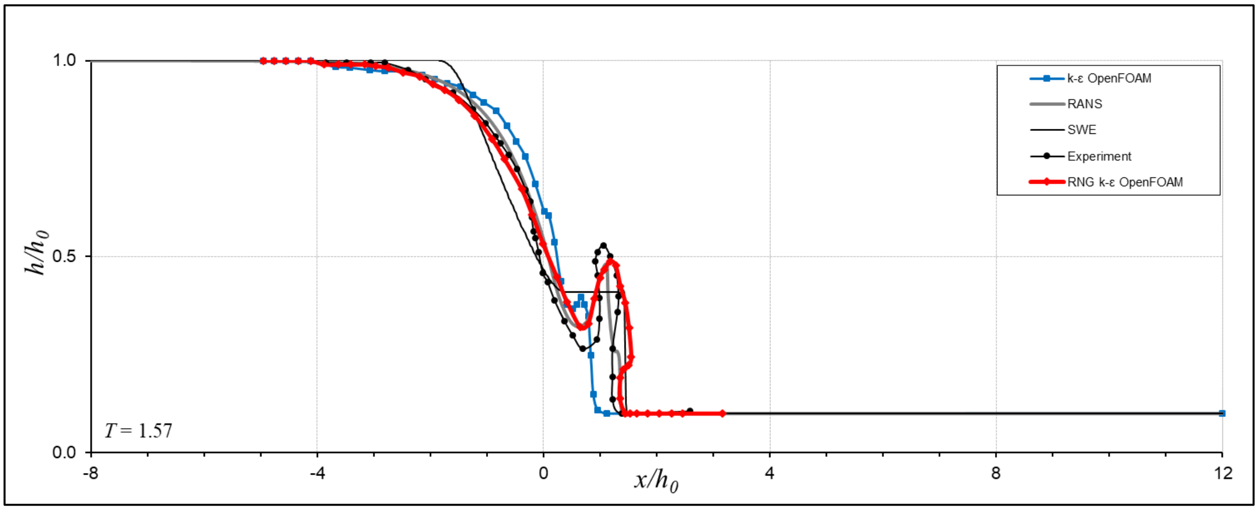

k-ε OpenFOAM
RANS
SWE
Experiment
RNG k-ε OpenFOAM
1.0
0.5
0.0
h/h_0
-8
-4
0
4
8
12
x/h_0
T = 1.57

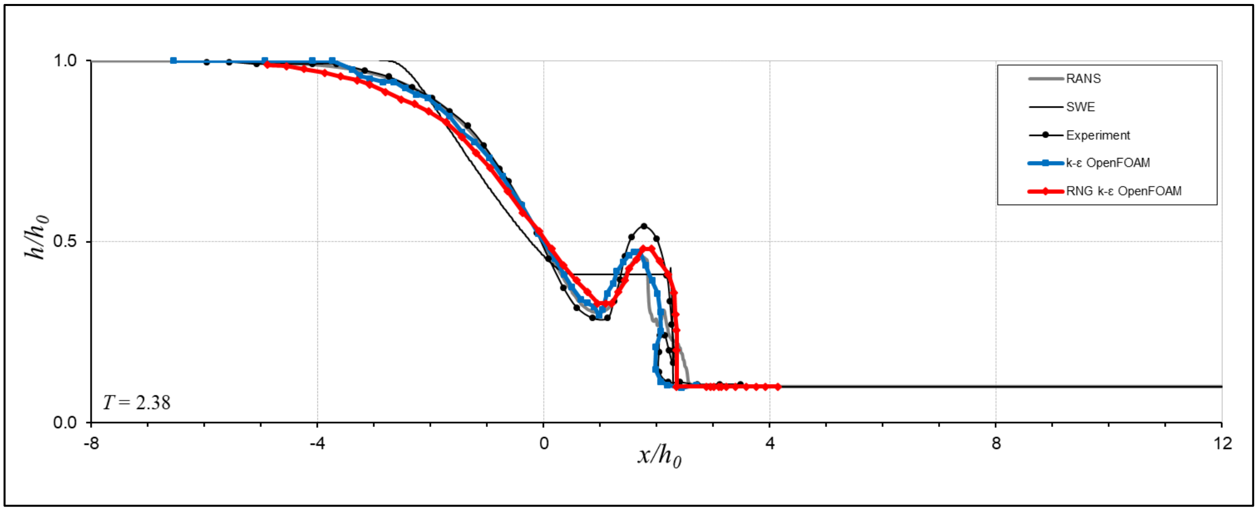

RANS
SWE
Experiment
k-ε OpenFOAM
RNG k-ε OpenFOAM
1.0
0.5
0.0
h/h_0
-8
-4
0
4
8
12
x/h_0
T = 2.38

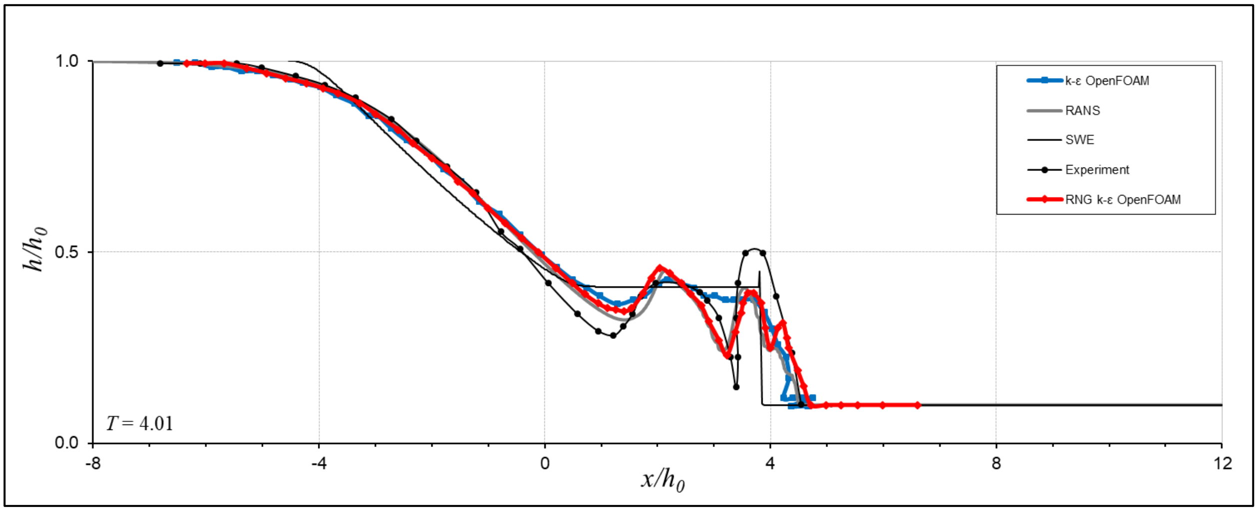

k-ε OpenFOAM
RANS
SWE
Experiment
RNG k-ε OpenFOAM
1.0
0.5
0.0
h/h_0
-8
-4
0
4
8
12
x/h_0
T = 4.01

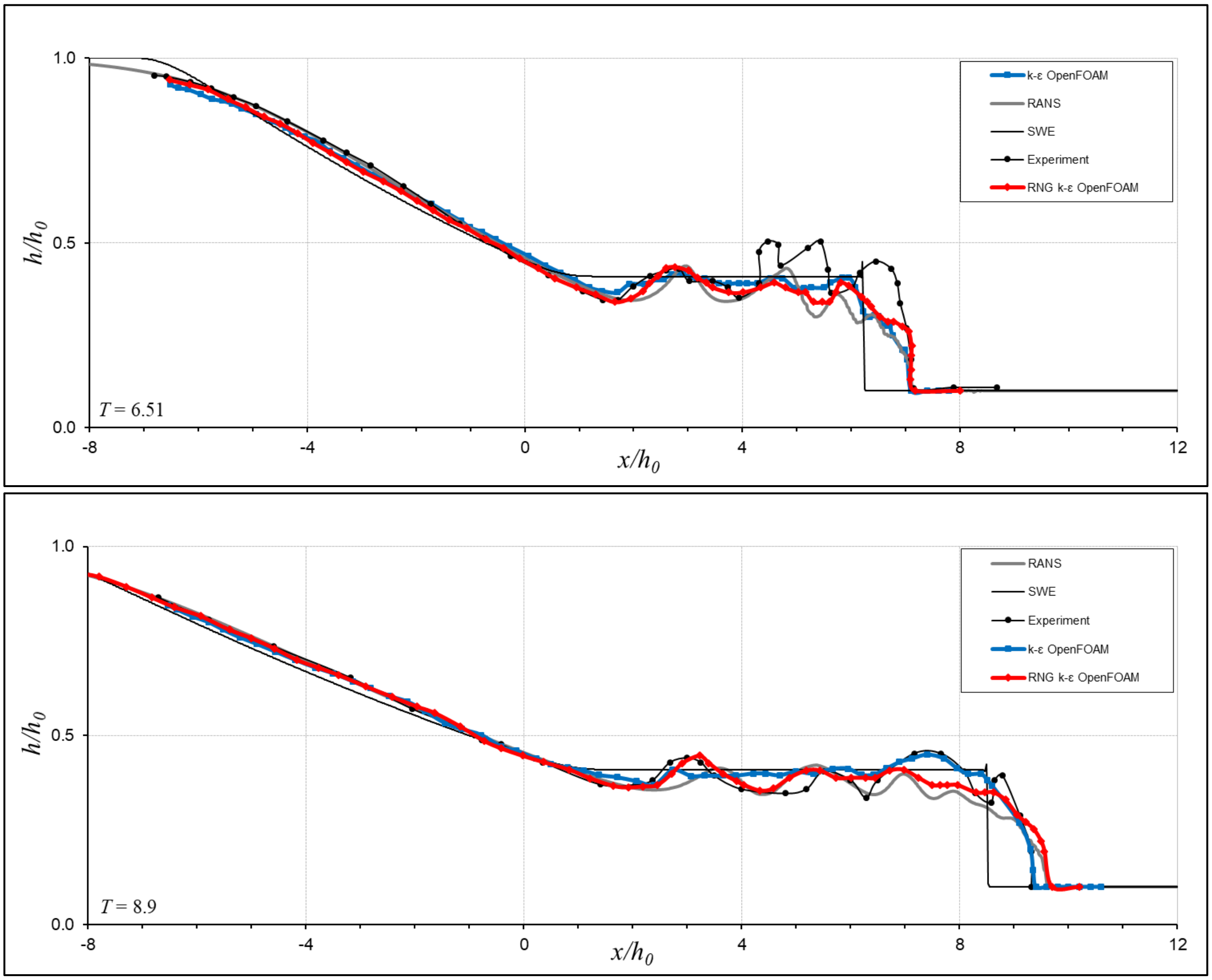

Figure 3.5. Model results of free surface profiles $h/h_0(x/h_0)$ during initial stages of dam break at various times $T=t(g/h_0)^{1/2}$ for wet bed with α=0.1. OpenFOAM models are for the current study.

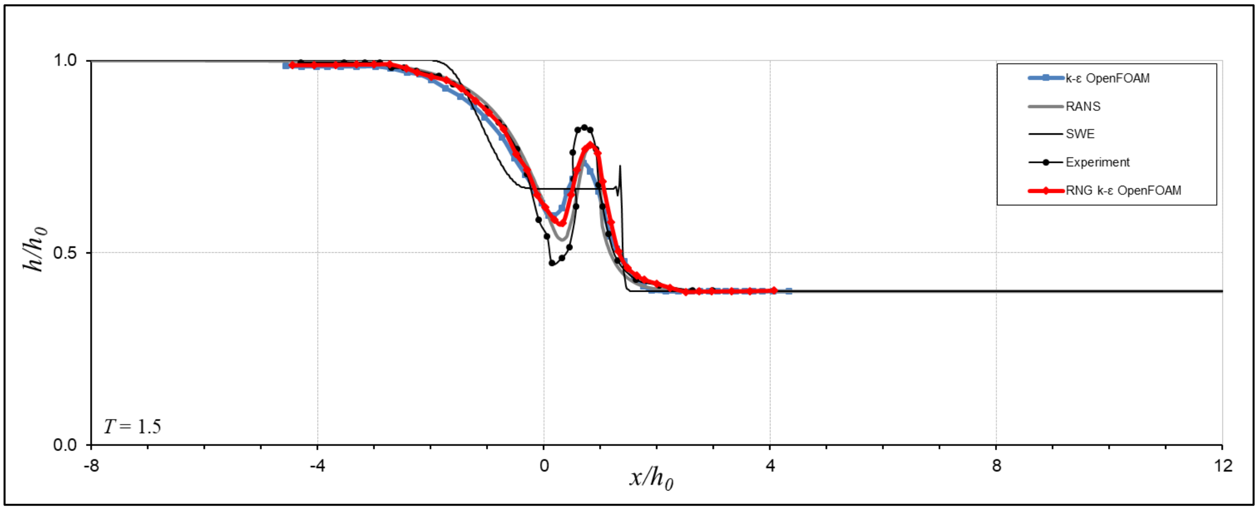

k-ε OpenFOAM
RANS
SWE
Experiment
RNG k-ε OpenFOAM
h/h_0
x/h_0
$T = 1.5$

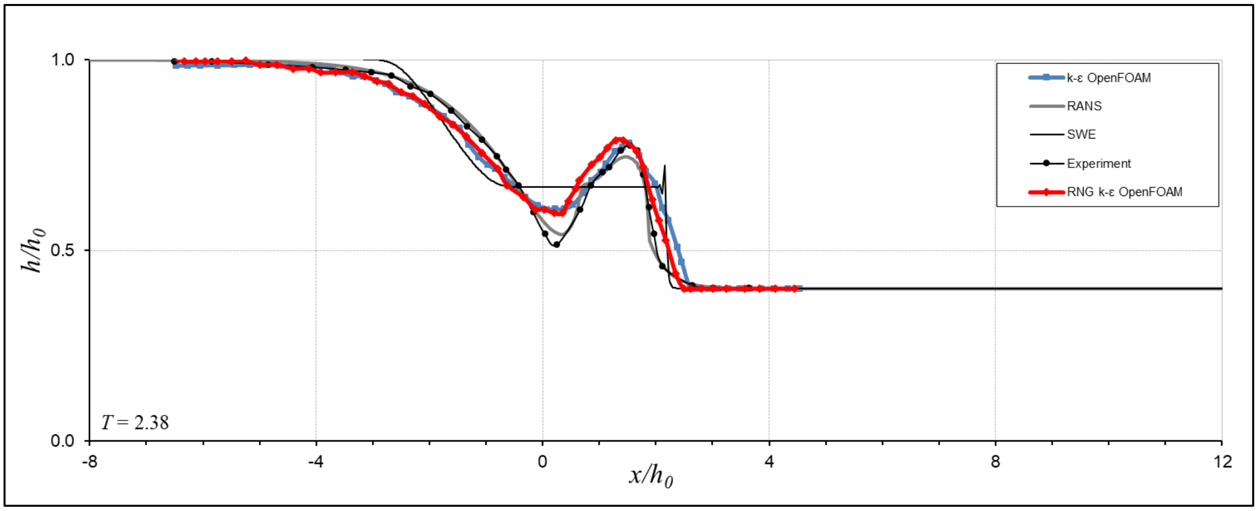

k-ε OpenFOAM
RANS
SWE
Experiment
RNG k-ε OpenFOAM
h/h_0
x/h_0
$T = 2.38$

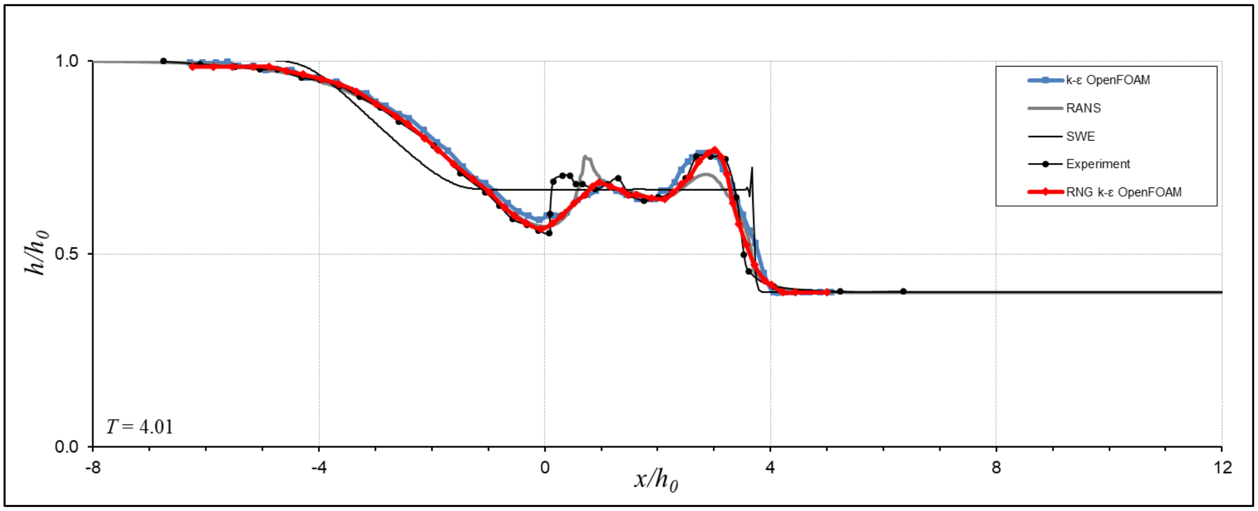

k-ε OpenFOAM
RANS
SWE
Experiment
RNG k-ε OpenFOAM
h/h_0
x/h_0
$T = 4.01$

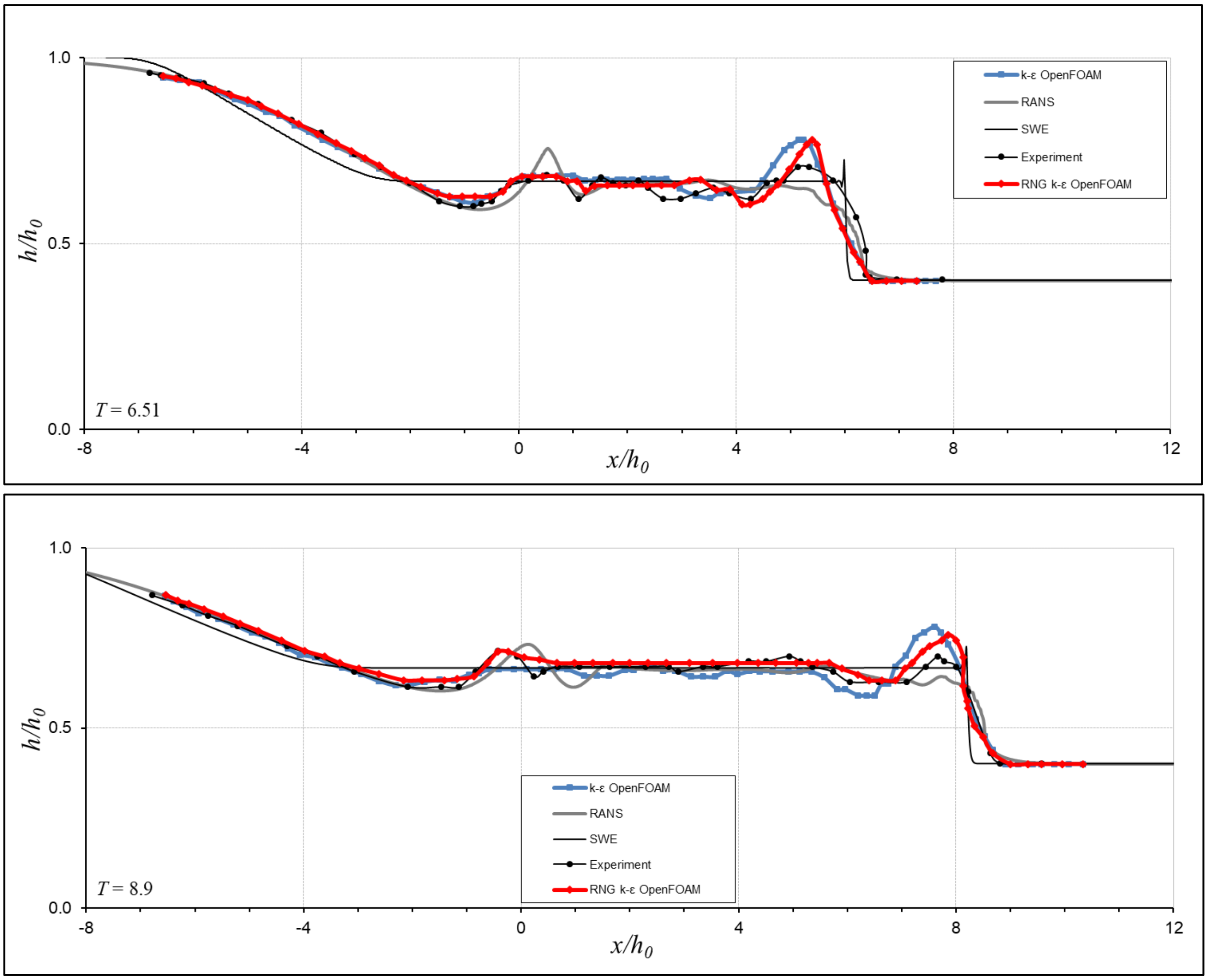

Figure 3.6. Model results of free surface profiles $h/h_0(x/h_0)$ during initial stages of dam break at various times $T=t(g/h_0)^{1/2}$ for wet bed with α=0.4. OpenFOAM models are for the current study.

3.4. Discussion

The dissipation properties and shear layer behavior of the turbulent flow immediately downstream of a dam break should be properly captured using the numerical model in order to resolve the flood wave developments. Flood wave characteristics downstream of a dam break are not often identical due to the downstream channel geometry and hydraulic initialization (i.e. tailwater in this study). Turbulent flows in presence of tailwater are often different than dry bed due to the perpendicular shear stresses where two water pockets meet, as well as other differences in flow characteristics.

The flood wave propagation is expected to be different, and thus the performance of turbulence models in capturing flood flows might be different for each condition. It is therefore vital to understand the differences between the two turbulence models used in this study. The main differences between the RNG and standard k-ε models are listed below:

- The RNG k-ε model has an additional term in its ε equation that improves the accuracy for rapidly strained flows.
- The effect of swirl on turbulence is included in the RNG k-ε model, enhancing accuracy for swirling flows.
- The RNG theory provides an analytical formula for turbulent Prandtl numbers, while the standard k-ε model uses user-specified, constant values.
- While the standard k-ε model is a high-Reynolds number model, the RNG theory provides an analytically-derived differential formula for effective viscosity that accounts for low-Reynolds number effects.

To improve the correlation between the existing models and the experimental data, turbulence model showing the best matches should be looked at closer and improved upon. In addition, different wall functions and Large Eddy Simulations (LESs) with higher resolution could be used to obtain results with higher levels of accuracy.

3.5. Conclusions

The current study was an effort to simulate the initial stages of a turbulent dam break flow using two different RANS turbulence models: standard and RNG k-ε models. k-ε models are the most common turbulence models and are widely used in both academia and industry. The previous experimental and numerical study by Cagatay and Kocaman (2010) was selected to verify the numerical model performances mainly in capturing the flood wave free surface profiles. Following is a summary of findings from the current study:

- The wave propagation (i.e. wave front shape and its travel time) differs if the breach downstream is dry or wet;

- The qualitative comparison between the present study and experimental data shows a reasonable agreement between the numerical models and experimental data for the evolution of free surface profiles in terms of capturing the wave front and the break process; and
- Quantitative comparison of the free surface profiles between the current study and previous data shows that RNG k-ε model performs better compared to the standard k-ε model.

Chapter 4. CFD Modeling of Initial Stages of Dam-Break Flow

4.1. Introduction

Dam failures often result in catastrophic floods that can have a significant impact on downstream areas due to the uncontrolled release of water from reservoirs. Extreme flooding events in downstream areas due to dam failures are a great concern, since they can have devastating consequences and significant ecological impacts. Investigating a dam-break flow is challenging when it propagates over irregular and complex channel topography such as natural channel expansions or contractions and with the presence of natural or artificial obstacles such as trees, debris, bridges, and buildings. In real life, natural or man-made obstacles can act as vertical walls during flooding from sudden dam failures, reflecting waves and creating negative bores that propagate in the upstream direction at high velocity. Varying channel topography also affects the flow regime and can lead to hydraulic jumps and reflected waves. Therefore, in order to minimize flood risks, it is important to investigate various flow characteristics such as variations in flow depth with time, flow velocity profiles, flood arrival times, and the formation and propagation of negative and positive waves in the presence of obstacles during flooding events.

In recent decades, theoretical studies for idealized dam-break waves have provided a way to theoretically characterize the hydrodynamics of dam-break flows (Ritter, 1892; Dressler, 1952; Chanson, 2006). Stoker (1957) extended Ritter's 1829 solution to relate dry and wet beds by solving Saint-Venant equations using the method of characteristics. However, most analytical solutions do not agree well with experimental data during the early stages of a dam break (Stansby et al., 1998; Cagatay and Kocaman, 2008). Also, they are not applicable for many complicated cases.

Recent experimental studies on dam-break waves have focused on their free surface profiles and water depths, while fewer studies have investigated flow velocity fields and pressure distributions. The early stages of dam-breaks have been investigated by many researchers experimentally (e.g., Dressler, 1954; Bell et al., 1992; Bellos et al., 1992; Lauber and Hager, 1998; Cagatay and Kocaman 2010). The effect of abrupt channel bottom variations on dam-break flow propagation and the formation and evolution of negative bores in the presence of an obstacle were studied by Cagatay and Kocaman in 2011 and 2014. In addition, Kocaman and Cagatay (2012; 2015) investigated the formation and propagation of dam-break flows and reflected waves in the presence of lateral channel contractions over a horizontal rectangular flume.

The accurate prediction of dam-break flow characteristics such as arrival times, free surface profiles, velocities, and pressure distributions is essential. Accordingly, numerical modelling has been employed to simulate complex dam-break flows and flood wave behaviour with detailed results. Shingematsu et al. (2004) solved RANS equations using the finite difference method, in which the volume of fluid (VOF) technique was used to capture the free surface, while Robb and Vasques (2015) studied the performance of three numerical models in reproducing dam-break flows in the presence of obstacles. Considering the rapid developments in computational fluid dynamics, dam-break flows can be reasonably well simulated by CFD numerical models to determine their fluctuation processes in detail. Yang et al. (2018) conducted a series of systematic comparisons between analytical solutions, experimental data, and numerical simulations of the generation and propagation of dam-break waves under both dry bed and wet bed downstream conditions.

In dam-break flood waves, turbulence effects which result from either bottom friction or wave-breaking are significant with regard to the reflected wave front, and the initial stages of a dam break are critical due to wave-breaking and the presence of turbulence. Consequently, precise predictions of flood parameters such as arrival times, free surface profiles, and flow velocity profiles are essential in order to mitigate flood hazards, and so selecting a suitable and accurate model to simulate complicated flood-wave behaviour is very important.

In this study, two dam-break cases are studied numerically in order to compare the propagation and formation of flood waves with available experimental data. First, an initial dam-break flow just after a sudden dam failure over horizontal dry and wet beds with two different tailwater levels is investigated numerically using a 3D OpenFOAM model. Second, the effect of abrupt channel bottom variations on flood wave propagation as well as the generation and time evolution of negative bores in the presence of a trapezoidal bottom obstacle are scrutinized using the 3D OpenFOAM model. This study was also focused on evaluating the performance and capability of an OpenFOAM model and various turbulence closure models such as the realizable $k - \varepsilon$ model, $k - \omega$ SST model, and $v^2 - f$ model in simulating a dam-break flow immediately downstream of a breach location. The results of the current study were compared to the experimental results from Cagatay and Kocaman (2010; 2011).

4.2. Numerical Model

OpenFOAM (OPEN Field Operation And Manipulation) is a free and open-source computational fluid dynamics model which was first produced by OpenCFD (1998) and has been further developed, with many users now employing it (Kheirkhah et al., 2021; Shaheed et al., 2018; Kheirkhah et al., 2015; Kheirkhah et al., 2014). OpenFOAM has an extensive range of features for solving complex fluid flows, and these features have been established under object-oriented C++ language. It also has the capability for changes, and new ideas can be provided by users to extend the software features. OpenFOAM uses the Finite Volume Method (FVM) and includes various numerical schemes that are implemented for both time and space integrations. Based on FVM with discretization, first a three-dimensional volume is created and divided into smaller volumes and meshes by OpenFOAM, and then, initial and boundary conditions are defined to solve the conservation equations that are applied to the geometry.

In this study, OpenFOAM is used to conduct simulations of dam-break flood wave, as reproducing flow fields using various numerical schemes and turbulence models is possible within the model. In this study, interFoam, which is mostly used to simulate incompressible free-surface turbulent flows, is chosen as the solver for the numerical model.

4.2.1 Governing Equations

In this study, Navier-Stokes and continuity equations have been used in the x, y, and z directions to describe the flow, as follows.

Momentum in the x-direction:

$$\frac{\partial}{\partial t}(\rho u) + \frac{\partial}{\partial x}(\rho uu) + \frac{\partial}{\partial y}(\rho vu) + \frac{\partial}{\partial z}(\rho wu) = -\frac{\partial P}{\partial x} + \mu\left(\frac{\partial^2 u}{\partial x^2} + \frac{\partial^2 u}{\partial y^2} + \frac{\partial^2 u}{\partial z^2}\right) \quad (4.1)$$

Momentum in the y-direction:

$$\frac{\partial}{\partial t}(\rho v) + \frac{\partial}{\partial x}(\rho uv) + \frac{\partial}{\partial y}(\rho vv) + \frac{\partial}{\partial z}(\rho wv) = -\frac{\partial P}{\partial y} + (v + v_t)\left(\frac{\partial^2 v}{\partial x^2} + \frac{\partial^2 v}{\partial y^2} + \frac{\partial^2 v}{\partial z^2}\right) \quad (4.2)$$

Momentum in the z-direction:

$$\frac{\partial}{\partial t}(\rho w) + \frac{\partial}{\partial x}(\rho uw) + \frac{\partial}{\partial y}(\rho vw) + \frac{\partial}{\partial z}(\rho ww) = -\frac{\partial P}{\partial z} + (v + v_t)\left(\frac{\partial^2 w}{\partial x^2} + \frac{\partial^2 w}{\partial y^2} + \frac{\partial^2 w}{\partial z^2}\right) \quad (4.3)$$

Continuity:

$$\frac{\partial}{\partial x}(\rho u) + \frac{\partial}{\partial y}(\rho v) + \frac{\partial}{\partial z}(\rho w) = 0 \quad (4.4)$$

where the y-axis of the Cartesian coordinate system is aligned in the vertical direction; $u, v,$ and w are the velocity components in the x, y, and z directions, respectively; ρ is the mass density; μ is the viscosity; v_t is the turbulent kinematic viscosity; t is the time; and P is the pressure.

4.2.2 Turbulence Models

The simulation of turbulent flows is considered to be one of the most complicated tasks for researchers and engineers due to their three-dimensionality, unsteadiness, and the inclusion of many scales (Tajnesaie et al., 2018). There are two main challenges for a turbulence model: boundary layer development, growth, and separation, and predicting the transfer of momentum after separation (Spalart and Flow, 2000). Therefore, it is a delicate task to choose the most appropriate turbulence model, and the selection process will depend on factors like the physics encompassed in the flow, the level of accuracy desired, and the computational resources available (Kheirkhah, 2013).

In this study, the simulation of dam break flood waves is conducted by adopting three widely used turbulence models: the realizable $k - \varepsilon$ model, the $k - \omega$ SST model, and the $v^2 - f$ model. These three RANS models have been selected due to their computational efficiency and their wide usage compared to other RANS models such as the LRR or Large Eddy Simulation (LES) models. The three models are described in the following.

4.2.2.1. Realizable $k-\varepsilon$ Model

Turbulence models are not simultaneously accurate and universal, as Reynolds equations are not able to capture all the small-case phenomena. Hence, developments and improvements for turbulence models are still required. The realizable $k-\varepsilon$ model is one of the most common turbulence models in the $k-\varepsilon$ category and was developed by Shih in 1995 for high Reynolds-number turbulence flows. When considering the differences between the realizable $k-\varepsilon$ turbulence model and the standard one, it can be noted that the realizable turbulence models provide a new formulation for the turbulent viscosity that is more robust compared to other two-equation turbulence models, and the realizable $k-\varepsilon$ turbulence model also has a new transport equation for the dissipation rate. In terms of predicting flows with complex secondary flow features, the realizable $k-\varepsilon$ turbulence model is more precise in many cases than the other $k-\varepsilon$ models due to the positivity of normal Reynolds stresses and Schwarz's inequality for turbulent shear stresses. The transport equation for k and the dissipation rate ε can be expressed by:

$$\frac{\partial k}{\partial t}+\frac{\partial k u_i}{\partial x_i}=\frac{\partial}{\partial x_j}\left(Dk_{eff}\frac{\partial k}{\partial x_j}\right)+G_k-\varepsilon \tag{4.5}$$

$$\frac{\partial \varepsilon}{\partial t}+\frac{\partial \varepsilon u_i}{\partial x_i}=\frac{\partial}{\partial x_j}\left(D\varepsilon_{eff}\frac{\partial \varepsilon}{\partial x_j}\right)+\sqrt{2}C_{\varepsilon 1}S_{ij}\varepsilon-C_{\varepsilon 2}\frac{\varepsilon^2}{k+\sqrt{\upsilon\varepsilon}} \tag{4.6}$$

$$Dk_{eff}=\nu+\nu_t \tag{4.7}$$

$$D\varepsilon_{eff}=\nu+\frac{\nu_t}{\sigma_\varepsilon} \tag{4.8}$$

$$\nu_t=C_\mu\frac{k^2}{\varepsilon} \tag{4.9}$$

where $Dk_{eff}=$ the effective diffusivity for k, $D\varepsilon_{eff}=$ the effective diffusivity for ε, and $G_k=$ the generation of turbulence kinetic energy due to the mean velocity gradients. For more details on the model and constants please see Shih et al. (1994).

4.2.2.2. $k - \omega$ SST Model

The $k - \varepsilon$ model is more suitable for flow regions away from the wall, whereas the $k - \omega$ model performs much better for regions close to the wall. Therefore, it would be quite useful to combine the advantages of these two models. Menter (1995) developed the $k - \omega$ SST (the shear stress transport $k - \omega$) model using the standard $k - \omega$ model and a transformed $k - \varepsilon$ model. In this model, the calculation method for the turbulent viscosity in order to account for the transport of the principal turbulent shear stress is different from previous models. This model triggers the standard $k - \varepsilon$ model far from the wall and the $k - \omega$ model near the wall. The transport equations for k and ω can be expressed by:

$$\frac{\partial k}{\partial t} + \frac{\partial k u_i}{\partial x_i} = \frac{\partial}{\partial x_j}\left(Dk_{eff}\frac{\partial k}{\partial x_j}\right) + G_k - \beta^* k\omega \tag{4.10}$$

$$\frac{\partial \omega}{\partial t} + \frac{\partial \omega u_i}{\partial x_i} = \frac{\partial}{\partial x_j}\left(D\omega_{eff}\frac{\partial \omega}{\partial x_j}\right) + 2\gamma S_{ij} - \beta\omega^2 + (1 - F_1)CD_{k\omega} \tag{4.11}$$

where $G_k =$ the generation of turbulent kinetic energy due to the mean velocity gradients. For detailed information about the parameters and constants, the reader is referred to Menter (1995).

4.2.2.3. $v^2 - f$ Model

Durbin (1995) developed a four-equation model by providing features for turbulence anisotropy and pressure-strain effects. The $v^2 - f$ model is based on the $k - \varepsilon - v^2$ model which includes turbulence kinetic energy (k), dissipation rate (ε), velocity variance (v^2), and a relaxing factor (f). The characteristics of the $v^2 - f$ model lie in between the $k - \varepsilon$ models and the Reynolds stress models. In this model, instead of kinetic energy (k), velocity variance (v^2) is used to estimate the eddy viscosity. The transport equations of the $v^2 - f$ model can be expressed by:

$$\frac{\partial k}{\partial t} + \frac{\partial k u_i}{\partial x_i} = \frac{\partial}{\partial x_j}\left(Dk_{eff}\frac{\partial k}{\partial x_j}\right) + S_k + P - \varepsilon \tag{4.12}$$

$$\frac{\partial \varepsilon}{\partial t} + \frac{\partial \varepsilon u_i}{\partial x_i} = \frac{C'_{\varepsilon 1} P - C_{\varepsilon 2} \varepsilon}{T} \frac{\partial}{\partial x_j}\left(D\varepsilon_{eff} \frac{\partial \varepsilon}{\partial x_j}\right) + S_\varepsilon \tag{4.13}$$

$$\frac{\partial \overline{V^2}}{\partial t} + \frac{\partial \overline{V^2} u_i}{\partial x_i} = kf - 6\overline{V^2} \frac{\varepsilon}{k} \frac{\partial}{\partial x_j}\left(Dk_{eff} \frac{\partial \overline{V^2}}{\partial x_j}\right) + S_{\overline{V^2}} \tag{4.14}$$

$$f - L^2 \frac{\partial^2 f}{\partial x_i^2} = (C_1 - 1) \frac{\frac{2}{3} - \frac{\overline{V^2}}{k}}{T} + C_2 \frac{P}{k} + \frac{\frac{5\overline{V^2}}{k}}{T} + S_f \tag{4.15}$$

where T = turbulence time, L = length scale, S_k, S_ε, $S_{\overline{V^2}}$, and S_f are user-defined source terms, and C_1, C_2, $C_{\varepsilon 1}$, $C_{\varepsilon 2}$, and $C'_{\varepsilon 1}$ are constants. For further details and constant values, the reader is referred to Durbin (1995).

4.2.3. Model Setup and Boundary Conditions

4.2.3.1. Test Case 1: CFD Modeling of Initial Stages of Dam-Break in Dry and Wet Bed Conditions (Cagatay and Kocaman, 2010)

In order to perform the numerical simulations, a rectangular horizontal tank 9.0 m long, 0.3 m high, and 0.3 m wide was modelled (Figure 4.1). All the channel surfaces were assumed as smooth. As the initial condition, the dam reservoir was defined as a volume of fluid 4.65 m long and 0.25 m high. To simulate dam-break flows in wet-bed conditions, an additional tailwater section 4.35 m long and two water depths of 0.025 m ($\alpha = 0.1$) and 0.10 m ($\alpha = 0.4$) were defined as tailwaters. The time steps δt were chosen as 0.02 s, which was determined based on the Courant–Friedrichs–Lewy (CFL) condition. The total running time of the modelling was about 1.5 s, since the objective was to investigate the immediate initial stages of dam-break flows.

In the numerical computations, the upstream, bottom, and sidewall boundaries were considered as walls due to the consistent reservoir length and there being no inflow into the reservoir. The downstream boundary was set as an outflow in the dry bed condition and a wall in the wet bed conditions since the downstream end was closed by a vertical steel plate to contain the tailwaters, and the top boundary was set as symmetry in order to account for the atmospheric pressure on the free surface. Since the water surface is defined by the VOF, zero shear stress and constant atmospheric pressure were applied as boundary conditions over the air–water interface (Hirt and Nichols, 1981). The standard wall function was employed to specify the boundary conditions at the walls. The effect of bed roughness was also investigated by setting the roughness values for bottom boundary and it was found that the results of the numerical models had not significant changes compared to the condition without bed roughness and the bed roughness was not so effective. The reason is that the length of flume at downstream of the gate was too short (4.35 m) and the total duration of the numerical simulation was quite short (1.5 s).

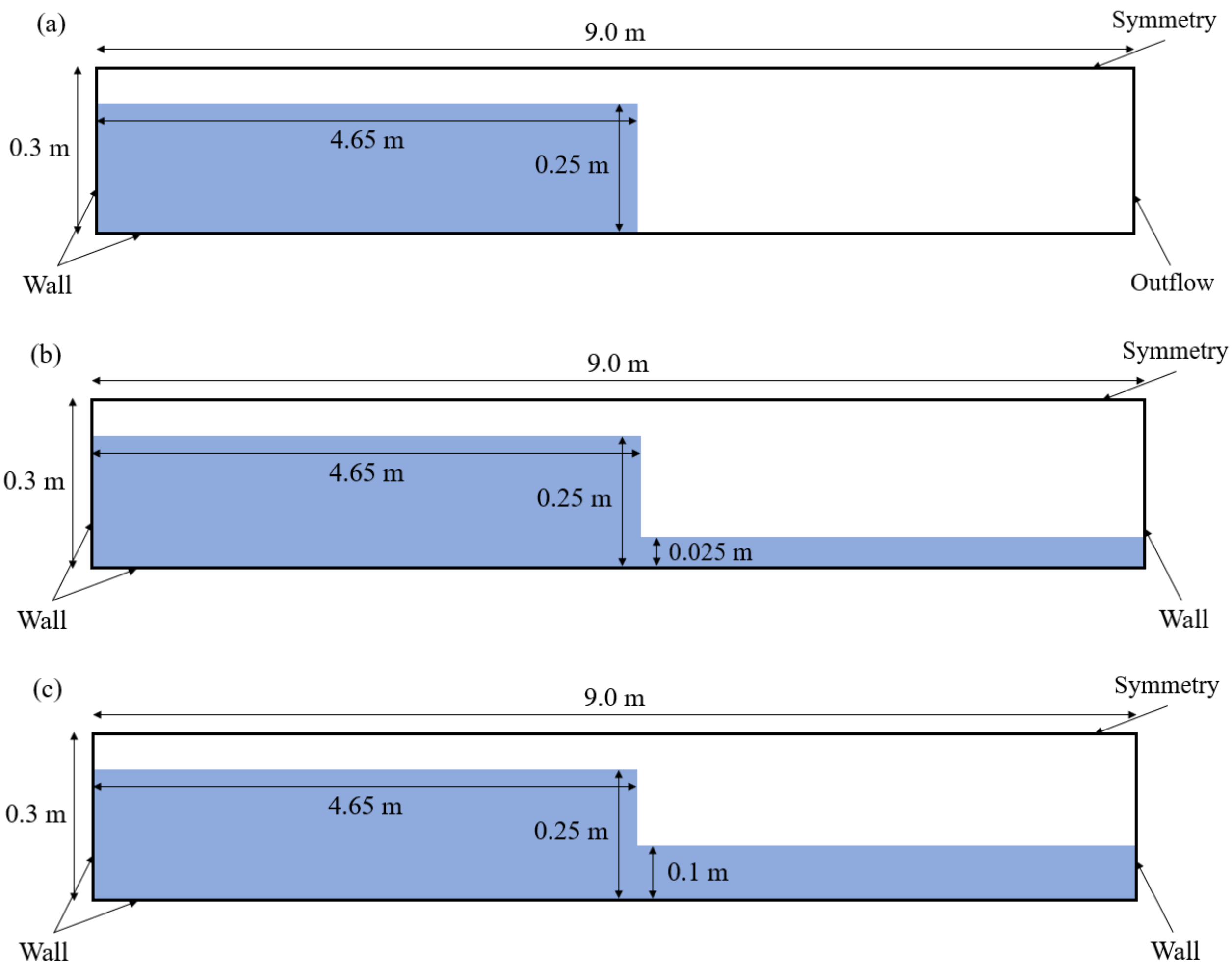

Figure 4.1. 2D view of numerical model setup and boundary conditions for Case 1 in: (a) dry bed condition, (b) wet bed condition with $\alpha = 0.1$, and (c) wet bed condition with $\alpha = 0.4$

The computational domain was subdivided into a mesh of fixed rectangular cells using Cartesian coordinates. Two block meshes were defined: the reservoir block mesh (upstream of the gate) and the main flume block mesh (downstream of the gate). Analysis of the mesh sensitivity for various grid sizes indicated that the mesh size was important only at the wave front, and consequently, the mesh sizes were not uniform in the simulations for Test Case 1 in the x and y directions. In the reservoir block mesh, the mesh size in the x direction ranged from 0.03 m at the upstream end to 0.004 m at the dam location. However, the mesh size in the x direction ranged from 0.004 m at the gate location to 0.03 m at the downstream end. The mesh size in the y direction ranged from 0.001 m at the bottom of the flume to 0.01 m at the top. The mesh size in the z direction was uniform at 0.005 m along the entire channel. The mesh systems consisted of a total of 3,132,000 cells for both the dry- and wet-bed conditions.

4.2.3.2. Test Case 2: CFD Modeling of Initial Stages of Dam-Break Flow in Presence of Trapezoidal Obstacle (Cagatay and Kocaman, 2011)

A rectangular horizontal tank 8.15 m long, 0.3 m high, and 0.3 m wide was modelled to set up the numerical simulation for Test Case 2. To define the initial condition, a volume of fluid 4.65 m long and 0.25 m high was considered as the reservoir of the dam. A symmetrical trapezoidal shaped obstacle 0.075 m high and with a base length of 1 m was defined and located 1.53 m downstream from the dam gate (Figure 4.2). The total duration of the simulation was 7.0 s, with time steps $\delta t =$ 0.02 s (based on the Courant–Friedrichs–Lewy condition). Similar to Test Case 1, all the channel and obstacle surfaces were assumed to be smooth.

In the numerical computations, the upstream, bottom, and sidewall boundaries were set as walls, since there was no flow into the channel and the reservoir length was constant. The top boundary was set as symmetry to account for the atmospheric pressure on the free surface, and the downstream boundary was set as an outflow, since the downstream end of the channel was open over the dry bed.

The computational domain consisted of a mesh with fixed rectangular cells using Cartesian coordinates. Various cell sizes were chosen to perform the mesh sensitivity analysis, and as a result, the mesh size in the x direction was ranged from 0.04 m at the upstream end to 0.004 m at the gate location. Downstream of the dam, the mesh size in the x direction was set to 0.004 m, while the mesh sizes in the y and z directions were uniform at 0.002 m and 0.005 m respectively along the entire channel. For Test Case 2, the mesh system consisted of 10,521,000 cells in total, which is very large in numerical modelling.

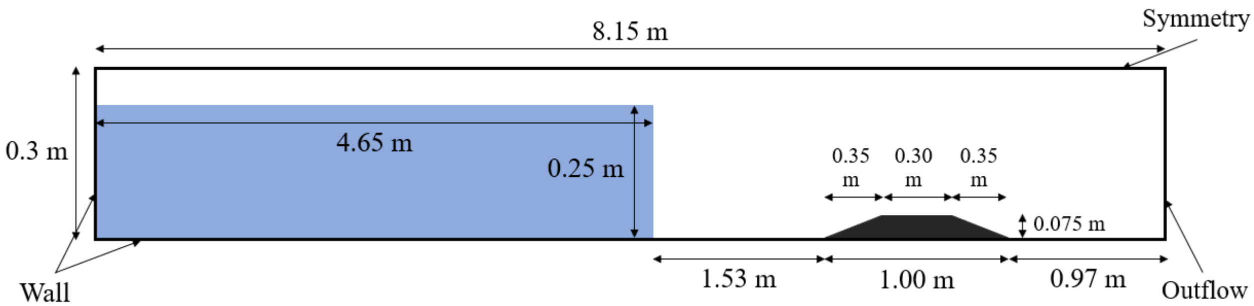

Figure 4.2. 2D view of numerical model setup and boundary conditions for Case 2 in the presence of a trapezoidal obstacle

4.3. Results and Discussion

4.3.1 Test Case 1: CFD Modeling of Initial Stages of Dam-break in Dry and Wet Bed Conditions

In this study, the initial stages of dam-break flows over a rectangular channel with dry bed and wet bed conditions were numerically investigated using a numerical model containing different turbulence models. Comparisons of the numerical results with experimental data (Cagatay and Kocaman, 2010) for all three turbulence models under one dry and two wet bed conditions with different tailwater depths are provided in Figures 4.3, 4.4, and 4.5, respectively. Flow depth (h) and distance along the channel (x) were non-dimensionalized by the initial reservoir depth h_0. Time t was also multiplied by $(g/h_0)^{1/2}$ in order to get the dimensionless time $T = t(g/h_0)^{1/2}$. The depth ratio, which is the tailwater depth over the reservoir depth, is defined as $\alpha = h_1/h_0$.

Three downstream bed conditions were investigated: a dry bed condition ($\alpha = 0$), a wet bed condition with a tailwater depth of 0.025 m ($\alpha = 0.1$), and a wet bed condition with a tailwater depth of 0.1 m ($\alpha = 0.4$).

Figure 4.3 illustrates the comparison between the predicted numerical results and the observed experimental data for the dry bed scenario with $\alpha = 0$. All the numerical models with the three turbulence closures adequately predicted the dam-break free surface profiles as time passed and as the flood waves travelled farther downstream; however, they overestimated the flow depth at the very early initial stage (T=1.13). Shigematsu et al. (2004) studied the turbulence effect during the initial stage of dam-breaks for dry bed cases and found that the surface profiles were mostly parabolic and the wave fronts became convex as time progressed, with pressure less than hydrostatic. As time passed, the pressure increased and became greater than hydrostatic due to bottom friction, caused a free surface vortex. For almost all the time frames, the numerical simulations overestimated the flow depth between $x/h_0 = -4$ and 0, while underestimating it at $x/h_0 > 0$. However, at *T*=2.75, the $k - \omega$ SST model well predicted the flow depth, while the realizable $k - \varepsilon$ and $v^2 - f$ models overestimated the wave-front flow depth. At the next time frame (T=3.88), the realizable $k - \varepsilon$ and $v^2 - f$ models agreed well with the measured free surface profile. In terms of flood wave arrival times, the results of the $k - \omega$ SST model perfectly matched with the experimental data except at *T*=1.13, while the flood waves moved more slowly in the realizable $k - \varepsilon$ and $v^2 - f$ models (Figure 4.3).

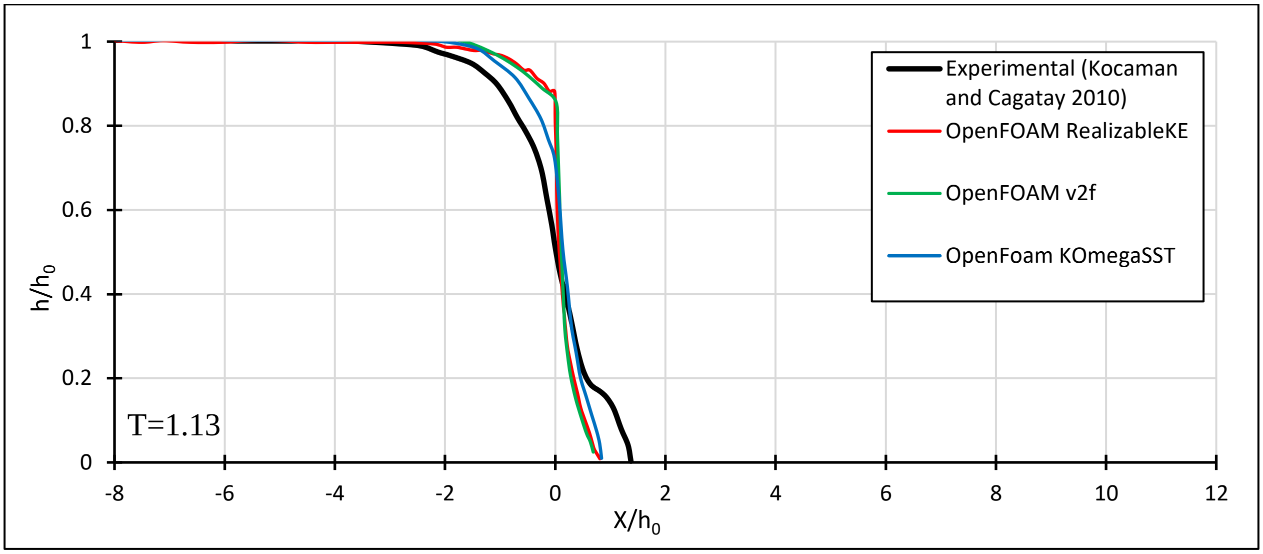
T=1.13
h/h0
X/h0
Experimental (Kocaman and Cagatay 2010)
OpenFOAM RealizableKE
OpenFOAM v2f
OpenFoam KOmegaSST
1
0.8
0.6
0.4
0.2
0
-8
-6
-4
-2
0
2
4
6
8
10
12

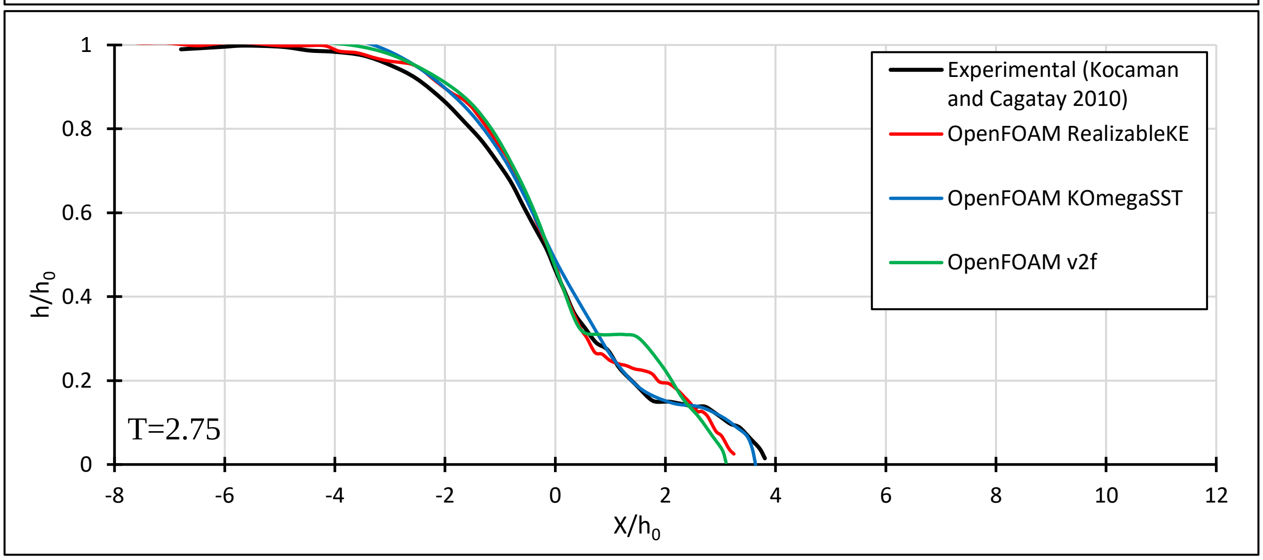
T=2.75
h/h0
X/h0
Experimental (Kocaman and Cagatay 2010)
OpenFOAM RealizableKE
OpenFOAM KOmegaSST
OpenFOAM v2f
1
0.8
0.6
0.4
0.2
0
-8
-6
-4
-2
0
2
4
6
8
10
12

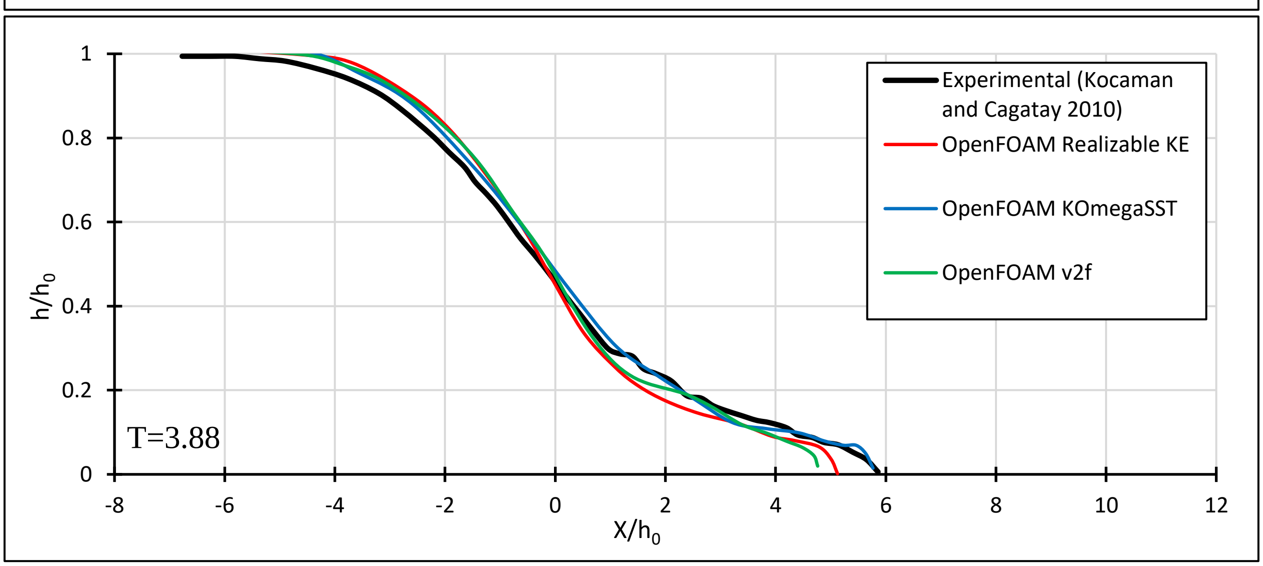
T=3.88
h/h0
X/h0
Experimental (Kocaman and Cagatay 2010)
OpenFOAM Realizable KE
OpenFOAM KOmegaSST
OpenFOAM v2f
1
0.8
0.6
0.4
0.2
0
-8
-6
-4
-2
0
2
4
6
8
10
12

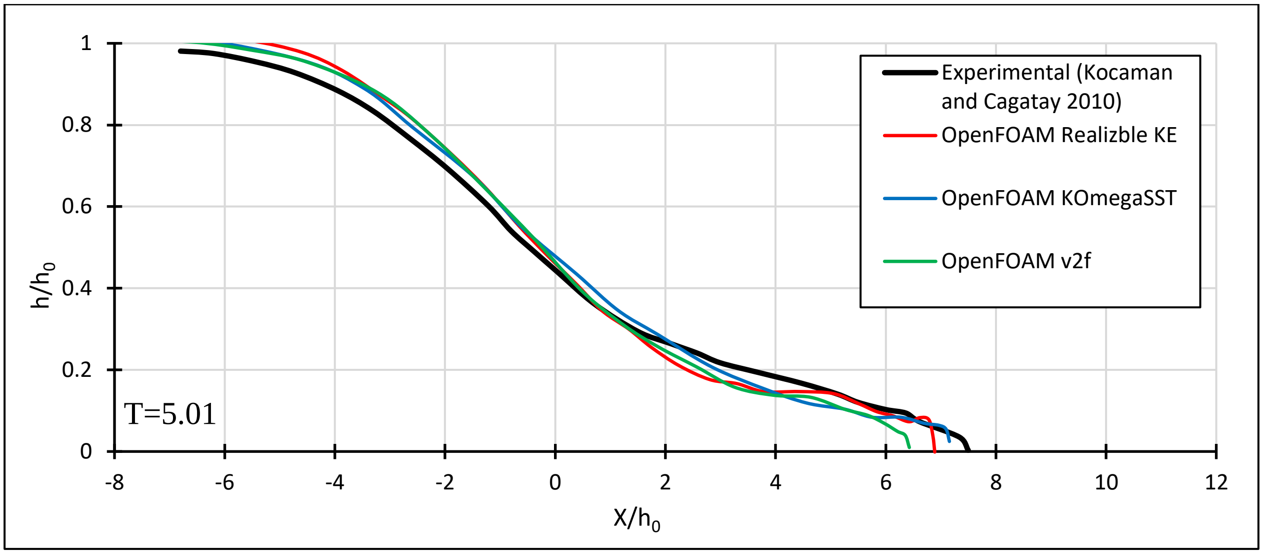

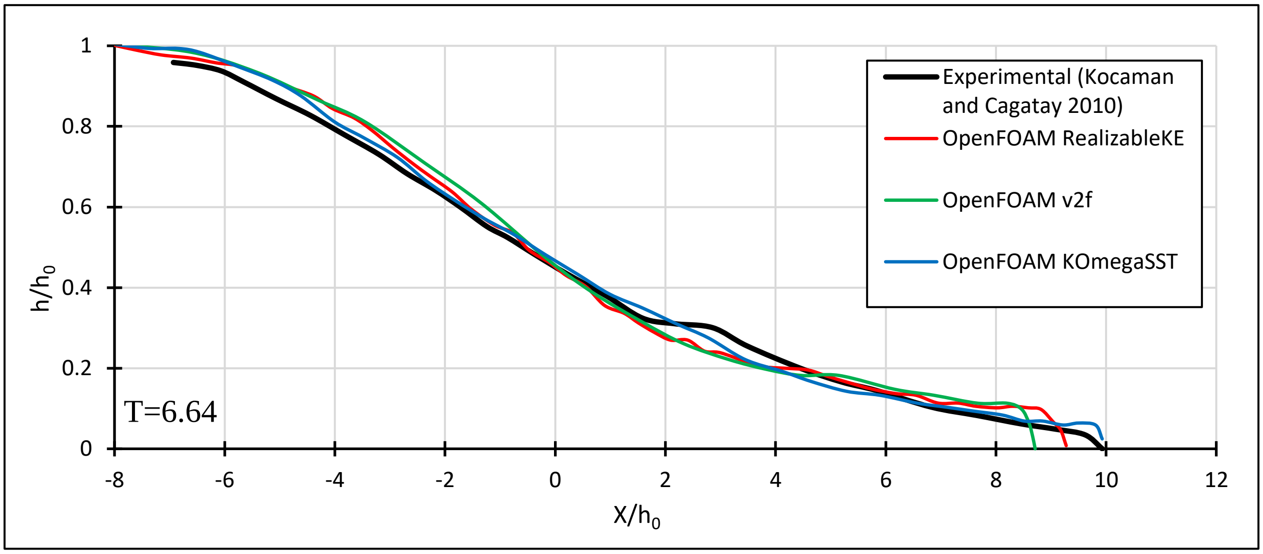

Figure 4.3. Model results of free surface profiles $h/h_0(x/h_0)$ during initial stages of dam break at various times $T=t(g/h_0)^{1/2}$ for dry bed with α=0.0

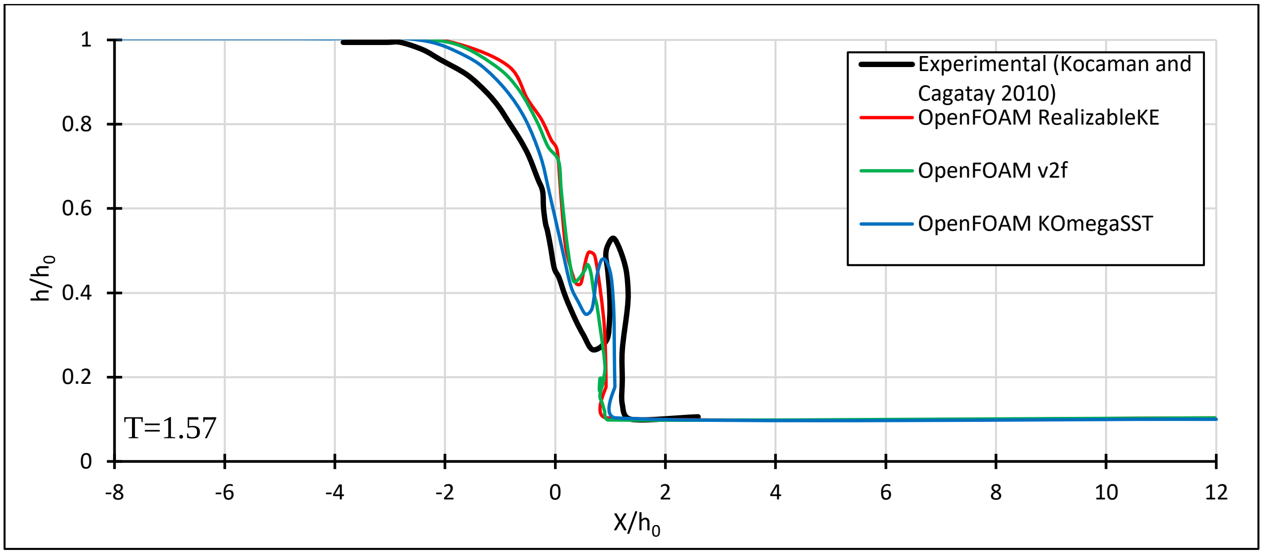
T=1.57
h/h0
X/h0
Experimental (Kocaman and Cagatay 2010)
OpenFOAM RealizableKE
OpenFOAM v2f
OpenFOAM KOmegaSST
1
0.8
0.6
0.4
0.2
0
-8
-6
-4
-2
0
2
4
6
8
10
12

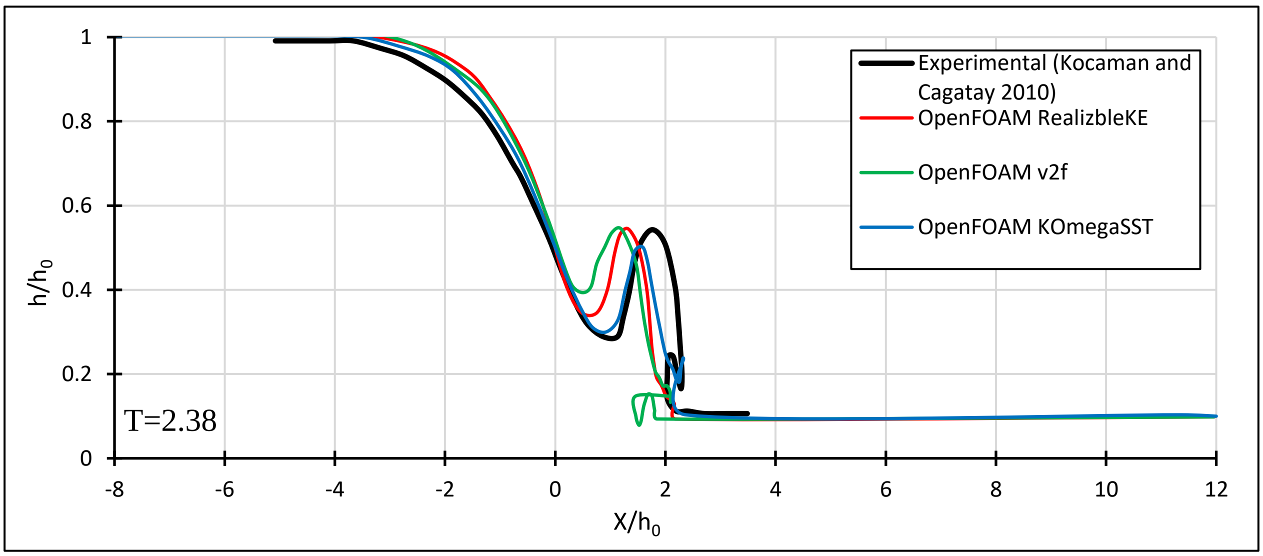
T=2.38
h/h0
X/h0
Experimental (Kocaman and Cagatay 2010)
OpenFOAM RealizbleKE
OpenFOAM v2f
OpenFOAM KOmegaSST
1
0.8
0.6
0.4
0.2
0
-8
-6
-4
-2
0
2
4
6
8
10
12

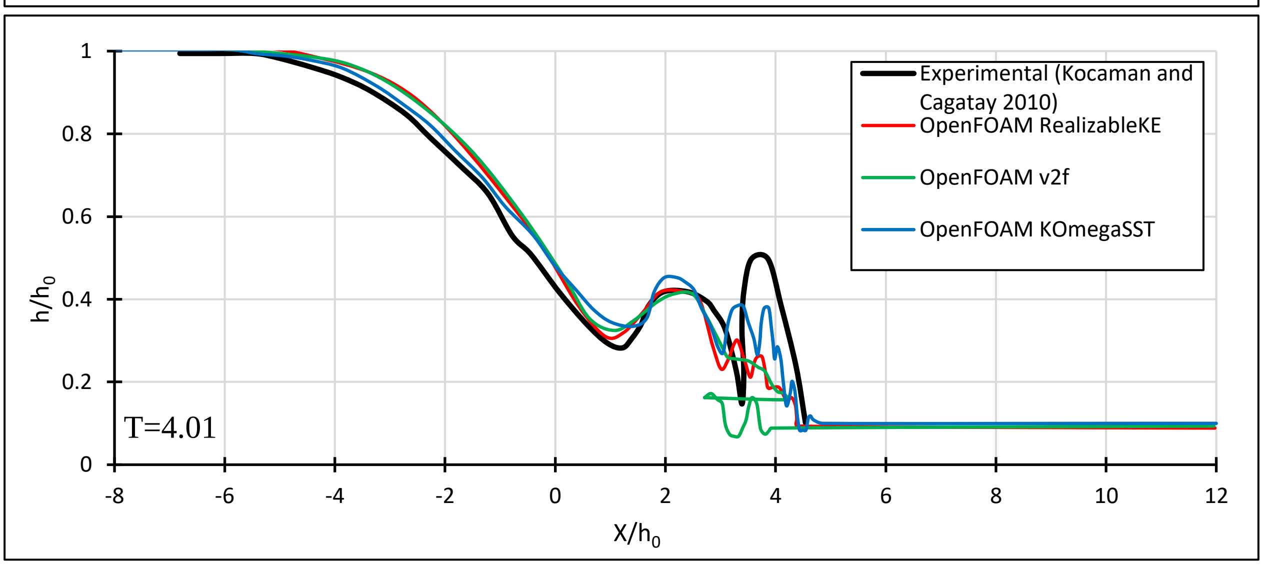
T=4.01
h/h0
X/h0
Experimental (Kocaman and Cagatay 2010)
OpenFOAM RealizableKE
OpenFOAM v2f
OpenFOAM KOmegaSST
1
0.8
0.6
0.4
0.2
0
-8
-6
-4
-2
0
2
4
6
8
10
12

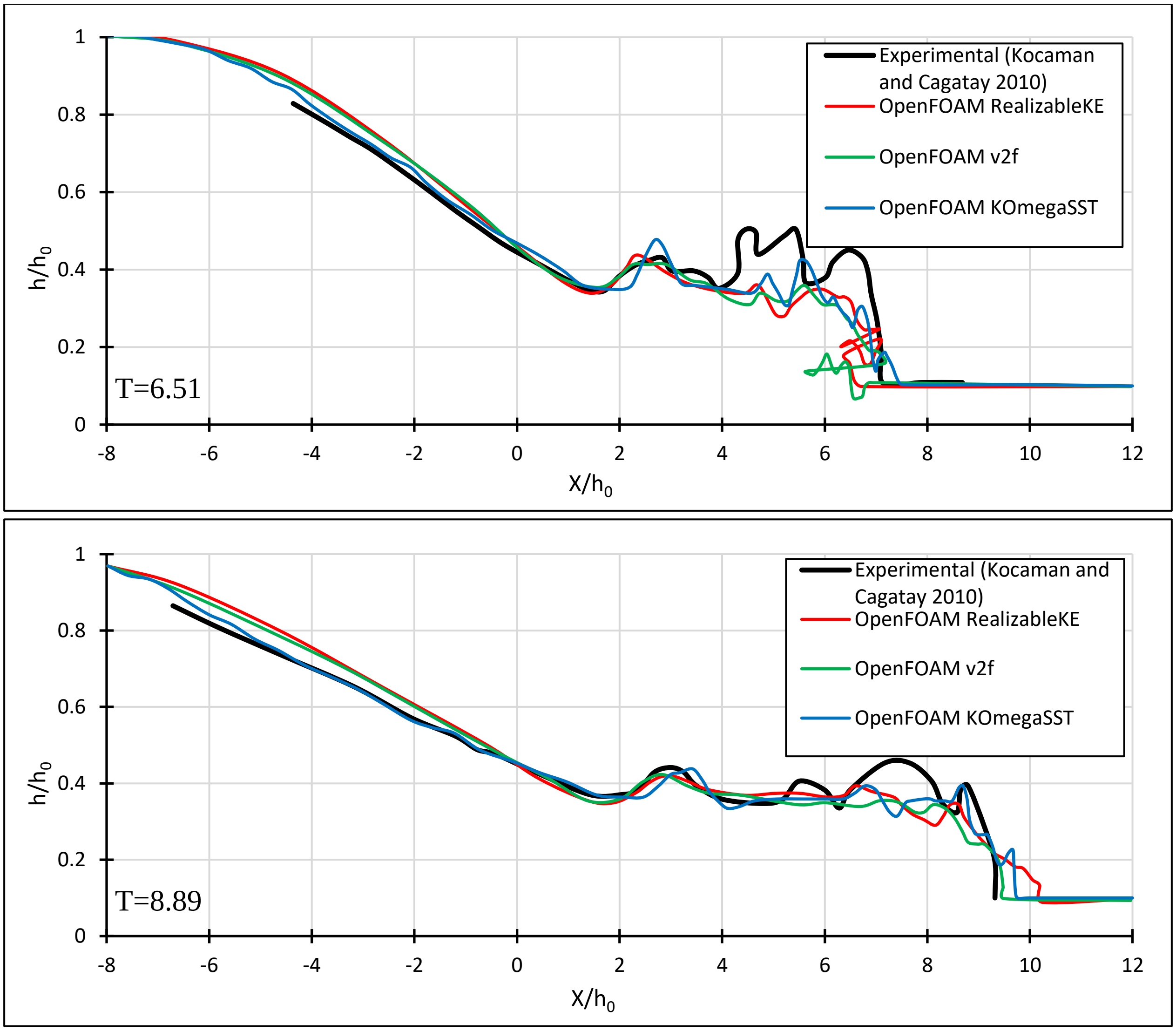

Figure 4.4. Model results of free surface profiles $h/h_0(x/h_0)$ during initial stages of dam break at various times $T=t(g/h_0)^{1/2}$ for wet bed with α=0.1

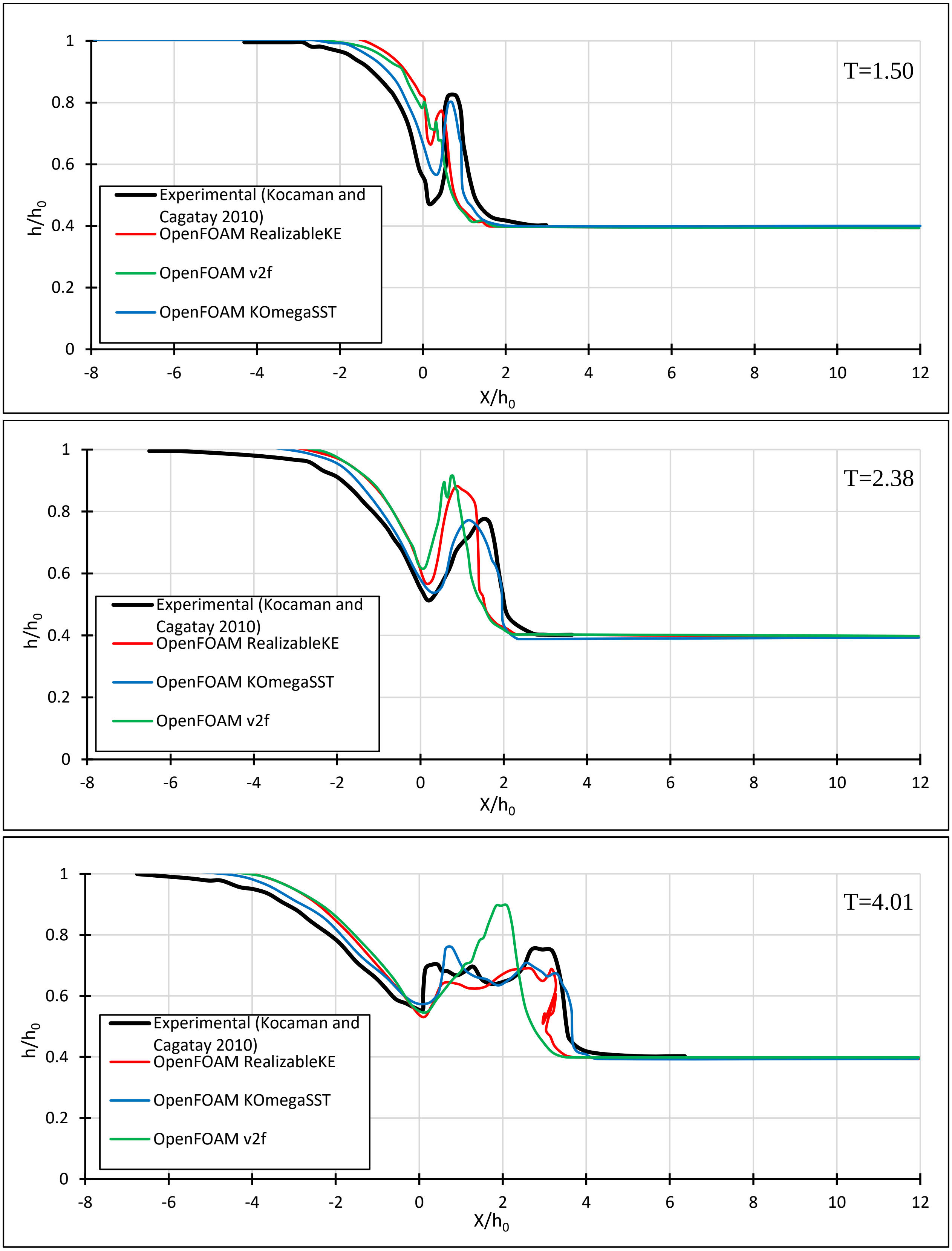

T=1.50
h/h0
X/h0
Experimental (Kocaman and Cagatay 2010)
OpenFOAM RealizableKE
OpenFOAM v2f
OpenFOAM KOmegaSST
T=2.38
h/h0
X/h0
Experimental (Kocaman and Cagatay 2010)
OpenFOAM RealizableKE
OpenFOAM KOmegaSST
OpenFOAM v2f
T=4.01
h/h0
X/h0
Experimental (Kocaman and Cagatay 2010)
OpenFOAM RealizableKE
OpenFOAM KOmegaSST
OpenFOAM v2f

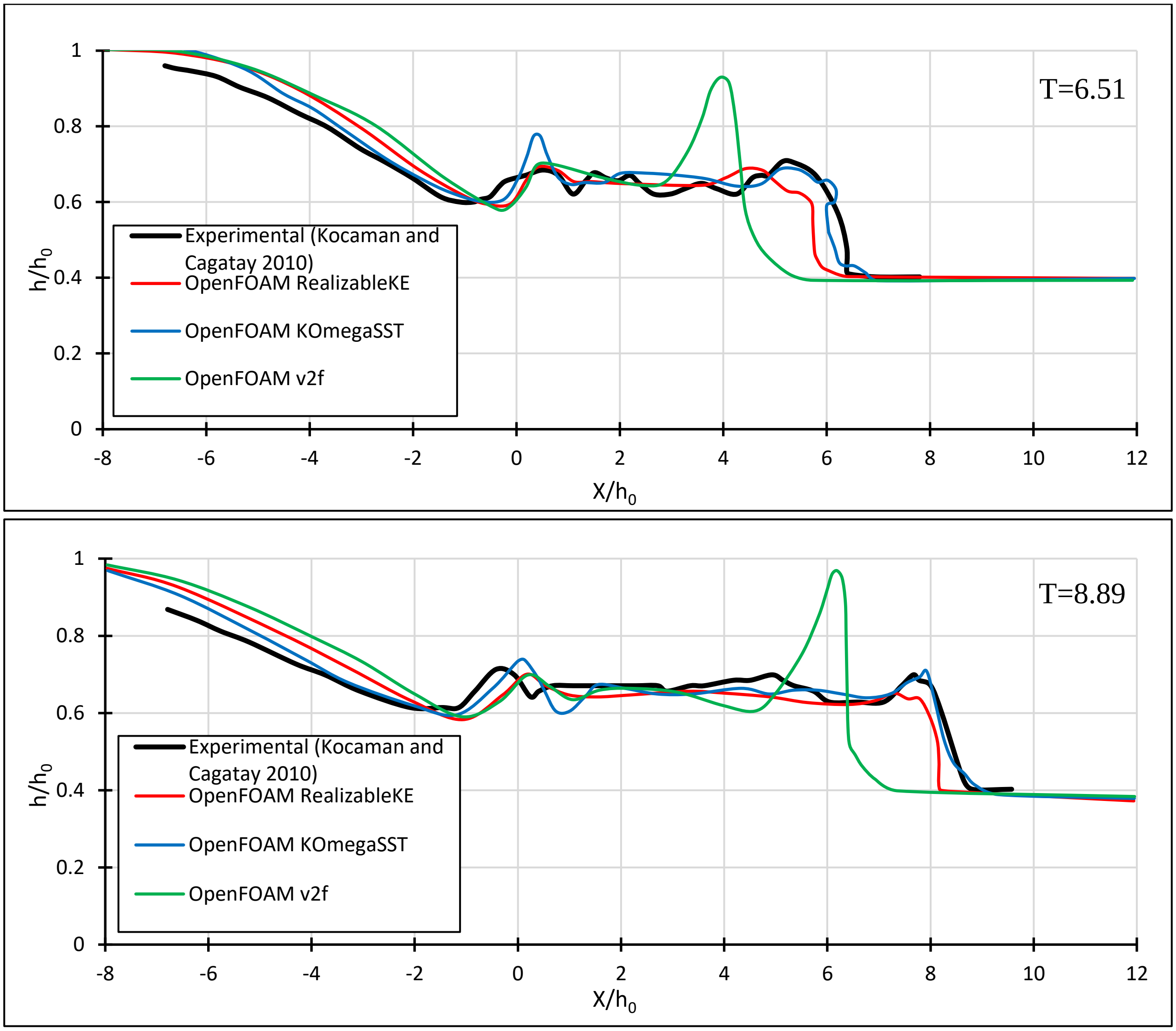

Figure 4.5. Model results of free surface profiles $h/h_0(x/h_0)$ during initial stages of dam break at various times $T=t(g/h_0)^{1/2}$ for wet bed with α=0.4

The comparison between the numerical results and the experimental data for the water free surface profile during the initial stages for the wet bed condition with $\alpha = 0.1$ are provided in Figure 4.4. After the dam-breaks in both of the wet bed conditions, the reservoir water would drag the tailwater, and the tailwater resisted the drag forces applied. Consequently, during the initial stage, the wave front would break and a jet-like flow would form downstream (Stansby et al., 1998). Based on the numerical results, it is obvious that the $k-\omega$ SST model performed better in capturing the water free surface profile than the realizable $k-\varepsilon$ and v^2-f models, with T=1.57 and T=2.38

respectively. However, in terms of flood peaks for the same time frames, the realizable $k-\varepsilon$ and v^2-f models had better results compared to the experimental data. For the subsequent time frames, the realizable $k-\varepsilon$ and v^2-f models were not able to properly reproduce the water free surface profiles, while the $k-\omega$ SST model had better results compared to the measured data. Also, there were some discrepancies in the flood timing in the results from the realizable $k-\varepsilon$ and v^2-f models for all time steps.

Figure 4.5 shows the comparison between the numerical simulations and the experimental results for the initial stages in the wet bed condition with deeper tailwater ($\alpha=0.4$). For almost all the time frames, the $k-\omega$ SST model had the capability of reproducing the water free surface profiles and maximum water depths with a reasonable agreement compared to the experimental results. The realizable $k-\varepsilon$ and v^2-f models underestimated the water free surface profiles and maximum water depths at *T*=1.50 and overestimated the flood peaks at *T*=2.38, while the $k-\omega$ SST model's results had a perfect match with the experimental data. For the next time frames (*T*>2.38), the results of the v^2-f model were not accurate compared to the measured data, while the $k-\omega$ SST and realizable $k-\varepsilon$ models were able to properly predict the water surface profiles and maximum water depths. In terms of flood arrival times, the $k-\omega$ SST model had the best results among all the models for almost all the time frames (Figure 4.5).

The initial stages of dam-break flood waves in both the dry- and wet-bed conditions could be predicted reasonably well using the numerical model combined with realizable $k-\varepsilon$, $k-\omega$ SST, and v^2-f models. However, for most of the scenarios and times, the performance of the $k-\omega$ SST model in capturing the wave front and water free surface profiles was significantly better than the other models.

4.3.2. Test Case 2: CFD Modeling of Initial Stages of Dam-Break Flow in Presence of Trapezoidal Obstacle

In this test case, the generation and propagation of dam-break flood waves and the formation of reflected waves over a rectangular channel in the presence of a symmetrical downstream trapezoidal obstacle has been investigated numerically by employing a numerical model with different turbulence closures. When the dam was removed, dam-break flood waves propagated downstream and travelled towards the obstacle. Once the flow reaches the obstacle, a part of the flow moves up the hump and travels towards the downstream end, while the other part is reflected off the obstacle; then, the reflected waves form a negative bore which moves in the upstream direction. The turbulence effects are significant, especially on the reflected wave front. The results of the numerical model were compared with previous experimental data (Kocaman and Cagatay 2011) in order to assess and evaluate the performance of the various turbulence models.

Figure 4.6 shows the comparisons between the computed water free surface profiles and the measured data for dam-break flood waves over a dry bed with a trapezoidal bottom obstacle at various times. Flow depth (h) and distance along the channel (x) were non-dimensionalized by the initial reservoir depth h_0, while time t was multiplied by $(g/h_0)^{1/2}$ to obtain the dimensionless time $T = t(g/h_0)^{1/2}$. At *T*=11.90, the free surface profile was accurately predicted by all three turbulence models. The realizable $k - \varepsilon$ and $v^2 - f$ models underestimated the free surface profile at the next time frame (*T*=17.54) and were not able to capture the maximum water depth, while the $k - \omega$ SST model adequately predicted both the free surface profile and the maximum flow depth. At *T*=20.67, the realizable $k - \varepsilon$ and $v^2 - f$ models underestimated the flow depth and were not capable of capturing the formation of the negative bore behind the bump compared to the experimental data, while the $k - \omega$ SST model performed better in predicting the maximum flow depth and reproducing the formation of the negative surge. The rising wave in the RANS models was steep and convex, while it was concave in the experiments. In terms of propagation of the reflected waves, the speed of the negative bore front was much lower in the numerical simulations compared to the measured data. These differences can be explained by the formation of a hydraulic jump and the occurrence of a mixed flow regime on the free surface profile behind the hump. Moreover, plunging-type wave-breaking in RANS models is generated, while spilling-type wave-breaking formed in the experiment. Despite the presence of some discrepancies, the $k - \omega$ SST model was able to accurately predict the free surface profiles and the formation and propagation of reflected waves.

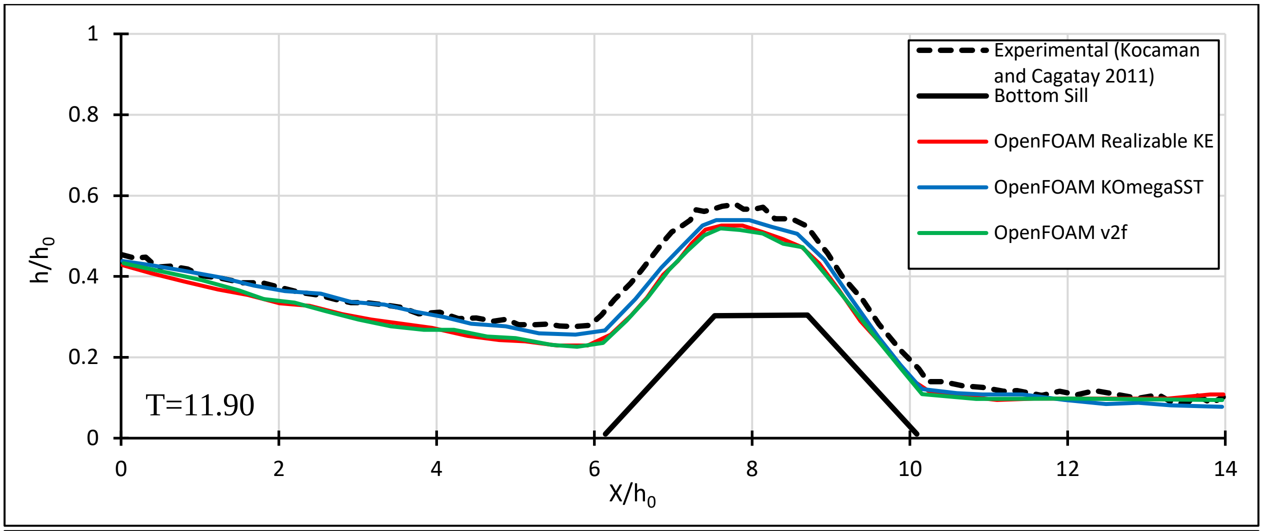

Experimental (Kocaman and Cagatay 2011)
Bottom Sill
OpenFOAM Realizable KE
OpenFOAM KOmegaSST
OpenFOAM v2f
T=11.90
h/h0
X/h0

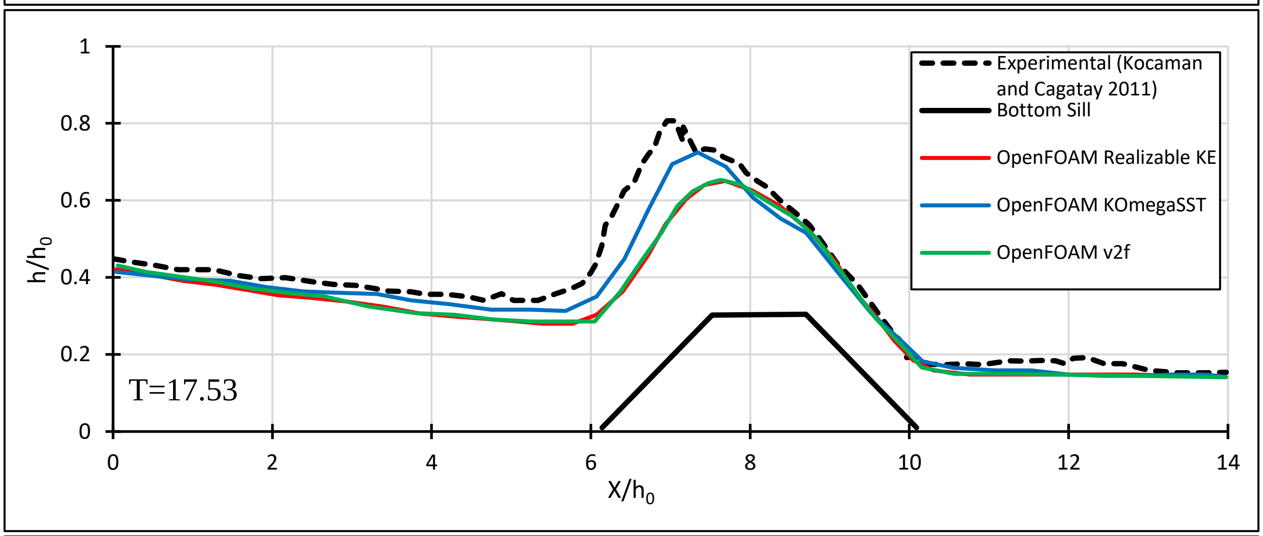

Experimental (Kocaman and Cagatay 2011)
Bottom Sill
OpenFOAM Realizable KE
OpenFOAM KOmegaSST
OpenFOAM v2f
T=17.53
h/h0
X/h0

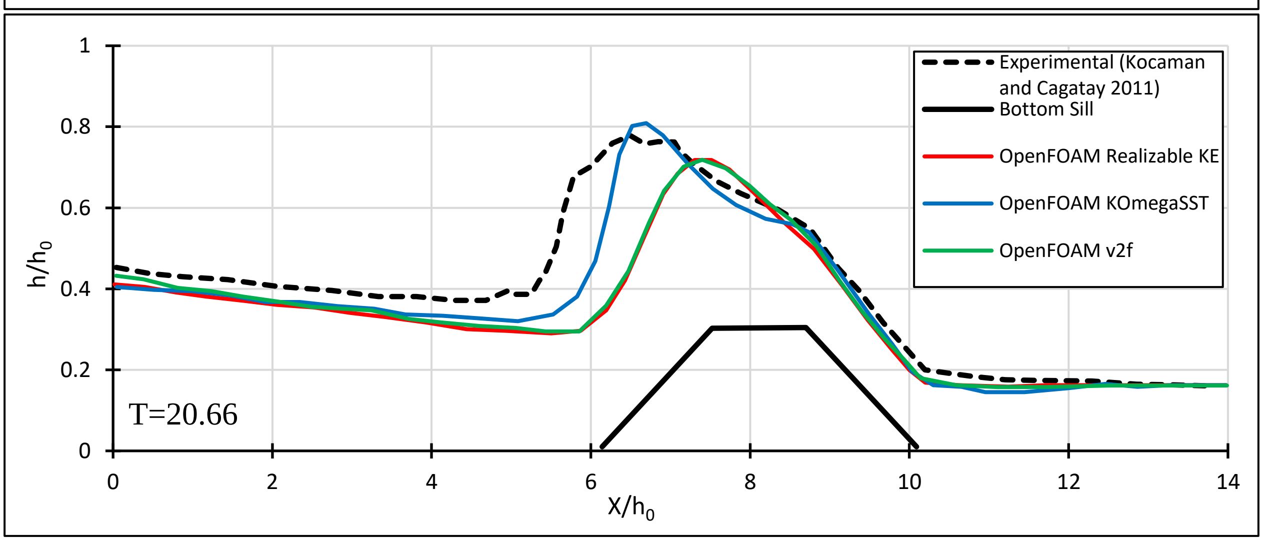

Experimental (Kocaman and Cagatay 2011)
Bottom Sill
OpenFOAM Realizable KE
OpenFOAM KOmegaSST
OpenFOAM v2f
T=20.66
h/h0
X/h0

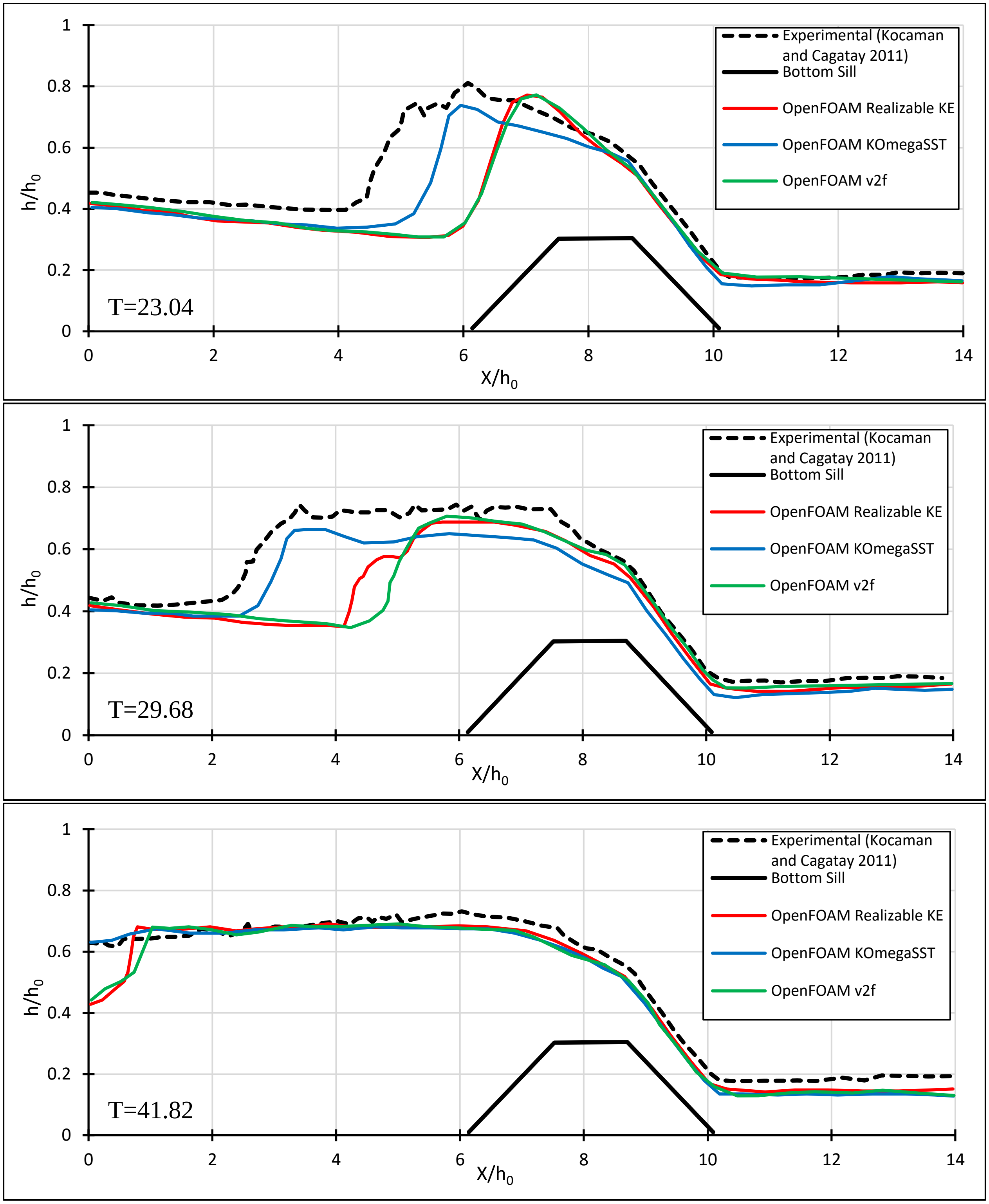

Figure 4.6. Model results of free surface profiles $h/h_0(x/h_0)$ at various times $T=t(g/h_0)^{1/2}$ for dam-break flow in presence of the trapezoidal obstacle

4.3.3. Numerical Model Evaluation

In order to evaluate the performance of the numerical model combined with the various turbulence models, the Root Mean Square Error (RMSE) method is used to measure the difference between the values estimated by the numerical model and the values observed from the experiments. The RMSE can be expressed as:

$$RMSE = \sqrt{\frac{\sum_{i=1}^{n}\left(X_{obs,i}-X_{model,i}\right)^2}{n}} \tag{4.16}$$

where $n =$ number of samples, $X_{obs} =$ observed values, and $X_{model} =$ modelled values at time/place i. The best fit between the modelled values and the observed data would have an RMSE=0.

Also, dimensionless forms of the RMSE are useful due to the capability of comparing RMSE with different units. In this study, the normalized RMSE is calculated by normalizing the RMSE to the range of the observed values, and can be expressed as:

$$NRMSE = \frac{RMSE}{X_{obs,max}-X_{obs,min}} \tag{4.17}$$

Error analyses of the free-surface profile results obtained by the different turbulence models for Test Cases 1 and 2 are summarized in Tables 4.1–4.3 and Table 4.4, respectively.

Table 4.1. RMSE and NRMSE values for the free surface profile for Test Case 1 with $\alpha = 0$

Dry Bed Condition $\boldsymbol{\alpha = 0}$		**Turbulence Models**		
		Realizable $k - \varepsilon$ Model	$k - \omega$ SST Model	$v^2 - f$ Model
T=1.13	RMSE	0.130	0.084	0.160
	NRMSE	0.264	0.172	0.326
T=2.75	RMSE	0.028	0.022	0.045
	NRMSE	0.031	0.025	0.051
T=3.88	RMSE	0.036	0.022	0.029
	NRMSE	0.039	0.023	0.031
T=5.01	RMSE	0.038	0.029	0.035
	NRMSE	0.041	0.032	0.038
T=6.64	RMSE	0.030	0.020	0.037
	NRMSE	0.034	0.023	0.042

Table 4.2. RMSE and NRMSE values for the free surface profile for Test Case 1 with $\alpha = 0.1$

Wet Bed Condition $\boldsymbol{\alpha = 0.1}$		**Turbulence Models**		
		Realizable $k - \varepsilon$ Model	$k - \omega$ SST Model	$v^2 - f$ Model
T=1.57	RMSE	0.185	0.064	0.178
	NRMSE	0.208	0.072	0.200
T=2.38	RMSE	0.140	0.088	0.141
	NRMSE	0.158	0.099	0.159
T=4.01	RMSE	0.099	0.062	0.090
	NRMSE	0.175	0.110	0.160
T=6.51	RMSE	0.060	0.053	0.060
	NRMSE	0.092	0.082	0.093
T=8.89	RMSE	0.049	0.027	0.045
	NRMSE	0.099	0.054	0.091

Table 4.3. RMSE and NRMSE values for the free surface profile for Test Case 1 with $\alpha = 0.4$

Wet Bed Condition $\boldsymbol{\alpha = 0.4}$		**Turbulence Models**		
		Realizable $k - \varepsilon$ Model	$k - \omega$ SST Model	$v^2 - f$ Model
T=1.50	RMSE	0.142	0.072	0.132
	NRMSE	0.245	0.125	0.228
T=2.38	RMSE	0.079	0.039	0.061
	NRMSE	0.134	0.066	0.102
T=4.01	RMSE	0.049	0.034	0.125
	NRMSE	0.086	0.059	0.220
T=6.51	RMSE	0.072	0.028	0.126
	NRMSE	0.226	0.089	0.398
T=8.89	RMSE	0.036	0.031	0.130
	NRMSE	0.180	0.155	0.657

Table 4.4. RMSE and NRMSE values for the free surface profile for Test Case 2

Dry Bed Condition		**Turbulence Models**		
		Realizable $k - \varepsilon$ Model	$k - \omega$ SST Model	$v^2 - f$ Model
T=11.90	RMSE	0.043	0.026	0.047
	NRMSE	0.143	0.085	0.155
T=17.53	RMSE	0.084	0.046	0.088
	NRMSE	0.321	0.175	0.335
T=20.66	RMSE	0.119	0.079	0.115
	NRMSE	0.449	0.298	0.437
T=23.04	RMSE	0.166	0.098	0.170
	NRMSE	0.692	0.410	0.706
T=29.68	RMSE	0.132	0.069	0.134
	NRMSE	0.501	0.263	0.510
T=41.82	RMSE	0.032	0.041	0.037
	NRMSE	0.072	0.091	0.082

Table 4.1 shows the calculation of the RMSE values for Test Case 1 in the dry bed condition ($\alpha = 0$) with the three turbulence models at various dimensionless times. It was observed that the three turbulence models generally had low RMSE values, with all of them below 0.170 at various time steps. Also, Table 4.1 reflects that all three turbulence models produced acceptable results compared to the experimental data during the initial stages for the dry bed condition, and that the $k - \omega$ SST model achieved the best RMSE result of 0.020 compared to the other turbulence models. Furthermore, the highest RMSE values for each turbulence model are observed at the earliest stage of the dam-break (*T*=1.13). As time passed, the RMSE values decreased, demonstrating the ability of numerical models to reproduce dam-break flows in a dry bed condition over time.

The RMSE values for Test Case 1 in the wet bed conditions with $\alpha = 0.1$ and $\alpha = 0.4$ are provided in Tables 4.2 and 4.3, respectively. Similar to the dry bed condition, the highest RMSE values were observed at the earliest stage (*T*=1.57 for $\alpha = 0.1$ and *T*=1.50 for $\alpha = 0.4$), with the highest value of 0.185 from the realizable $k - \varepsilon$ model in the wet bed with shallower tailwater. As time passed, the RMSE values decreased for all the turbulence models. However, the RMSE result from the $k - \omega$ SST model increased at *T*=2.38 for the wet bed condition with $\alpha = 0.1$, and the RMSE values from the $v^2 - f$ model also increased over time (*T*=4.01-8.89) in the wet bed condition with $\alpha = 0.4$.

The RMSE values for Test Case 2, which are provided in Table 4.4, show that all three turbulence models are able to predict the formation and propagation of positive and negative bores in the presence of an obstacle. The performance of the $k - \omega$ SST model was slightly better than those of the other two models at different times, since it had lower RMSE values. The highest RMSE values for each turbulence model were observed at *T*=23.04, when the flood waves were reflected and started travelling in the upstream direction. At the initial stage (T=11.90), the $k - \omega$ SST model performed better in predicting the free surface profile, with RMSE=0.026, while at *T*= 41.82, the flow depth estimations of the realizable $k - \varepsilon$ and $v^2 - f$ models were better, with RMSE=0.032 and 0.037, respectively.

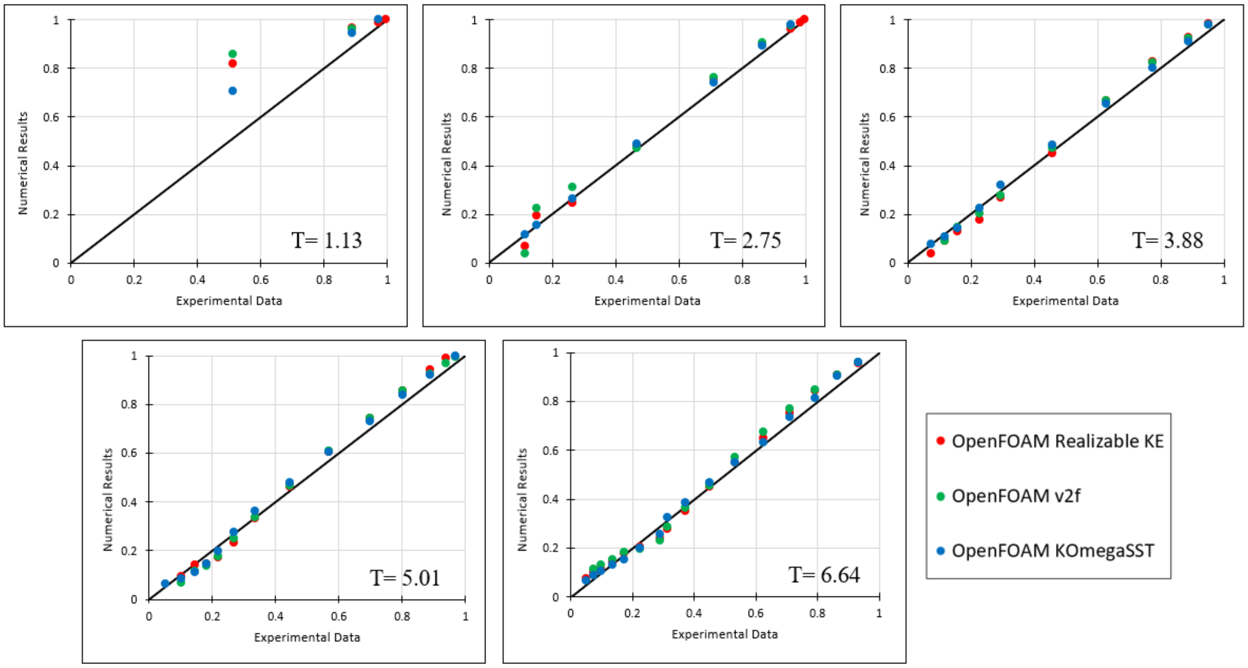

Figure 4.7. Numerical results versus the experimental data for Test Case 1 with $\alpha = 0$

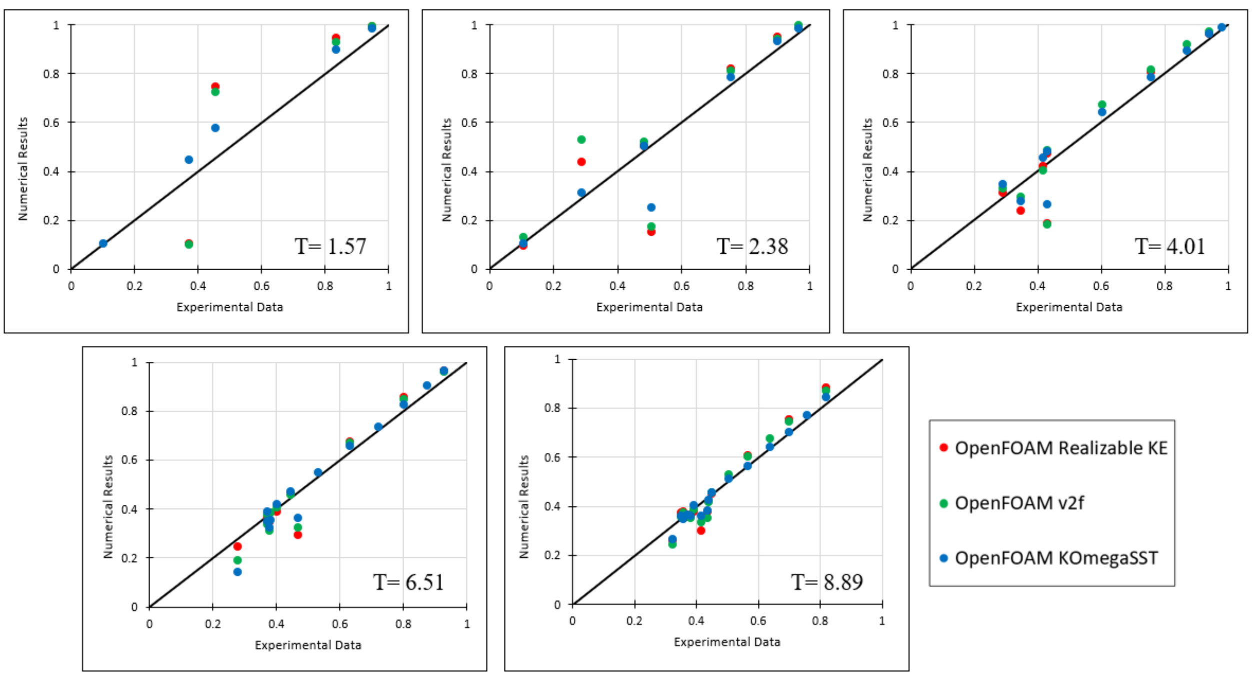

Figure 4.8. Numerical results versus the experimental data for Test Case 1 with $\alpha = 0.1$

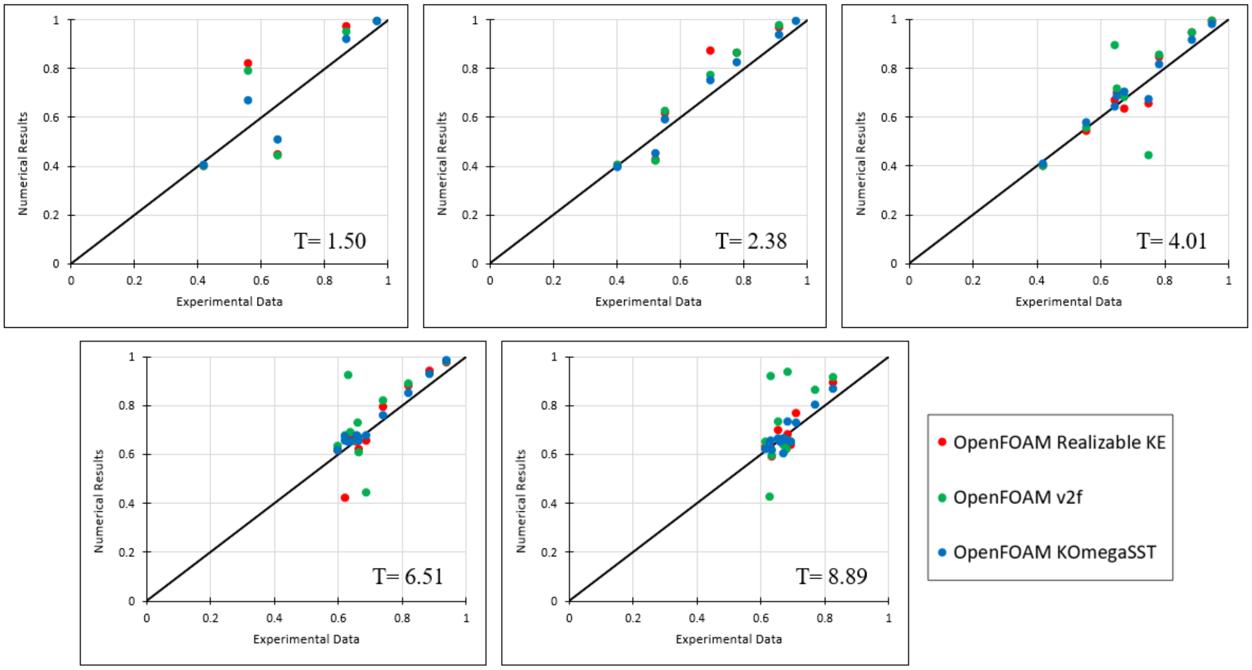

Figure 4.9. Numerical results versus the experimental data for Test Case 1 with $\alpha = 0.4$

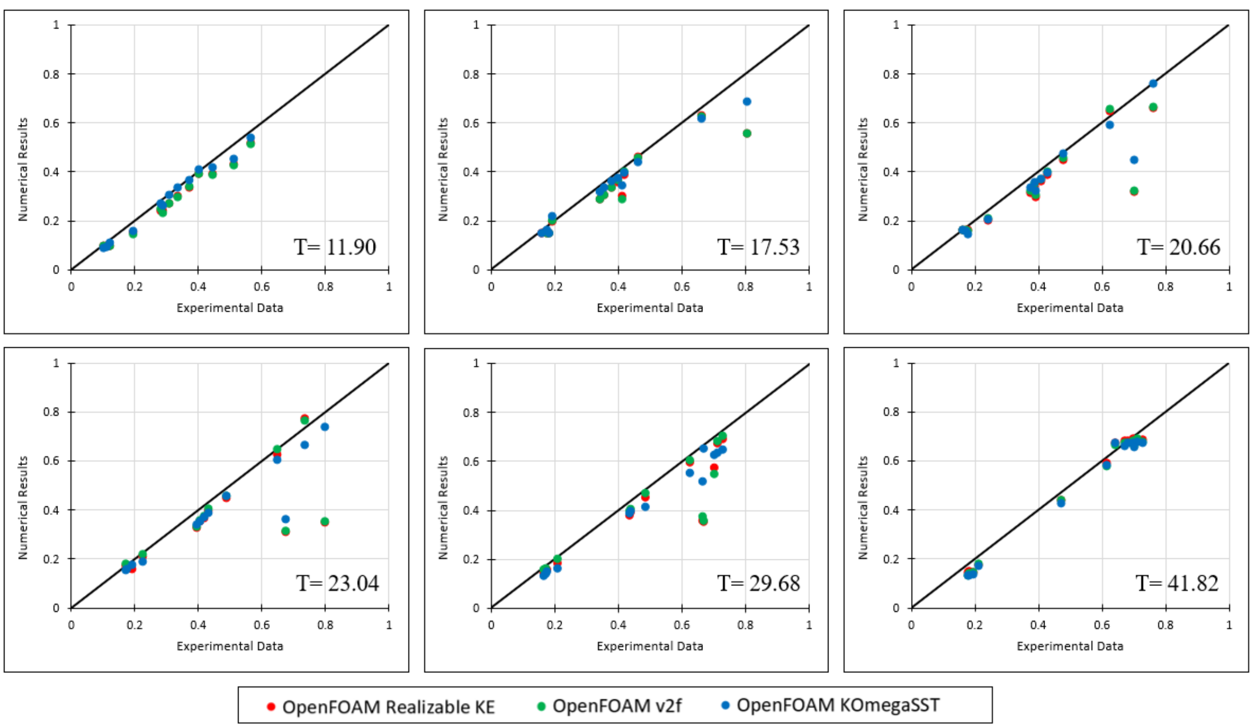

Figure 4.10. Numerical results versus the experimental data for Test Case 2

Figures 4.7 to 4.10 illustrate the accuracy of each turbulence models to predict the experimental data. Considering Test Case 1, in the dry bed condition (Figure 4.7), all the turbulence models had good accuracy in predicting the experimental data, except for the very first time frame. From Figures 4.8 and 4.9, it can be seen that the performance of the $k-\omega$ SST turbulence model in reproducing the experimental data was slightly better than those of the other turbulence models. The ability of the turbulence models in estimating the measured data for Test Case 2 (Figure 4.10) showed that the $k-\omega$ SST model performed reasonably well, while the realizable $k-\varepsilon$ and v^2-f models had a good agreement with the experimental data only for the first and last time steps (T=11.90 and T=41.82 respectively). For both the test cases and most of the time steps, the $k-\omega$ SST model was capable of reproducing the free surface profiles with an acceptable accuracy compared to the other turbulence models.

The $k-\omega$ SST model often performs well when dealing with a single-phase fluid running on a surface due to its ability to account for the flow separation and transport of the shear stress. The shear stress between the water and bed determines the runout distance from the breach location, and therefore this model can better capture the free surface boundary in terms of wave front propagation downstream. Moreover, the flow separation feature of the $k-\omega$ SST model can better predict the complex wave breaks that were observed in the simulations performed in this study.

4.4. Conclusions

In this study, two recent experimental studies on dam-break flows were investigated numerically to reveal the effect of an abrupt channel bottom variation on unsteady flows, and to better understand dam-break flow characteristics during the initial stages over both dry and wet bed conditions. Three-dimensional numerical models were employed using OpenFOAM to solve Reynolds-Averaged Navier-Stokes equations with different turbulence models. First, the initial stages of dam-break flows over a horizontal rectangular channel with one dry-bed and two wet-bed conditions with two tailwater depths were scrutinized (Kocaman and Cagatay, 2010). Next, the formation and propagation of reflected waves and negative bores in a rectangular channel with a dry bed condition in the presence of a symmetrical trapezoidal bottom obstacle were investigated

(Kocaman and Cagatay, 2011). To evaluate and assess the performance of the numerical models in capturing and predicting the flow characteristics, three different RANS turbulence models were used: the realizable $k - \varepsilon$ model, the $k - \omega$ SST model, and the $v^2 - f$ model. For all the test cases, the results of the free surface profiles from the numerical simulations were compared to the results of experiments, and a summary of the findings from the current study is provided as follows:

- Solutions of RANS equations with various turbulence models can reasonably simulate and predict the overall process of the formation and propagation of dam-break flood waves under both dry and wet bed conditions and in the presence of a bottom obstacle.
- In the dry-bed condition, except for the very early dam-break stage, all the turbulence models accurately predicted the free surface profiles, with the best results coming from the $k - \omega$ SST turbulence model.
- For the wet bed conditions, except for the $v^2 - f$ model, the performances of the numerical models were reasonably acceptable in reproducing the free surface profile with $\alpha = 0.4$. However, comparisons of the results of the realizable $k - \varepsilon$ and $v^2 - f$ models showed some deviations in predicting the free surface profiles in the wet bed condition with $\alpha = 0.1$, specifically at early stages.
- The $k - \omega$ SST model is capable of predicting the formation and propagation of dam-break flows and reflected waves in the presence of a bottom obstacle, while the realizable $k - \varepsilon$ and $v^2 - f$ models showed some discrepancies in predicting the formation and propagation of negative bores behind the obstacle.
- Comparisons of the free surface profiles from the experimental data and the numerical models and analysis of the performance of the turbulence models illustrate that the $k - \omega$ SST model performs better in capturing and accurately reproducing dam-break flow characteristics compared to the realizable $k - \varepsilon$ and $v^2 - f$ models.

Chapter 5. Conclusions and Recommendations for Future Research

5.1. Conclusions

The current study was performed in an effort to investigate the mechanisms and behavior of dam-break flows in a horizontal rectangular channel with various downstream bed conditions. The initial stages of dam-break propagation over dry- and wet-bed conditions were studied numerically and compared to available experimental data from the literature. Also, the effect of the presence of a trapezoidal-shaped bottom obstacle on the behavior of dam-break flood waves and reflected waves was investigated and compared to measured data. Three-dimensional (3-D) Computational Fluid dynamics (CFD) models were developed and used to solve the unsteady RANS (Reynolds-averaged Navier-Stokes) equations in order to determine the free surface profiles, and the performance of different RANS turbulence models has been assessed, with the standard $k-\varepsilon$, RNG $k-\varepsilon$, realizable $k-\varepsilon$, $k-\omega$ SST , and v^2-f turbulence models being studied using an OpenFOAM model. The results of the numerical simulations were collected and comprehensively compared to the experimental data. A summary of the most important conclusions is provided below:

- Flow characteristics observed during the initial stages of dam breaks over dry- and wet-bed conditions exhibited various patterns.
- Despite the presence of some discrepancies in prediction of dam-break flows under different conditions, the developed numerical models were able to simulate dam-break flows with a reasonable accuracy.
- The effect of water depth present on the bed downstream of the releasing gate was investigated, and it was found that the free surface has a smooth, curved profile for the dry-bed case, while for wet-bed conditions, jet-like and mushroom-like wave fronts were observed during the earliest stage of the dam-breaks for shallower and deeper tailwater depths, respectively.

- The evaluation of the performance of the various turbulence models demonstrated that the RNG $k - \varepsilon$ turbulence model performed slightly better than the other turbulence models in accurately predicting dam-break flow characteristics during the initial stages over both dry- and wet-bed conditions.
- When investigation the dam-break flow features in the presence of a bottom obstacle, the $k - \omega$ SST model was able to predict and estimate the formation and propagation of reflected waves with more accuracy compared to the other turbulence models.

5.2. Recommendations for Future Research

Based on the results obtained from this study, the following recommendations are proposed for the numerical modeling of dam-break flows in future studies:

- More three-dimensional numerical models are needed to better understand the formation and propagation of dam-break flows in presence of more shapes of obstacles.
- A wide range of numerical models using various turbulence models have been applied for the cases considered in this study. However, evaluation and comparison of the performance of more turbulence models, including LES and DNS models, are needed in order to obtain more reliable and accurate data on dam-break flow characteristics.
- The effect of reservoir geometry on the generation of dam-break flood waves should be investigated both experimentally and numerically to assess its effect on the flow in both upstream and downstream reaches of the dam.
- In this study, dam-break flow characteristics were studied over a horizontal rectangular channel; however, in reality, dam-break flood waves propagate over channels with various topographies. Therefore, further investigations on the effects of irregularities present in a channel cross-section, such as channel contractions and expansions, need to be performed.
- In this study, the influence of downstream water depth (i.e., under wet-bed conditions) was studied for the initial stages of dam-break flows; however, further analyses of the effects of various bed conditions with a wider range of depth ratios on dam-break flood-wave propagation are needed.

References

1. Abdolmaleki, K., Thiagarajan, P., Morris-Thomas, M.T. (2004). Simulation of the dam break problem and impact flows using a Navier-Stokes Solver. 15th Australasian Fluid Mechanics Conference Sydney, Australia, 13–17.
2. Atabak Feizi Khankandi , Ahmad Tahershamsi & Sandra Soares-Frazão (2012) Experimental investigation of reservoir geometry effect on dam-break flow, Journal of Hydraulic Research, 50:4, 376-387. https://doi.org/10.1080/00221686.2012.690974
3. Bell, S.W., Elliot, R.C., Chaudhry, M.H. (1992). Experimental results of two dimensional dam-break flows. J. Hydraulic Res. 30(2), 225–252.
4. Bellos, C.V., Soulis, J.V., Sakkas, J.G. (1992). Experimental investigation of two-dimensional dam-break induced flows. J. Hydraulic Res. 30(1), 47–63.
5. Biscarini, C., Di Francesco, S., Manciola, P., (2010). CFD modelling approach for dam break flow studies. Hydrol. Earth Syst. Sci. 14 (4), 705.
6. Cagatay, H., Kocaman, S. (2008). Experimental study of tail water level effects on dam-break flood wave propagation. River Flow 2008 Cesme, Turkey 1, 635–644.
7. Cagatay, H., Kocaman, S. (2008). Dam break flows during initial stage using SWE and RANS approaches. J. Hydr. Res., 48:5, 603-611.
8. Chanson, H. (2006). “Analytical solutions of laminar and turbulent dam break wave.” River Flow 2006: Proc., the International Conf. on Fluvial Hydraulics, Taylor and Francis, London, 465–474.
9. Dressler, R.F. (1954). Comparison of theories and experiments for the hydraulic dam-break wave. Association of Scientific Hydrology, Rome 38, 319–328.
10. Durbin PA (1995) Separated flow computations with the k-ε-v^2 model. AIAA J 33(4):659-664.
11. Fennema, R. J. and Chaudhry, M. H.: Explicit methods for twodimensional transient free-surface flows, JHE, 116(8), 1013–1034, 1990.
12. Fraccarollo, L., Toro, E. (1995). Experimental and numerical assessment of the shallow water model for two-dimensional dam-break type problems. *J. Hydraulic Res.* 363(6), 843–864.

13. Hirt, C. W., & Nichols, B. D. (1981). Volume of fluid (VOF) method for the dynamics of free boundaries. Journal of Computational Physics, 39(1), 201–225.
14. Hu, H., Zhang, J., Li, T. (2018). Dam-Break Flows: Comparison between Flow-3D, MIKE 3 FM, and Analytical Solutions with Experimental Data. Appl. Sci., 8, 2456. https://doi.org/10.3390/app8122456
15. Kocaman, S., Ozmen-Cagatay, H., (2012). The effect of lateral channel contraction on dam break flows: Laboratory experiment. Journal of Hydrology, Volumes 432–433,Pages 145-153, ISSN 0022-1694, https://doi.org/10.1016/j.jhydrol.2012.02.035
16. Kocaman, S., Ozmen-Cagatay, H., (2015). Investigation of dam-break induced shock waves impact on a vertical wall. J. Hydrol. 525, 1–12.
17. Kocaman, S., Ozmen-Cagatay, H., (2015). Dam-break flow over abruptly contracting Channel. International Journal of Mechanical And Production Engineering, Volume- 3, Issue-8.
18. Kheirkhah Gildeh H (2013) Numerical modelling of thermal / saline discharges in coastal waters. Master of Applied Science Thesis in Civil Engineering. University of Ottawa, Ottawa, Canada.
19. Kheirkhah Gildeh, H., Mohammadian, A., Nistor, I., and Qiblawey, H. (2014). "Numerical modelling of 30° and 45° inclined dense turbulent jets in stationary ambient.", J. Environ. Fluid Mech.,15(3): 537-562.
20. Kheirkhah Gildeh, H., Mohammadian, A., Nistor, I., and Qiblawey, H. (2014). "Numerical modelling of turbulent buoyant wall jets in stationary ambient water.", J. Hydraul. Eng., 140(6), 04014012.
21. Kheirkhah Gildeh, H., Mohammadian, A., Nistor, I., Qiblawey, H., and Xiaohui, Y. (2015). "CFD modelling and analysis of the behavior of 30° and 45° inclined dense jets; New Numerical Insights.", J. Appl. Water. Eng. & Res., https://doi.org/10.1080/23249676.2015.1090351
22. Kheirkhah Gildeh, H., Mohammadian, A. & Nistor, I. (2021). Inclined dense effluent discharge modelling in shallow waters. Environ Fluid Mech 21, 955–987. https://doi.org/10.1007/s10652-021-09805-6

23. LaRocque, L.A., Imran, J., Chaudhry, M.H., (2012). Experimental and numerical investigations of two-dimensional dam-break flows. J. Hydraul. Eng. 139 (6), 569–579.
24. Larocque, L.A., Imran, J., Chaudhry, M.H., (2013). 3D numerical simulation of partial breach dam-break flow using the LES and k–ε turbulence models. Journal of Hydraulic Research Vol. 51, No. 2 (2013), pp. 145–157 http://dx.doi.org/10.1080/00221686.2012.734862
25. Lauber, G., Hager, W.H. (1998). Experiments to dam-break wave: Horizontal channel. J. Hydraulic Res. 36(3), 291–308.
26. Lin, P. and Liu, P.L.F. (1998a). "A numerical study of Breaking Waves in the Surf Zone." J. Fluid Mech. 359, 539-264.
27. Liu, H. and Liu, H. (2016). Experimental study on dam-break hydrodynamic characteristics under different condition. Journal of disaster research, Vol. 12, No.1, Pages 197-207.
28. Menter FR (1994) Two-equation eddy-viscosity turbulence models for engineering applications. AIAA Journal, 32(8):1598-1605
29. Olsen NRB (2000) CFD algorithms for hydraulic engineering. Department of Hydraulic and Environmental Engineering, The Norvegian University of Science and Technology.
30. OpenCFD Limited. (2018). OpenFOAM - User Guide, Version 5.1.0.
31. Ozmen-Cagatay, H., Kocaman, S., (2010). Dam-break flows during initial stage using SWE and RANS approaches. J. Hydraul. Res. 48 (5), 603–611.
32. Ozmen-Cagatay, H., Kocaman, S., (2011). Dam-break flow in the presence of obstacle: experiment and CFD simulation. Eng. Appl. Comput. Fluid Mech. 5 (4), 541–552.
33. Ozmen-Cagatay, H., Kocaman, S., (2012). Investigation of dam-break flow over abruptly contracting channel with trapezoidal-shaped lateral obstacles. J. Fluids Eng. 134 (8), 081204.
34. Ozmen-Cagatay, H., Kocaman, S., Guzel, H., (2014). Investigation of dam-break flood waves in a dry channel with a hump. J. Hydro-Environ. Res. 8 (3), 304–315.
35. Quecedo, M., Pastor,M., Herreros, M.I., Merodo, J.A.F., Zhang, Q. (2005). Comparison of two mathematical models for solving the dam break problem using the FEM method. Comput. Methods Appl. Mech. Engng. 194(36–38), 3984–4005.
36. Ritter, A. Die Fortpflanzung der Wasserwellen (The propagation of water waves). Z. Ver. Dtsch. Ing. 1892, 36, 947–954.

37. Robb, Daniel & Vasquez, Jose. (2015). Numerical simulation of dam-break flows using depth-averaged hydrodynamic and three-dimensional CFD models. Canadian Society for Civil Engineering 22nd Hydrotechnical Conference. Montreal, Quebec.
38. Soarez Fraz˜ao, S. and Zech, Y.: Dam Break in channels with 90 bend, J. Hydraul. Eng.-ASCE, 128(11), 956–968, 2002.
39. Soares Fraz˜ao, S.: Dam-break induced flows in complex topographies. Theoretical, numerical and experimental approaches, PhD Thesis, Louvain-la-Neuve: Universit`a catholique de Louvain, Civil Engineering Department, Hydraulics Division, 116(8), 2002.
40. Shaheed, R., Mohammadian, A., Kheirkhah Gildeh, H. (2018). A comparison of standard k–ε and realizable k–ε turbulence models in curved and confluent channels. J. Environ. Fluid Mech. DOI: 10.1007/s10652-018-9637-1.
41. Shaolin Yang, Wanli Yang, Shunquan Qin & Qiao Li (2018): Comparative study on calculation methods of dam-break wave, Journal of Hydraulic Research, https://doi.org/10.1080/00221686.2018.1494057
42. Shaolin Yang, Wanli Yang, Shunquan Qin, Qiao Li, and Bing Yang (2018): Numerical study on characteristics of dam-break wave. Journal of Ocean Engineering, volume 159, pages 358-371.
https://doi.org/10.1080/00221686.2018.1494057
43. Shigematsu, T., Liu, P.L.-F., Oda, K. (2004). Numerical modeling of the initial stages of dam-break waves. J. Hydraulic Res. 42(2), 183–195.
44. Shih TH, Liou WW, Shabbir A, Yang Z, Zhu J (1994) A new k-ε eddy viscosity model for high Reynolds number turbulent flows- Model development and validation. Computers Fluids 24(3):227–238
45. Spalart, P. R. J. I. J. o. H. and F. Flow (2000). "Strategies for turbulence modelling and simulations." 21(3): 252-263.
46. Stansby, P.K., Chegini, A., Barnes, T.C.D. (1998). The initial stages of dam-break flow. J. Fluid Mech. 374, 407–424.
47. Stoner W. Bell , Robert C. Elliot & M. Hanif Chaudhry (1992) Experimental results of two-dimensional dam-break flows, Journal of Hydraulic Research, 30:2, 225-252.
https://doi.org/10.1080/00221689209498936

48. Stoker, J.J. Water Waves: The Mathematical Theory with Applications; Wiley and Sons: New York, NY, USA, 1957; ISBN 0-471-57034-6.
49. Tajnesaie M, Nodoushan EJ, Barati R, Moghadam MA. (2018). Performance comparison of four turbulence models for modeling of secondary flow cells in simple trapezoidal channels. ISH Journal of Hydraulic Engineering, doi:10.1080/09715010.2018.1469053.
50. Versteeg HK, Malalasekera W (1995). An introduction to computational fluid dynamics. 1st ed. Longman Science & Technical, Harlow.
51. Yakhot, V., Orszag, S.A., (1986). Renormalization group analysis of turbulence. Journal of Scientific Computing 1, 3–51.